8-12-2015 12:00 AM

Characterizing the Function of Helix Five of the Ku70 von Willebrand A Domain in Non-Homologous End Joining

Sarah M. Hoffer
The University of Western Ontario

Supervisor
Dr. Caroline Schild-Poulter
The University of Western Ontario

Graduate Program in Biochemistry
A thesis submitted in partial fulfillment of the requirements for the degree in Master of Science

CHARACTERIZING THE FUNCTION OF HELIX FIVE OF THE KU70 VON WILLEBRAND A DOMAIN IN NON-HOMOLOGOUS END JOINING

(Thesis format: Monograph)

by

Sarah M. Hoffer

Graduate Program in Biochemistry

A thesis submitted in partial fulfillment
of the requirements for the degree of
Master of Science

The School of Graduate and Postdoctoral Studies
The University of Western Ontario
London, Ontario, Canada

Abstract

DNA double strand breaks (DSBs) are a toxic and dangerous form of DNA damage repaired primarily by non-homologous end joining (NHEJ) in mammals. The Ku70/80 heterodimer rapidly responds to DSBs, stimulating recruitment of downstream NHEJ factors to protect, process, and ligate broken DNA ends. Work in our lab has shown that a D192A/D195R mutation in helix five of the Ku70 von Willebrand A (vWA) domain leads to an NHEJ defect. However, little is known about the function of this region in NHEJ. We hypothesized that helix five of the Ku70 vWA domain mediates a protein-protein interaction that is crucial for DNA repair. We optimized a laser microirradiation protocol and used microirradiation and in vitro binding assays to assess helix five's ability to recruit and interact with a variety of NHEJ factors. Surprisingly, the D192A/D195R mutation did not prevent recruitment of NHEJ factors to laser-induced DNA damage, nor did it impede several protein-protein interactions that we assessed in vitro. Overall, while the role of helix five of the Ku70 vWA domain in DNA repair remains unknown, our investigations have ruled out several possible binding partners and suggest that this helix could interact with a yet unidentified DNA repair factor.

Keywords

Ku70/80, non-homologous end joining, DNA double strand breaks, microirradiation, protein-protein interactions, lysine signaling, ionizing radiation

Co-Authorship Statement

This thesis was written by Sarah Hoffer and edited by Caroline Schild-Poulter. Experiments were performed by Sarah Hoffer. Sources of cell lines and constructs that were not cloned by Sarah Hoffer are highlighted in the Methods section. Mass spectrometry analyses were performed by Kristina Jurcic. Victoria Fell generated Figure 3-12 with data and images collected and compiled by Sarah Hoffer.

Acknowledgments

First and foremost, I would like to express my sincerest gratitude to my supervisor Dr. Caroline Schild-Poulter. Thank you for your guidance, mentorship, support, and your patience throughout this project. Thank you for being understanding and for being a great role model.

Thank you as well to Dr. Brandl, Dr. Berube, and Dr. Shilton, my committee members. From the start, I was thrilled to work with the three of you. Our very different backgrounds allowed for many great perspectives and ideas for my work at every committee meeting.

I would also like to thank the members of the Schild-Poulter lab for their friendship and support. Vicki, thank you for your mentorship and your sense of humor. Wesley, thank you for your patience (even though you say you are impatient) and for taking the time to help me with bacterial expression when you were busy writing your thesis. Louisa, thank you for always listening and for giving great advice (about things in the lab and things outside of the lab), despite your schedule. Long science days were much better when you were also having a long science day at the bench across from mine. Xu, thank you for keeping everything going in the lab and for all of the great conversations we've had during our wait times. Elisabeth, thank you for teaching me how to teach someone! And to all of the undergraduate volunteers and summer students, thank you for making busy days a little bit easier by helping with mini preps and cloning!

This work was highly collaborative and would not have been possible without all of the people who contributed to it by providing constructs, protocols, and reagents. Throughout my project, I have had the opportunity to reach out to members of the DNA repair "community" from around the world. My thesis includes constructs from three continents! I am very thankful for the kind attitudes and generosity I encountered from many research groups while seeking GFP-tagged repair protein constructs and advice about microirradiation. It was truly inspiring! Dr. van Gent and Dr. Hendzel, thank you for your support and advice in developing a microirradiation protocol for my experiments. Thank you especially to Darin McDonald from the Hendzel lab for providing me with the protocol for your system and answering the many questions that I asked you through e-mails while I translated the protocol

to our microscope. As well, thank you to Dr. Chen, Dr. Modesti, Dr. Junop, Dr. Yasui, Dr. Hordjik, and Dr. Pfeifer for the constructs that you have provided for this work. Thank you to Dr. Ferguson, Dr. Meakin, Dr. Poulter and Dr. Creuzenet for providing equipment and antibodies for some of my experiments. No matter where life takes me, I will remember with fondness the cooperative, enthusiastic spirit of the scientists I've encountered, whether they were down the hall from our lab at Robarts or e-mailing me from across the world!

As well, I would like to express my gratitude to Dr. Fabiana Caetano. I had a very limited knowledge of confocal microscopy when I began to pursue my work with microirradiation and if you had not sat down with me, taught me how to use the microscope and software, and gone through the Hendzel lab's protocol with me, I would not have a thesis to write right now!

I would also like to thank Dr. Eric Ball for taking me on as an undergraduate volunteer four years ago and allowing me to experience a lab environment for the first time. Thank you as well for being someone who I could go to for advice during my graduate studies. Your support and patience with undergraduate students has inspired many to pursue graduate degrees, myself included and I am truly thankful for this.

Thank you to my boyfriend Tamas for the love and support you have given me as I worked through my Master of Science. Thank you for understanding when I was in the lab, even when it was 1:00am and we had to miss Sunfest or when I ruined our cottage weekend three weeks before this was due because I wanted to see the results of my Western blot. Thank you for putting up with me when I was upset about failed experiments and thank you for picking me up from the lab on the days when I stayed later than the last bus (and for bringing me back when I thought I left something on).

Finally, I would like to thank my family for standing by me as I pursued my degree and trusting me to make the right choices. Thank you Mom for believing in me and for reminding me that hard work pays off in the end, even when my experiments were failing. Dad, thank you for being proud and supportive (I may have seemed a bit embarrassed when you showed all of your friends the Biochemistry brochure I'm on, but I am honored that you did). Alex, thank you for making me smile and surprising me with a visit the day the microscope broke down.

It was hard for me to choose a person to dedicate my thesis to. Should it be for the amazing community of scientists who have provided advice and materials for this work? Should I dedicate it to the women in science who have inspired me, a student in an all-female lab? Or should it be for my loved ones, who have been endlessly supportive throughout my degree? In the end, I've decided that this is for all of you. I wouldn't have made it here without any of you and this is as much yours as it is mine.

Table of Contents

List of Tables

List of Figures

List of Appendices

List of Abbreviations

aNHEJ	Alternative end joining
APLF	Aprataxin and PNK-like factor
APTX	Aprataxin
ATF2	Activating transcription factor 2
ATM	Ataxia telangiectasia mutated (protein)
ATR	Ataxia telangiectasia and Rad3-related protein
Bax	Bcl-2-associated X protein
CBP	Creb binding protein
CDK	Cyclin dependent kinase
Chk1	Checkpoint kinase 1
Chk2	Checkpoint kinase 1
CO_2	Carbon dioxide
CSK+R	Sucrose, detergent, and RNase A pre-extraction solution
Cul1	Cullin 1
DDR	DNA damage response
DNA-PK	DNA-dependent protein kinase
DNA-PK_{cs}	DNA-dependent protein kinase catalytic subunit
DSB	Double stranded break
DMEM	Dulbecco's modified eagle medium
DTT	Dithiothreitol
ECL	Enhanced chemiluminescence
EDTA	Ethylenediaminetetraacetic acid
EGFP	Enhanced green fluorescent protein
Exo1	Exonuclease 1
FAR	Fraction of activity released
Fbxl12	F-box and leucine-rich repeat protein 12
GFP	Green fluorescent protein
GST	Glutathione S-transferase
Gy	Abbreviation for the IR dose unit Gray
HEPES	Hydroxymethyl piperazineethanesulfonic acid
HR	Homologous recombination
IPTG	Isopropyl β-D-1-thiogalactopyranoside
IR	Ionizing radiation
KCl	Potassium chloride
KO	Knockout
LigIV	DNA ligase IV
MDC1	Mediator of DNA damage checkpoint 1
MEF	Mouse embryonic fibroblast
Mre11	Mitotic recombination 11 Homolog A
MRN	Mre11, Rad50, and Nbs1 complex
Mrx	Mre11-Rad50-Xrs2 complex
Na_3VO_4	Sodium orthovanadate
NaCl	Sodium chloride
NaF	Sodium fluoride
Nbs1	Nijmegen breakage syndrome protein 1

NEDD8	Neural precursor cell expressed, developmentally down-regulated 8
NHEJ	Non-homologous end joining
NIR	Near infrared
NLS	Nuclear localization signal
NP-40	Nonidet P-40
P53	Tumor protein p53
PAGE	Polyacrylamide gel electrophoresis
PARP1	Poly (ADP-Ribose) Polymerase
PAXX	Paralog of XRCC4 and XLF
PBS	Phosphate buffered saline
PFA	Paraformaldehyde
PFGE	Pulsed field gel electrophoresis
PMSF	Phenylmethylsulfonyl fluoride
PNKP	Bifunctional polynucleotide phosphatase/kinase
POT1	Protection of telomeres protein 1
PP1	Protein phosphatase 1
RAG	Recombination activating gene 1
Rap1	Ras-proximate-1
RNF8	Ring finger protein 8
SCF	Skp1-Cul1-Fbox
SDS	Sodium dodecyl sulfate
SIM	3D structured super-resolution microscopy
SSB	Single strand break
TIN2	TERF1-interacting nuclear factor 2
TPP1	Tripeptidyl peptidase I
TRF1	Telomeric repeat binding factor 1
TRF2	Telomeric repeat binding factor 2
Tris	Tris-hydroxymethyl amino methane
UV	Ultraviolet
vWA	von Willebrand A
Wrn	Werner syndrome helicase/exonuclease
WT	Wild-type
XAF-1	XIAP associated factor 1
XLF	XRCC4-like factor
XRCC4	X-like complementing gene 4 protein
X4-L4	XRCC4-XLF-DNA ligase IV complex
YFP	Yellow fluorescent protein
γ-H_2AX	Phosphorylated histone H_2AX

CHAPTER 1: INTRODUCTION

This chapter provides an introduction to DNA double strand breaks (DSBs), the mammalian DSB repair process of non-homologous end joining (NHEJ), and the Ku heterodimer. Techniques in studying DNA repair protein recruitment to DSBs will be outlined. This section will also introduce the newly identified yet poorly understood importance of helix five of the Ku70 von Willebrand A domain in NHEJ. The overall goal of my project was to characterize the function of this helix and its ability to recruit NHEJ factors to DNA damage.

1.1 DNA double strand breaks

Throughout their lifetime, many, if not all, cells experience DNA damage. While damage is common, it can cause mutations and chromosomal aberrations that have negative impacts on cells, tissues, and organisms as a whole[1]. Failure to repair DNA lesions results in a multitude of conditions including immunodeficiency, aging, cancer, and neurodegenerative disorders[2]. To prevent these affects, several repair mechanisms have evolved for the various types of DNA damage that can occur. The work herein will focus on the DNA double strand break (DSB) and its repair.

DSBs, which can lead to chromosomal rearrangements, mutations, and DNA loss, occur when both strands of a DNA helix are broken[3]. They are thought to be particularly toxic, with one DSB having potential to yield a 100 million base pair loss, and if unrepaired, they can lead to cell death or cancer[4,5]. DSBs can arise from exogenous sources or natural cellular processes. Ionizing radiation (IR), which occurs naturally in the atmosphere or can arise from X-rays, is a major external source of DSBs[6]. Ionizing radiation is defined as energy that increases electron energy levels in atoms within a given tissue to the extent that electrons are released from the atoms[7]. The released electrons can interact with DNA directly to alter and damage it or they can form radicals that indirectly oxidize DNA. Several medical applications including plane X-rays, X-ray computed tomography scans, and radiation therapy used for cancer involve tissue exposure to IR[8]. Since use of these techniques is fairly common, understanding cells' ability to respond to and repair the IR-

induced DNA damage that these applications can yield is of fundamental importance in current healthcare.

X-rays are frequently used to induce DNA damage in cells for the study of DNA damage and repair. In X-ray machines, groups of electrons are accelerated towards a tungsten or gold medium with an electric current[7]. Collision between the electrons and the medium results in a rapid conversion of the electrons' kinetic energy to waves of electric or magnetic energy, or photons. These photons interact with target tissue to excite its electrons and create DNA damage as discussed above.

Additional DSB sources exogenous to the cell include chemotherapeutic drugs, such as topoisomerase inhibitors, rare cutting endonucleases, and radiomimetic drugs[9]. While these agents can be useful in cancer treatment, the genetic instability that occurs as a side effect must be acknowledged and understood. Risks of these drugs in eliciting genetic instability and tumorigenicity was exemplified in the case of mitoxantrone, a topoisomerase II inhibitor which is thought to have caused acute promyelocytic leukemia in four patients who had used the drug as a breast cancer treatment[10]. Each patient's leukemia appeared to stem from a chromosome translocation at the same position. This is thought to be a side effect of the drug. Refining therapies to prevent side effects like secondary cancers requires improved knowledge of cellular responses and adaptations to DSBs.

DSBs can also arise from sources within the cell. Like free radicals produced by IR-induced electron excitation, free radicals and reactive oxygen species produced inside of cells through processes such as cellular respiration can generate DNA damage sites referred to as oxidative clustered DNA lesions[11]. These sites contain several forms of DNA damage, including DSBs.

Single strand breaks (SSBs), another form of DNA damage, can also lead to DSB formation[12]. Like DSBs, SSBs can arise from reactive oxygen species, drugs, and ionizing radiation. SSBs occur at a higher frequency than DSBs, with approximately 10 SSBs estimated to occur for every 1 DSB induced by IR, and they are repaired by single strand break repair[13]. This process is different than DSB repair and is initiated by

recruitment of PARP1 to damage [14]. PARP1 promotes chromatin remodeling for repair and recruits XRCC1, a scaffold for several repair proteins, including PNKP, Aprataxin, and DNA Polymerase β, which process and fill gaps in the broken DNA. The DNA can then be ligated by DNA Ligase 1 or DNA Ligase 3α. When two SSBs occur within one helical turn of one another on opposite strands of the DNA helix, a DSB will result[12]. Furthermore, replication forks can be stalled upon encountering a base lesion or single strand break in DNA[5]. This is thought to be a major cause of DSB formation within cells and exemplifies their vulnerability to internal sources of DNA damage.

Some natural cellular processes rely on DSB formation and without it, many cellular systems would not be able to function normally. In development, DSBs are required for recombination between parental chromosomes[15]. DSB formation is also critical in topoisomerase II-mediated topological modification of DNA, which prevents physical strain on DNA[16]. Furthermore, the process of V(D)J recombination, which leads to production of T-cell receptors and immunoglobulins, relies on DSB formation by recombination activation gene (RAG) proteins[17,18]. Thus, while DNA DSBs can be detrimental and affect genomic integrity, their occurrence is a normal part of cellular and human physiology.

Regardless of their source, repair of DSBs is crucial for cell survival and function. Response to and repair of DSBs is accomplished by several mechanisms and processes. With particular relevance to this work are the DNA damage response and non-homologous end joining.

1.2 The DNA damage response and DSB repair

1.2.1 The DNA damage response

The DNA damage response (DDR), a signaling cascade initiated by DSBs, can pause cell cycle progression to allow cells to commence in DNA repair, cell death, or senescence depending on the severity of damage[2]. It begins with recruitment of kinases Ataxia telangiectasia mutated (ATM) kinase and ataxia telangiectasia and Rad3-related protein (ATR) to broken DNA ends. These proteins activate additional kinases, checkpoint kinase 1 (CHK1) and checkpoint kinase 2 (CHK2) to inhibit cyclin dependent kinases

(CDKs) and arrest the cell cycle while also stimulating DNA repair factor recruitment. This is accomplished through phosphorylation, ubiquitation, or acetylation of repair proteins. In result, this response prevents damaged DNA from being replicated until it is repaired.

1.2.2 DSB repair

The two main processes of DNA DSB repair are homologous recombination (HR) and non-homologous end joining (NHEJ). HR occurs during the S and G2 phases of the cell cycle while non-homologous end joining (NHEJ) is required for cells in G1[19]. Recent work has sought to gain insights into the mechanisms by which cells "choose" between undergoing NHEJ and HR. While much is still unknown regarding DSB repair pathway choice, it is clear that 53BP1 and BRCA1 play a major role in this avenue of repair, with BRCA1 promoting HR and 53BP1 activating NHEJ[4]. Additionally, it is expected that the first proteins recruited in HR, the MRN complex (Mre11, Rad50, and Nbs1) and CtIP, compete with Ku70, the first factor recruited in NHEJ in order to mediate pathway choice. Consistent with this theory, CtIP was shown to be upregulated in stages of the cell cycle where HR is favoured. This could lead to end resection outcompeting Ku-binding to DNA ends and consequently a switch from NHEJ to HR, indicating that activity of molecules influencing repair pathway choice is highly cell-cycle dependent. Interestingly, initiation of HR can be reversed and there is evidence that Ku can be cleaved from the DNA ends by HR machinery, suggesting that a "choice" can still be made after these proteins bind the broken DNA[20,21].

When neither NHEJ nor HR can occur, perhaps due to mutation, repair is carried out by a third pathway known as alternative NHEJ (aNHEJ)[20]. aNHEJ is thought to use short regions of microhomology at either end of the DSB to align and ligate broken ends. Little is understood about aNHEJ and although PARP1 and the MRN complex are said to be major players in the process, it is currently unclear whether aNHEJ is a single pathway or a subset of smaller, independent, repair mechanisms. However, aNHEJ is thought to be highly error-prone and elicits chromosome translocation[20,22]. Thus, while aNHEJ is active throughout the cell cycle, NHEJ and HR predominate. Detailed descriptions of HR and NHEJ are provided below.

Homologous recombination

During phases of the cell cycle where DNA has been replicated for mitosis, cells can undergo homologous recombination[19]. This process uses a sister chromatid template for repair of broken DNA[20]. Thus, HR is considered to have relatively high fidelity, as compared to the other DSB repair processes. HR is initiated by binding of MRN (a complex comprised of (Mre11, Nbs1, and Rad50) to the DNA ends[23]. This complex resects the ends, yielding a 3' OH overhang. Rad51 associates with the overhang and scans the template sister chromatid for regions of homology, forming a D-loop with template sister chromatid DNA by invading it with the overhang. Next, DNA polymerase I elongates the broken DNA using the homologous DNA as a template. The result is a Holliday junction.

Following formation of the Holliday junction, two models are proposed for HR: the double strand break repair (DSBR) model and the synthesis-dependent strand-annealing model[24,25]. In the DSBR model, overhangs from either side of the DSB form Holliday junctions[24]. Junctions are then cleaved by endonucleases and ligated by DNA ligase I[23,24]. Depending on the site of cleavage, this can result in crossing over and this model is thus considered to be favored in meiosis[24]. In the synthesis-dependent strand-annealing model, strand invasion by the 3' OH overhang on one side of the DSB and the consequent formation of a Holliday junction leads to synthesis of enough DNA that the newly synthesized strand can be annealed to the 3' OH overhang on the opposite end of the DSB and used as a template for repair[25]. Unlike DSBR, this model does not result in crossing over.

Non-homologous end joining

NHEJ, which is thought to be the major DNA repair process for mammalian cells, will be the focus of our work and is outlined in Figure 1-1[26].

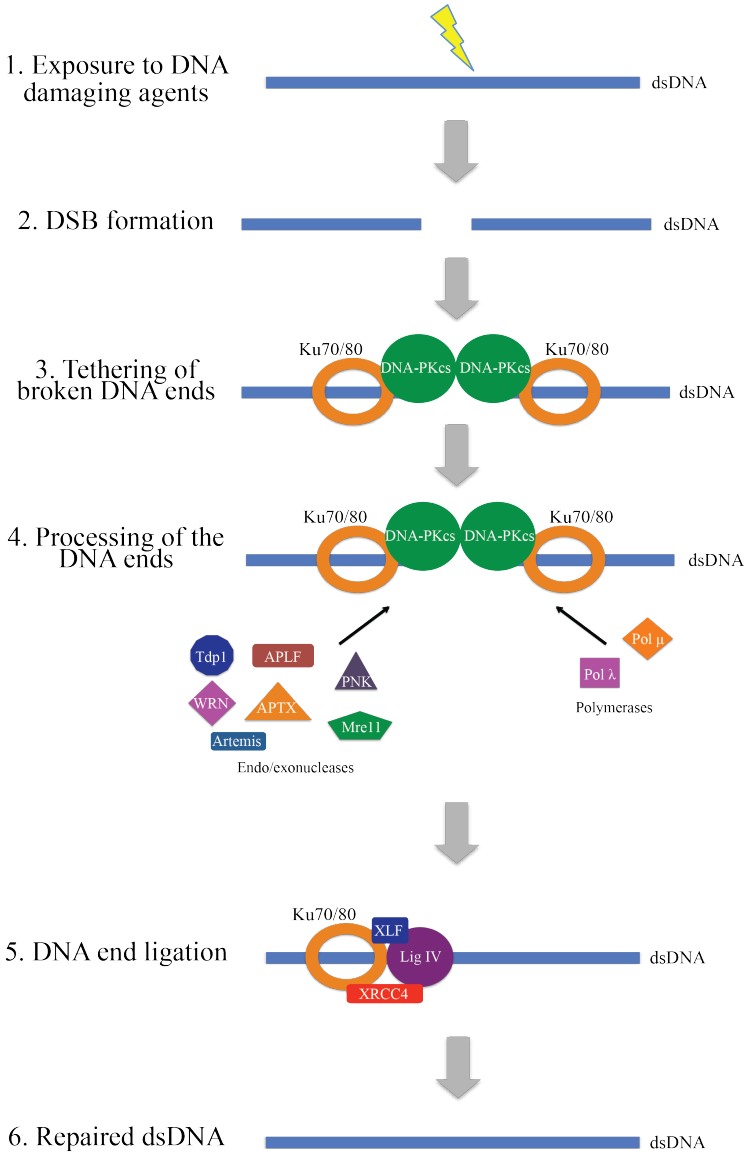

Figure 1-1: Non-homologous end joining. Following DSB formation, NHEJ is initiated by binding of the Ku heterodimer to broken DNA (dsDNA) ends. Ku recruits DNA-PK, which tethers the broken ends to protect them from degradation. Several accessory factors then process the ends, removing non-ligateable groups and filling in gaps in the DNA such that the ends can be re-ligated by XRCC4-XLF-DNA Ligase IV complex. As a result of this process the DNA ends are rejoined, restoring DNA integrity.

Non-homologous end joining begins with recruitment of the Ku70/80 heterodimer to broken DNA ends[27]. The heterodimer translocates along the DNA, making space for two DNA-PK molecules to associate with the break. DNA-PK transphosphorylates the DNA ends and is thought to regulate its own activity through autophosphorylation. The association of Ku70/80 and DNA-PK ultimately yields tethered DNA ends that cannot be degraded by endonucleases within the cell[27].

Following tethering of the DNA ends, the ends can be processed[28]. Small nucleotide gaps in the broken DNA are repaired by DNA polymerases μ and λ and non-ligateable groups are removed from the DNA ends by the DNA 3' phosphatase/ 5'kinase polynucleotide phosphatase kinase (PNKP), as well as tyrosyl-DNA phosphodiesterase 1 (TDP1) and possibly aprataxin (APTX). Nucleases such as Mre11, Artemis, exonuclease 1 (Exo1), and Werner syndrome helicase/exonuclease (WRN) are thought help align broken DNA ends by detecting regions of the ends with microhomology. The ultimate goal of this processing step is to make the DNA ends ligateable.

Following processing, the DNA ends can be ligated by the X4-L4 complex, which contains x-like complementing gene 4 protein (XRCC4), XRCC4-like factor (XLF), and DNA ligase IV[27]. This complex is recruited to the DSB in the presence of Ku70/80 and its ligation function is carried out by DNA ligase IV while XRCC4 is thought to serve as a scaffolding protein. The overall result is the restoration of the DNA double helix.

While many of the key players in NHEJ are recognized, it has been postulated that additional factors involved in the NHEJ complex exist and have yet to be identified. This principle was exemplified in the recent identification of paralog of XRCC4 and XLF (PAXX), a protein similar in structure to XRCC4 and XLF which was shown to be required for NHEJ and to directly interact with Ku[29,30]. Further characterization of NHEJ and factors involved in the process is needed.

NHEJ is considerably error prone. Processing of broken DNA ends can cause nucleotide losses or alterations[28]. Furthermore, the X4-L4 complex is more tolerant of mispairings and nucleotide damage at DNA ends than other ligases[31]. While the low fidelity of NHEJ could result in loss of genetic information and jeopardized genomic integrity, the process

restores DNA's structural integrity, preventing chromosome aberrations and overall more severe cellular and genetic consequences.

DSB repair has long been considered as a potential target process for cancer therapeutics. NHEJ inhibiting drugs like Garcinol, which does not allow chromatin remodeling for NHEJ after IR, are promising for use with radiation therapy since NHEJ is the main repair process to occur after IR[32]. Another drug, SRC7, inhibits DNA ligase IV in NHEJ to slow tumor growth in mice and increase mouse tumor sensitivity to radiation or DSB-forming chemotherapeutic drugs[33]. By developing an understanding of DSB repair and the proteins involved, we create potential for identifying new therapeutic targets.

1.3 The Ku Heterodimer

The focus of this work was Ku70, a component of the Ku70/80 heterodimer, which is the first complex recruited to DSBs in NHEJ[27]. Overall, Ku is highly conserved from yeast to mammals highlighting the importance of Ku-mediated DNA repair in even simple organisms[34]. Here, I will discuss basic features of Ku as well as its role in repair and signaling.

1.3.1 The Ku heterodimer: A brief history and overview

Ku was first identified more than thirty years ago in an immunological study of antibodies in a patient with polymyositis-scleroderma overlap, a connective tissue disease[35]. The objective of this study was to find biomarkers for the disease and at this time, the role of Ku in repair was not apparent. However, antibodies designed for Ku indicated that it was localized to the nucleus. Later work from the same group showed that double stranded DNA precipitated with anti-Ku antibodies[36]. The DNA-binding ability of Ku was found to be dependent on the availability of free DNA ends while Ku dimerization was DNA-independent in vitro[37]. However, the role of Ku in repair was not elucidated for over 10 years following its initial discovery until a DNA repair defect in radiosensitive hamster cells was attributed to Ku deficiency[38]. Several studies have since shown a link between Ku-deficiency and impaired DNA repair in multiple cell lines and the significance of Ku for repair, particularly in NHEJ is well-documented[34].

1.3.2 Ku in DNA repair

A.) NHEJ

Ku's primary roles in NHEJ are to act as a sensor to breaks, as well as a scaffold for recruitment of other NHEJ factors. As discussed in section 1.2.2, Ku is the first repair factor to be recruited in the process of NHEJ[27]. Ku binds to double stranded DNA, but not single stranded DNA, with a high affinity (approximately 2nM), with Ku80 interacting with the DNA minor groove and Ku70 interacting with the major groove[39]. Ku encircles the DNA such that Ku80 faces the length of the DNA while Ku70 faces the break[40]. Upon binding, Ku translocates along the DNA by approximately one turn of the helix such that the DNA-PK catalytic subunit (DNA-PKcs) can bind the broken DNA ends[41]. Together, Ku and DNA-PKcs form the DNA-PK complex. DNA-PKcs subunits on either end of the DSB can interact to tether the broken ends, protecting them from nuclease degradation[27]. It has also been suggested that Ku itself is directly involved in DNA end bridging[34]. In addition to its protective function, Ku is important in recruiting several members of the NHEJ complex that carry out downstream functions (see 1.2.2 for an overview of NHEJ). Among the NHEJ factors that interact with Ku are DNA polymerases μ and λ, XRCC4, XLF, DNA ligase IV, APLF, and WRN[39].

Following NHEJ, Ku is removed from repaired DNA via polyubiquitination of Ku80. In a Xenopus system, Ku removal was shown to be mediated by a Skp1-Cul1-Fbox (SCF) E3 ubiquitin ligase complex containing the F box protein F-box and leucine-rich repeat protein 12 (FBxl12), which recognizes Ku80 as a substrate[42]. Truncation experiments indicate that the E3 recognition site within Ku80 is located within the DNA-binding core domain. In humans, Ku removal via ubiquitination is attributed to RING finger protein 8 (RNF8), a ubiquitin ligase[43]. Additionally, a recent study suggested that Ku ubiquitination and removal is mediated through Ku neddylation by NEDD8[44]. While it is suspected that DNA-bound Ku70 is also degraded or removed by ubiquitination, regions of Ku70 required for this have not been identified[39]. It has also been argued that Ku could be removed by nicking by members of the HR complex MRX (Mre11-Rad50-Xrs2) followed by end resection[21,45]. Overall, the molecular mechanisms underlying Ku removal from the break are not yet clear.

B. Other repair roles of Ku

The primary repair functions of Ku lie in the heterodimer's role in NHEJ. However, Ku has been implicated in various types of DNA repair. Several studies have identified an interaction between Ku and base excision repair intermediates called AP sites[46]. A recent study suggested that Ku80-deficient cells displayed impairments in the initial steps of base excision repair and that the absence of Ku80 yielded vulnerability to single-strand break (SSB)-inducing reactive oxygen species and alkylating agents[47]. Surprisingly, deletion of Ku70 did not affect base excision repair. Consistent with the idea that Ku80 is more important for base excision repair than Ku70 is the observation that Ku80-depleted cells are more sensitive than Ku70-depleated cells to the SSB-inducing agents streptonagrin and paraquat[48]. However, these results should be interpreted cautiously and may be the result of deficient cells' background phenotypes, as Ku is thought to exist primarily in its heterodimeric state and depletion of Ku70 or Ku80 respectively has been shown to lead to absence of the other member of the heterodimer[49,50].

Additionally, Ku may play a role in ribosomal DNA repair. Ku was shown to interact with ABH2, a protein linked to protection of ribosomal DNA (rDNA) in response to alkylating damage[51]. Repair of rDNA, which encodes ribosomal RNA and is highly transcribed in the nucleolus, is not yet well-understood and it could be possible that Ku plays a novel role here.

Beyond its involvement in particular repair processes, Ku also plays a key role in suppressing other repair pathways when NHEJ is favorable. By outcompeting members of the HR complex during the G1 phase of the cell cycle as well as the alternative end joining player PARP1 when aNHEJ is not favorable, Ku ensures that NHEJ predominates over the other pathways[34].

1.3.3 Additional functions of Ku

A.) Ku in telomere function

Ku is essential for normal telomere function[34]. Telomeres, as the linear double stranded end components of chromosomes, pose the problem of being recognized as DSBs by

NHEJ machinery[52]. Recognition and "repair" of telomere ends could have dire consequences for the cell, such as chromosome fusions and overall genetic instability. Comprised of telomeric repeat binding factor 1 (TRF1), telomeric repeat binding factor 2 (TRF2), Ras-proximate-1 (Rap1), TERF1-interacting nuclear factor 2 (TIN2), tripeptidyl peptidase I (TPP1), and protection of telomeres protein 1 (POT1), the shelterin complex protects DNA ends from this fate[53]. Specifically, TRF2 is thought to inhibit NHEJ at the telomere[52]. Surprisingly, Ku plays a key role in this by interacting with TRF2, despite its function in NHEJ, and it is also involved in preventing HR and alternative end joining at telomeres[52,54,55].

In addition to downregulating repair at telomeres to maintain telomere integrity, Ku may be involved in recruiting telomerase to lengthen telomeres, a function proposed to act through the Ku80 vWA domain[56]. The implications of Ku-deficiency in terms of telomere length vary across organisms[34]. However, structural disruptions and loss of telomeres occur in human cells that do not express Ku suggesting that Ku's role in telomere maintenance is physiologically relevant[57]. It is not clear whether Ku binds telomeres directly via its DNA binding domain or whether it indirectly interacts with telomeres via a protein-protein interaction, but reported binding partners of Ku within the telomere include telomeric repeat binding factor 1 (TRF1), telomeric repeat binding factor (TRF2), and Ras-proximate-1 (Rap1)[34].

B.) DNA damage signaling and apoptosis

The DNA damage response (DDR) is a signaling cascade mediated mainly by members of the PIKK family that modifies chromatin to prepare DSBs for repair and signals for cell cycle arrest and apoptosis[58]. The latter is carried out through ATM and ATR-regulated phosphorylation of p53 and Chk1/2. Ku's link to the DDR is through ATM. ATM activity is regulated by Ku and cells lacking Ku70 were impaired in ATM-mediated ATR activation while cells without Ku80 display increased ATM activity and consequently inability to enter S phase[59,60].

Work in our lab has shown a role for S155 within the Ku70 von Willebrand A domain in DNA damage signalling[61]. An alanine substitution at S155 led to increased cell survival

after IR, accelerated growth, and abnormal expression of genes related to DNA damage-induced apoptosis[61,62]. Further investigation indicated that the S155A substitution led to misregulation of activating transcription factor 2 (ATF2) and its targets[61]. Conversely, an S155D phosphomimetic substitution led to increased IR sensitivity and activation of ATF2, suggesting that S155 could be phosphorylated to mediate DNA damage signaling. This was confirmed by mass spectrometry analyses (Fell *et al*., submitted). Characterization of the S155D mutant revealed upregulation of the apoptotic and G2/M checkpoint regulator XAF-1 along with downregulation of cell cycle progression proteins Cyclin D1, cyclin dependent kinase 6 (CDK6), and protein phosphatase 1 (PP1). This suggests that phosphorylation of Ku70's S155 mediates cell cycle progression. A large-scale screen suggested that Ku could interact with Aurora B, a kinase that mediates G1/S and G2/M progression. S155D-expressing cells displayed arrest in these stages and gene expression in cells treated with an Aurora B inhibitor was comparable to that of S155D mutant-expressing cells. Considering the similarities between the Aurora B inhibition and S155D phenotypes, as well as the interaction between Ku and Aurora B, it was proposed that phosphorylation of S155 in Ku70 inhibits Aurora B activity. This could promote cell cycle arrest during DNA repair and, in cases of more severe damage, lead to senescence and apoptosis.

Beyond our studies in the role of S155 in Ku-mediated DNA damage signaling, other groups have considered the role of Ku in apoptosis through its binding to Bcl-2-associated X protein (Bax)[34]. However, these studies are limited in that Bax is a cytoplasmic protein whereas Ku is localized to the nucleus.

1.3.4 Localization of the Ku heterodimer

Ku is localized to the nucleus throughout the lifetime of a cell. Ku70's nuclear localization signal (NLS) is a bipartite basic sequence comprised of amino acids 539 to 556[63]. Within this, two basic clusters from 542-544 and 553-556 are essential for nuclear localization. A Ku80 NLS was reported at residues 561-569 and its import is thought to occur via PTAC58 and PTAC97, two proteins within the nuclear pore-targeting complex[64]. Ku NLS mutants, when co-expressed with wild-type binding partners (for example a Ku70 NLS mutant co-expressed with wild-type Ku80), can localize to the

nucleus suggesting that NLS integrity in only one member of the heterodimer is sufficient to promote nuclear localization of the full Ku heterodimer [63].

1.3.5 Medical relevance of the study of Ku

There is evidence that Ku could be linked to immune system disorders, aging, and cancer[34]. Although there is no Ku-deficient human phenotype, studies in Ku-deficient mice have provided insights into the adverse effects of Ku dysfunction in mammals. In the context of the immune system, Ku80-deficient mice are incapable of T cell and B cell maturation by V(D)J recombination[65,66]. Ku70-deficient mice display low levels of mature T cells, with poor overall T cell development[67]. They are also impaired in B cell development and class switch recombination[68]. The Ku80-deficient phenotype is thought to be more similar to recombination activating gene (*RAG*) deficient mice as lymphocytes cannot mature within the animals' thymus[65]. While DJ junctions form in the mice, at low levels, V(D)J recombination cannot be completed. These data imply that Ku plays a vital role in the immune system.

In the context of aging and cancer, it has been reported that Ku70/80 double knockout mice display an increased aging phenotype[69]. There have also been reports that Ku70-deficient mice are predisposed to thymic tumors[67]. However, these data must be interpreted cautiously as double knockout experiments did not indicate an increased likelihood of tumor growth in Ku70 and Ku80-deficient mice raised in the same environment and genetic background[69]. Nevertheless, abnormal Ku expression has been reported in cancers and Ku80-deficiency, in combination with p53 deficiency leads to tumor development[34,70].

In addition to being causative in tumor formation, Ku deficiency could be exploited by cancer therapies. This was exemplified in a study showing that Imatinib, a drug whose functions include inhibition of homologous recombination, could be used to sensitize Ku-deficient bladder cells[71]. The authors of this study argued that since muscle invasive bladder cancer is deficient in Ku (and therefore NHEJ) whereas healthy tissue maintains normal Ku expression, inhibiting HR could specifically sensitize bladder cancer cells.

However, this work was highly preliminary and sensitization of muscle invasive bladder cancer cells by Imatinib has not yet been illustrated in vivo.

1.3.6 Structural characteristics of Ku70/80

Ku70/80 is a heterodimer and removing either subunit of the dimer likely compromises the stability of the other component. This is exemplified by low Ku80 expression in Ku70 knockout cells and by low Ku70 levels in cells harboring Ku80 loss of function mutations[49,50]. The crystal structure of the Ku heterodimer, which is depicted in Figure 1-2, has provided important insights into how Ku binds DNA and how Ku70 and Ku80 interact to achieve this[72]. Ku70 and Ku80 interact with one another via three beta hairpins from each of the two proteins[73]. The binding domains of Ku70 and Ku80, which connect the two proteins together, deviate from one another in sequence to ensure that they form heterodimers, rather than homodimerizing[72]. However, Ku70 and Ku80 have a considerable degree of structural similarity. Although the two proteins diverge in their C-termini, which for Ku70 contains a SAP domain and for Ku80 contains a domain thought to bind DNA-PK, they share similarity in their core domains[74]. These have beta barrel structures which form grooves that facilitate the proteins' DNA binding[72]. In addition to this, the two proteins share the similarity of having N-terminal Von Willebrand A (vWA) domain-like motifs[75].

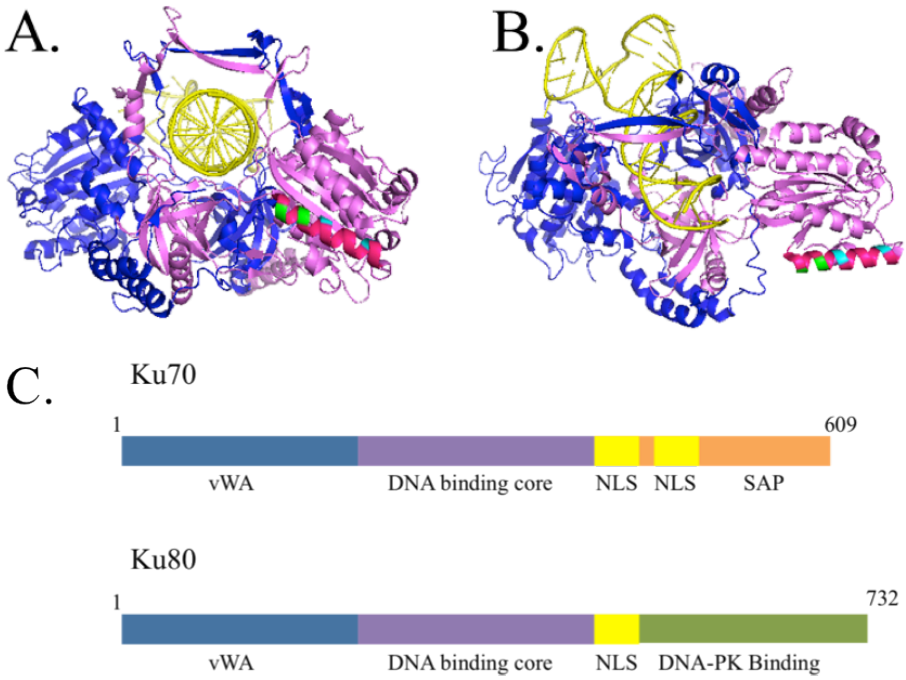

Figure 1-2: Structure of the Ku70/80 heterodimer with front (A) and side (B) views and a linear representation of both Ku subunits (C). In A and B, D192 (right) and D195 (left) are indicated in green and K182 (right) and K189 (left) are indicated in cyan. Crystal structure images are adapted from the crystal structure solved by Walker *et al*. using the PyMOL Molecular Graphics System Version 1.3 (Schrödinger LLC, USA)[72]. (Adapted by permission from Macmillan Publishers Ltd: [Nature] ([72]), copyright 2001). (See Appendix C). In C, domains of Ku70 and Ku80 are colour-coded, with the von Willebrand A domains in blue, the DNA binding cores in purple, and the NLS signals in yellow. The SAP domain of Ku70 is depicted in orange and the C-terminal/DNA-PK binding domain of Ku80 is shown in green.

1.3.7 Function of von Willebrand A-like domains in the Ku70/80 heterodimer

Generally, vWA domains are thought to be sites of protein-protein interactions[76]. The Ku80 vWA-like domain is involved in yeast telomere function and there is evidence that it interacts with aprataxin and PNK-like factor (APLF), whose recruitment was recently shown to stabilize the NHEJ complex[40,77]. Additionally, Werner's syndrome helicase/exonuclease (WRN) interacts with the region of Ku80 containing the vWA domain[78]. Despite the discovery of these roles of Ku80's vWA domain, the function of the Ku70 vWA domain is not well-understood.

Recent evidence suggests that helix five of the Ku70 vWA domain may be important in DNA repair. This helix displays high conservation across organisms, suggesting that it could be key for survival (Figure 1-3A). In fact, a study searching for significant residues in Ku indicated that the helix five was conserved in a manner comparable to Ku70's critical DNA-binding region, suggesting it could have functional significance[40]. The authors mutated D195 and D198 in helix five of the yeast Ku70 vWA domain and indeed, this led to impaired NHEJ, as evaluated by in vivo plasmid repair assays[40] (yeast Ku70's D195 is homologous to human Ku70's D192, and yeast D198 corresponds to human D195). While both D195A and D195R substitutions led to a repair defect, a D198A substitution did not impair repair while repair was affected by a D198R substitution. This work prompted our lab to study the effects of mutating the acidic residues of helix five in mammalian cells. Ku70 D192A/D195R in a retroviral expression vector was introduced into Ku70 knockout mouse embryonic fibroblasts (MEFs)[61]. This resulted in cells stably expressing Ku70 D192A/D195R and no wild-type Ku70. Using clonogenic cell survival assays, the authors found that compared to Ku70 knockout MEFs expressing wild-type Ku70, Ku70 knockout MEFs expressing Ku70 D192A/D195R showed impaired survival in response to IR (Figure 1-3B). Levels of survival were similar to those measured for Ku70 knockout MEFs expressing an empty retroviral vector. Ku70 knockout mice and Ku70 knockout embryonic stem cells are radiosensitive and have NHEJ defects, and consistently the Ku70 knockout MEFs displayed impaired DNA repair[50,68]. The similarity of survival levels between Ku70 knockout MEFs and MEFs with the Ku70

D192A/D195R mutation indicates that Ku70 D192A/D195R had lost its function in conferring cell survival following IR. Pulsed-field gel electrophoresis (PFGE), which measured DNA repair at various time points, indicated that the Ku70 D192A/D195R mutant had impaired DNA repair, suggesting that the mutant was deficient in NHEJ (Figure 1-3C)[61]. This indicates that helix five of the Ku70 vWA domain, in which residues D192 and D195 are located, may be important for DNA repair. However, the function of this helix in repair is unknown.

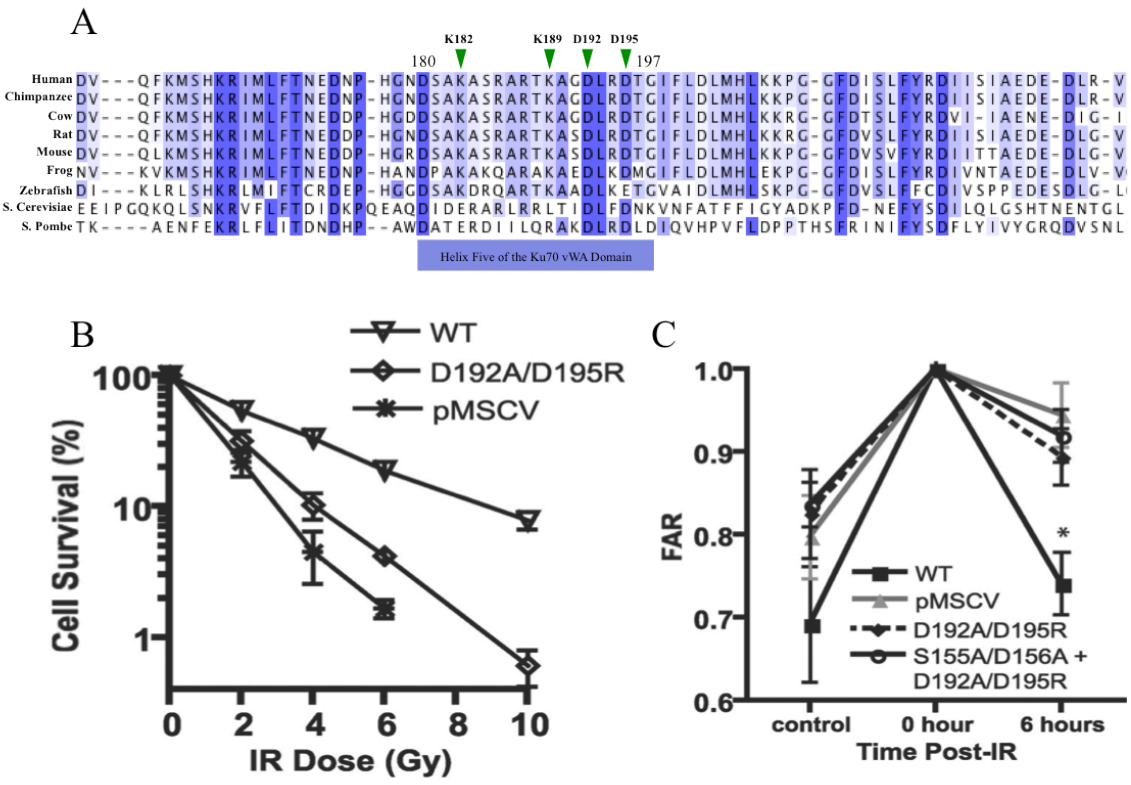

Figure 1-3: Conserved helix five of the Ku70 vWA domain is important for NHEJ. Sequence alignment of several eukaryotic organisms indicates high conservation in helix five of the Ku70 vWA domain in mammals (A). The alignment was performed using the COBALT alignment tool and formatted in Jalview software, Version 2 (Barton Group, University of Dundee, Scotland)[79,80]. Residues are colour-coded, with dark purple indicating residues with the highest percent identity and brighter colour intensity indicating a higher degree of residues' conservation. D192, D195, K182, and K189 within helix five are indicated with green arrows. Clonogenic cell survival assays with Ku70 knockout MEFs expressing wild-type Ku70 (WT), Ku70 D192A/D195R (D192A/D195R), or the pMSCV puro empty vector (pMSCV) indicate that Ku70 knockout MEFs expressing Ku70 D192A/D195R have impaired survival as a function of IR, as compared to wild-type Ku70-expressing cells (B)[61]. Pulsed field gel electrophoresis confirmed that the mutant displayed impaired DNA repair as a function of time (C)[61]. FAR=fraction of activity released, a ratio of unrepaired DNA to total DNA loaded in the experiment. Panels B and C were obtained from[61] in the journal Molecular Cell Biology with permission from the editors, the American Society for Microbiology (see Appendix C).

A recent study reported that the Ku70 vWA domain might contribute to Ku70's association with the shelterin complex, which prevents the DNA damage response from occurring at telomeric ends[52]. The authors also argued that Ku70 self-associates in a tetramer via helix five of the Ku70 vWA domain. They suggested Ku tetramerization could bridge DNA ends and that this bridging function could define the helix's role in repair. However, this study was not conduced in the context of DNA damage. Thus, it remains a mystery whether Ku tetramerizes in DSB repair and whether this is truly dependent on helix five of the Ku70 vWA domain.

1.4 Covalent modification of helix five of the Ku70 vWA domain

Helix five of the Ku70 vWA domain contains two conserved lysines at positions 182 and 189 (Figure 1-3A). The conservation of these residues indicates that they may have an important function and as they are located within a helix important for repair, we considered the possibility of their involvement in NHEJ. In support of the idea that these lysines could be sites of signaling or modification, several proteins have been shown to modify lysines in the Ku heterodimer in past studies, discussed herein.

A. Ku ubiquitination

There is evidence that ubiquitination of Ku80 is integral for effective NHEJ and this could be true of Ku70 as well. MDC1, a DNA damage response factor, recruits the E3 ubiquitin ligase RNF8 to DSBs where it ubiquitinates Ku80[43,81]. Work by Feng and Chen (2012) indicated that RNF8-mediated ubiquitination of Ku80 may be important for removing Ku80 from broken DNA ends[43]. In support of this Postow *et al.* developed an assay showing Ku80 dissociation from DNA is dependent on ubiquitination and showed that removal of Ku80 from DNA may be mediated by the proteasome[82]. Furthermore, siRNA silencing of RNF8 led to prolonged retention of Ku80 at sites of DNA damage and an NHEJ defect was observed in RNF8 knockout MEFs[43,83].

Considering the key role of Ku80 ubiquitination as well as the high structural and functional similarities of Ku70 and Ku80, it is possible that like Ku80, Ku70 is

ubiquitinated in NHEJ. This ubiquitination may occur at K182 or K189 of helix five of the Ku70 vWA domain. If this is the case, the Ku70 D192A/D195R repair defect mutation could prevent this ubiquitination by reducing the availability of these sites for modification or by preventing recruitment of factors responsible for their ubiqutination, such as RNF8 or the upstream MDC1. The possibility of Ku70 ubiquitination is supported by a global ubiquitination study which indicated that K182 of Ku70 can be ubiquitinated[84].

B. Ku acetylation

It is also possible that Ku70 is acetylated at the conserved K182 and K189 residues. Some evidence suggests that Ku70 is acetylated in response to ionizing radiation and this is thought to be dependent on CREB binding protein (CBP)[85]. Such acetylation may lead to cell death in response to IR. The specific residues that are acetylated by CBP have not been identified and it is possible that this role is assumed by K182 and K189 in helix five of the Ku70 vWA domain.

1.5 Involvement of helix five of the Ku70 vWA domain in a protein-protein interaction

Helix five of the Ku70 vWA domain is positioned in the Ku70/80 heterodimer such that the helix protrudes from the dimer, making it an ideal site for protein-protein interactions. The helix's surface is predicted to be altered by the D192A/D195R mutation, which affects both the charge and surface morphology of helix five (Figure 1-4). Because of the repair-deficient phenotype observed in the Ku70 D192A/D195R mutant, it was suspected that helix five might recruit a factor involved in NHEJ or the DNA damage response. No protein-protein interactions have been reported between helix five and NHEJ factors, but Ku80's vWA domain interacts with NHEJ accessory factors Werner syndrome recombinase/exonuclease (WRN) and APLF[77,78]. With this in mind, it is possible that the structurally similar Ku70 vWA domain is involved in a similar interaction. To understand the role of helix five of the Ku70 vWA domain in protein-protein interactions, factor recruitment in the Ku70 D192A/D195R mutant must be analyzed.

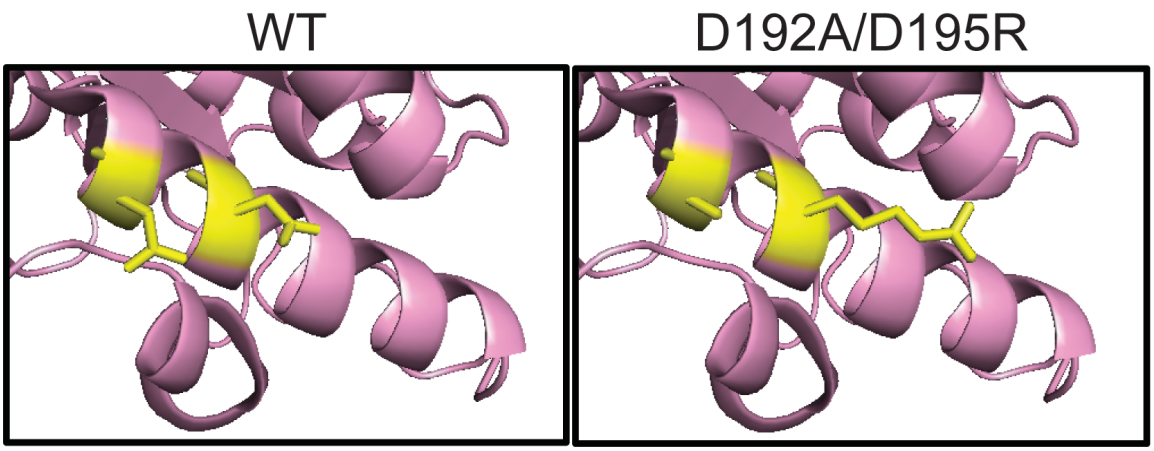

Figure 1-4: Comparison of helix five of the Ku70 vWA domain in WT Ku70 and Ku70 D192A/D195R. D192 (right) and D195 (left) are indicated in yellow. Images were adapted from Walker *et al*. using PyMOL Molecular Graphics System Version 1.3 (Schrödinger LLC, USA)[72]. (Adapted by permission from Macmillan Publishers Ltd: [**N**ature] ([72]), copyright 2001). (See Appendix C).

1.6 Candidate factors that may be recruited via the Ku70 vWA domain

1.6.1 DNA-PKcs

Ku70 and the DNA-PK catalytic subunit (DNA-PKcs) form the DNA-PK complex, which bridges DNA ends and phosphorylates various NHEJ factors at the DSB[27]. While there is evidence that DNA-PKcs's recruitment is mediated by the C-terminus of Ku80, it is possible that the Ku70 vWA domain strengthens the interaction[86]. Cells with Ku80 lacking its C-terminal domain cannot recruit DNA-PK to DSBs and display a radiosensitive phenotype, as observed with the Ku70 D192A/D195R mutant and it is possible that both phenotypes result from impaired DNA-PK recruitment[61,86].

1.6.2 DNA-processing NHEJ factors

Several proteins and accessory factors, including Artemis, DNA polymerases μ and λ, WRN, APLF, and PNKP have been implicated in processing DNA ends for repair[27]. Artemis is thought to act as an endonuclease that becomes active in cleaving overhangs in broken DNA in the presence of DNA-PK[87]. DNA polymerase μ and λ are thought to fill in small gaps in the broken DNA ends[27]. Pol μ's ability to form a complex with DNA was found to be Ku-dependent and perhaps the region of Ku important for this association is the vWA domain[88]. While pol λ's association with broken DNA is thought to be Ku-independent, it is possible that Ku70's vWA domain facilitates its recruitment through a protein-protein interaction, as well[89]. As mentioned previously, Werner's syndrome recombinase helicase (WRN) and APLF are accessory factors whose association with NHEJ complexes relies on the Ku80 vWA domain[77,78]. Since the Ku70 vWA domain is structurally similar to that of Ku80, it is possible that it shares this function in binding these proteins, as well. Finally, PNKP, which is thought to process non-ligatable end groups of broken DNA by acting as a 3' phosphatase and 5' kinase, may be recruited to the Ku70 vWA domain[27]. In the absence of this protein, cells display radiosensitivity as observed in the Ku70 D192A/D195R mutant, although there is little evidence that the association of PNKP with DSBs is Ku-dependent[27,90].

1.6.3 Proteins of the X4-L4 complex

Recruitment of the X4-L4 complex to DSBs for ligation of DNA ends was reported to be dependent on the presence of Ku in vitro[91]. Furthermore, studies using laser-induced DNA damage showed that Ku80 colocalized with XRCC4 and a direct interaction between Ku70/80 and XRCC4 was confirmed using immunoprecipitation[92]. Helix five of the Ku70 vWA domain may play a role in this interaction or may be involved in stabilizing the complex.

1.6.4 PAXX

PAXX was recently characterized as a novel NHEJ factor within the same structural superfamily as XLF and XRCC4[29]. PAXX depletion by siRNA knockdown or knockout by CRISPR-Cas9 gene editing led to radiosensitivity and GFP-PAXX was recruited to sites of laser microirradiated damage, suggesting that the protein is involved in DSB repair. Furthermore, GFP pulldown assays identified Ku70 and 80 as PAXX binding partners and mutagenesis studies revealed that the Ku-PAXX interaction is mediated via the PAXX C-terminus. Re-expression of PAXX in PAXX-deficient cells led to rescued survival after IR while reexpressing PAXX without its C-terminus did not, implying that the PAXX-Ku interaction may be key for DSB repair. However, the regions of Ku involved in the Ku-PAXX interaction have not been characterized and it is possible that this interaction occurs via helix five of the Ku70 vWA domain.

1.7 Qualitative analysis of DNA repair factor recruitment

DNA repair factor recruitment can be analyzed qualitatively using immunofluorescence. Following IR-induced DNA damage, some proteins form foci, clusters that can be observed with microscopy, at the broken DNA ends[93]. One such factor is phosphorylated histone H_2AX, (γ-H_2AX), which forms one nuclear focus per DSB[94]. These foci can be used to quantify DNA damage derived from sources like X-rays. γ-H_2AX foci are thus often considered to be markers for DNA damage and can be observed with immunofluorescence, minutes after IR treatment[94,95]. Additional foci-forming proteins related to the DNA damage response include p53 binding protein 1 (53BP1) and ataxia telangiectasia mutated protein (ATM)[94].

Limitations arise in the X-ray-immunofluorescence approach for visualizing protein recruitment to DNA damage as only low levels of NHEJ proteins accumulate at the break. As a result, protein recruited to damage cannot always be distinguished from free protein in the nucleus (see example in Figure 1-5A).[96] Thus, while X-ray induced DNA damage, which creates DSBs throughout the nucleus, can be used to visualize factors that form foci at DSBs, an alternative means of visualizing factor recruitment to DSBs must be used in observing NHEJ factors.

Microirradiation, a technique that induces DNA damage using lasers, has allowed effective visualization of proteins involved in NHEJ and the DDR at DSBs, regardless of whether the factors form foci[96]. Laser-induced DNA damage is stimulated in pre-defined regions, with relatively high levels of damage localized to a specified area. This results in a concentration of repair proteins at microirradiated sites, such that the damage-associated protein can be resolved and distinguished from protein that is not associated with DSBs in immunofluorescence and live-imaging studies (see example in Figure 1-5C). In addition to laser microirradiation, a study has suggested that Ku foci can be observed by immunofluorescence when cells are treated with a pre-extraction method that removes non-DSB associated Ku from the nucleus (Figure 1-5B). We considered both Ku visualization methods in our study.

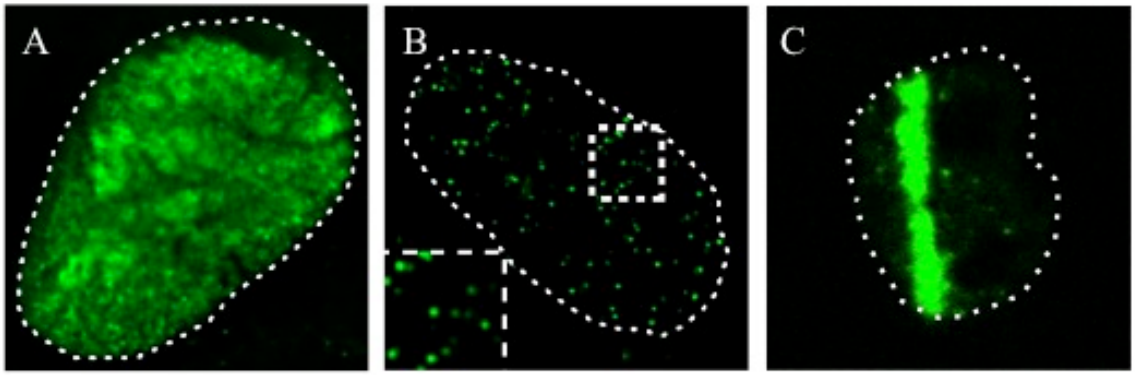

Figure 1-5: Methods for visualizing Ku. Images of Ku80 in cells treated with 10Gy IR (A), 10Gy IR and preextraction with cytoskeleton buffer and RNase A (CSK+R) (B), or laser microirradiation (C). Images in panels A and B were adapted from[97] in the Journal of Cell Biology with permission from the RUP permissions department (see Appendix C) and C was taken in our lab under conditions described in Chapter 2. Without pre-extraction or concentration of damage to predefined sites by microirradiation, Ku stains diffusely throughout the nucleus and Ku localized to breaks cannot be distinguished from Ku throughout the nucleus.

1.7.1 Mechanisms for laser-induced DNA damage

Laser-induced DNA damage is thought to occur by four mechanisms reviewed by Kong *et al*[96]. These mechanisms are outlined below.

1. Increased temperature due to photon absorption

DNA is thermally denatured in temperatures above 66.85°C[98]. Laser microirradiation of nuclei leads to photon absorption which, in turn, can lead to a rise in temperature[96]. For laser systems that deliver multiple pulses to target DNA, the heat from subsequent pulses can be retained and thus, the DNA will be heated not only by each pulse, but by the cumulative effect of multiple pulses[96]. This will generate multiphoton absorption that can further increase temperature to damage DNA.

2. Thermo-eleastic stress

Thermo-elastic stress is a form of physical stress influenced by the length of laser pulses irradiating the DNA as well as the time needed for thermal stress induced by the laser to move through the DNA[96]. It can be generated from laser systems using multiple pulses due to the short time interval between pulses and has potential to affect DNA integrity. However, thermo-elastic stress generated by the laser parameters used to induce DNA damage is thought to be relatively low and overall, thermo-elastic stress is considered a minor player in formation of damage induced by lasers with multiple pulses.

3. Oxidative and crosslinking damage generated by photochemical processes following photon absorption

Photon absorption can lead to reactive oxygen species and free radical formation which can, in turn, cause damage[96]. This source of damage is particularly significant for UVA lasers. For these lasers, DNA damage is not limited to DSBs, but also to pyrimidine dimers due to the photochemical effects of UV light[99]. Other lasers, such as NIR lasers can also create photochemical damage in a manner similar to that formed by UV lasers as a result of UV effects created by non-linear multiphoton absorption of laser energy[96].

4. Plasma formation

NIR lasers' irradiances result in the production of plasma, free electrons which can become involved in DNA-damaging reactions. Multiphoton processes and ionization processes can occur as a result of plasma and plasma is thought to trigger thermal, mechanical, and chemical DNA damage.

1.7.2 Laser systems used for inducing DNA DSBs

Microirradiation is generally performed with lasers coupled to confocal microscopes. These lasers vary in wavelength and type and different laser wavelengths can be used to achieve specific types of damage. Thus, when choosing a laser system for a study one must consider the types of damage that a given laser can induce and which DNA repair pathways will be stimulated by this damage. Ideal for our study was a system that could effectively create DSBs while keeping UV-induced damage, which could stimulate other repair pathways, minimal. Highlighted below are three commonly used laser types for microirradiation studies.

1. UVA lasers

UVA lasers can be used to induce DSBs in cells pretreated with photosensitizing compounds such as BrdU, IdU, or Hoechst with or without thymidine analogues[100]. Increasing the laser dose allows DNA damage without use of these compounds[96]. UVA lasers induce damage at a relatively long pulse width and are thought to do so via temperature and chemical changes to DNA. While such lasers have been used in several studies to observe protein recruitment to DSBs, caution must be used in interpreting results obtained with these lasers[101,102]. Because these lasers use UV light, they can form UV-induced DNA damage to a greater extent than other damage-inducing laser systems[96].

2. Green lasers

DNA DSBs can also be induced by nanosecond-green lasers at wavelengths of approximately 535nm. It can be used with pulse widths at the nanosecond or picosecond time range, with less formation of 6-4 photoproducts, products of UV-induced DNA

damage, at the picosecond time range[96]. These lasers are able to induce DNA damage and can be used to visualize factor recruitment to DSBs via two-photon absorption by DNA molecules that cause thermal and chemical DNA alterations.

3. fs Ti: sapphire near infrared lasers

Femtosecond Ti: Sapphire near infrared (NIR) laser systems are able to induce damage to which Ku can be recruited with lower 8-oxoguanine production than UVA laser systems[96]. Prior to damage, cells can be sensitized with the DNA dye Hoechst which is excited by the laser light to stimulate damage.[103] However, the necessity of Hoechst for damage induction is debated and some studies have produced damage in the absence of Hoechst[92]. NIR lasers are thought to induce damage through plasma formation and multiphoton processes. They employ rapid, repetitive, short (50-300fs) pulses of light with a high peak intensity within a targeted region in a cell at relatively low power whereas UV-based lasers require use of higher power that can lead to cytotoxicity[103]. UV-wavelength laser light can be absorbed by cellular components, but NIR lasers avoid this due to their relatively long wavelengths. This system thus creates well-localized damage to the target region in a cell without the confounding effects of damage to other portions of the cell[103]. Live imaging of the recruitment of NHEJ factors has been well-documented and reviewed using the NIR system with a variety of proteins including Ku[92,104]. Due to the many benefits of NIR systems, microirradiation discussed herein was performed using a 750nm NIR laser.

1.7.3 Kinetics of Ku and NHEJ protein recruitment to laser-induced DNA damage

Work by Reynolds *et al*. assessing Ku recruitment to sites of NIR laser-induced damage showed that Ku, XRCC4, and DNA-PK are rapidly recruited to the DSB, with fluorescence at sites of microirradiation peaking within one minute of damage. The amount of Ku localized to breaks declines rapidly within 10-15 minutes until about 30% of damage has been repaired, and then it slowly declines for approximately one hour during what is thought to be repair of more complex damage. XRCC4 fluorescence at sites of damage declines in a similar manner, although slightly slower, as its activity occurs following Ku association with DSBs. DNA-PK declines steadily, without a

differentiation between complex and simple damage evident in its kinetics[104]. γ-H_2AX, a marker of DSBs, also appears rapidly following damage, but its fluorescence peaks after 30 minutes to one hour[103].

1.7.4 Pre-extraction of non-DSB associated Ku

In a recent study, treating irradiated cells with a solution of sucrose, detergent, and RNAse A (CSK+R) was presented as an alternative to microirradiaton[97]. It was argued that Ku associated with chromatin via RNA, so treating cells with the pre-extraction solution prior to immunofluorescence would remove background Ku70 from the nucleus, allowing resolution of Ku foci using 3D structured illumination super-resolution microscopy (SIM). Use of the technique was demonstrated with both X-ray induced DSBs and laser-induced damage and we tested the technique in our study. However, it has not been widely used or replicated.

1.8 Hypothesis and objectives

Previous work in our lab and a yeast study conducted by Ribes-Zamora *et al* implicated helix five of the Ku70 vWA domain in repair[40,61]. However, the molecular mechanisms underlying this role are unclear. Helix five of the Ku70 vWA domain is located on the outer surface of the Ku heterodimer, with D192 and D195 oriented such that their side chains face outward from the protein's surface. Due to the residues' surface position, it has been speculated that they could mediate a protein-protein interaction[40]. Furthermore, von Willebrand A domains are often involved in protein-protein interactions and the Ku80 vWA domain has been implicated in interacting with the NHEJ factors APLF and Wrn[77,78]. Taking this into consideration, it could be possible that Ku70's vWA domain has a similar function.

Helix five of the Ku70 vWA domain could mediate a protein-protein interaction with an NHEJ factor in several ways. One possibility was that the helix could mediate a protein-protein interaction via conserved lysines 182 and 189 within the same helix or recruit a factor that modifies these residues. Recent studies have suggested that lysine modifications such as ubiquitination and neddylation are important for Ku removal from DSBs and ubiquitination of K182 has been reported in a global mass spectrometry

study[43,44,84]. Furthermore, lysine residues in the Ku N-terminus have recently been suggested to be involved in lyase activity to remove abasic sites close to DNA ends[105]. It is therefore plausible that K182 and K189 are involved in Ku function. Alternatively the helix could be involved in Ku self-association, as a recent study has implicated helix five in Ku tetramerization, a process that may occur to bridge DNA ends prior to DNA-PKcs binding after damage[52]. Another possibility is that helix five is involved in interacting with the newly identified NHEJ factor PAXX. PAXX and Ku are thought to interact and while the region of PAXX involved in this interaction has been established, the region of Ku needed for its association with PAXX has yet to be identified[29]. Finally, we also considered the possibility that helix five interacts directly with another NHEJ protein which may or may not have been identified as part of the NHEJ complex in the past.

Overall, we hypothesized that *helix five of the Ku70 vWA domain is involved in a protein-protein interaction and that the D192A/D195R mutation prevents this interaction from occurring*. To address this hypothesis, we investigated the possibilities that: 1. The protein-protein interaction mediated by helix five could be regulated by signaling at conserved K182 and K189 residues within the same helix. 2. The interaction could occur directly between helix five and an NHEJ factor. 3. The helix could mediate Ku tetramerization and 4. The helix could interact with the newly identified NHEJ factor PAXX. Our objectives were to:

1. Test the significance of K182 and K189 in cell survival in response to IR to determine whether these residues play a role in helix five's repair function

2. Using GST pulldowns, test the ability of the Ku N-terminus and specifically helix five to mediate Ku tetramerization and binding to PAXX

3. Identify novel factors that interact with and contribute to the function of helix five using a GST pulldown

4. Optimize laser microirradiation with a 750nm infrared multiphoton laser to assay NHEJ factor recruitment to DNA damage in live cells.

5. Using microirradiation, compare recruitment of known conserved NHEJ factors in WT Ku70 and Ku70 D192A/D195R expressing cells. This could allow us to identify a factor that cannot be recruited in the repair mutant

CHAPTER 2: METHODS

2.1 Chemicals and reagents

Cell Culture Reagents

Trypsin, phosphate buffered saline (PBS), L-glutamine, sodium pyruvate, and Dubecco's modified eagle medium (DMEM) were purchased from Wisent Inc. (St. Bruno, Quebec, Canada). DMEM and PBS were purchased from Gibco by Life Technologies Inc. (Burlington, Ontario, Canada) as well. Puromycin was purchased from BioShop Inc. (Burlington, ON, Canada).

Immunofluorescence reagents

Triton X-100, PIPES, and RNase A were purchased from BioShop Inc. (Burlington, ON, Canada). Sucrose was purchased from ThermoFisher Scientific Inc (Rockford, Illinois, USA). Paraformaldehyde (PFA) and sodium dodecyl sulfate (SDS) were purchased from Wisent Inc. (St. Bruno, Quebec, Canada). Hoechst 33342, Trihydrochloride, Trihydrate and ProLong Gold antifade reagent with DAPI and DAPI-free mounting medium were purchased from Life Technologies, ThermoFisher Scientific Inc (Rockford, Illinois, USA).

In vitro assay reagents

Sodium chloride (NaCl), hydroxymethyl piperazineethanesulfonic acid (HEPES), potassium chloride (KCl), Tris-hydroxymethyl amino methane (Tris), ethylenediaminetetraacetic acid (EDTA), and sodium dodecyl sulfate (SDS) were purchased from Wisent Inc. (St. Bruno, Quebec, Canada). Glycerol was purchased from Caledon Laboratory Chemicals Ltd. (Georgetown, ON, Canada). Dithiothreitol (DTT), pheylmethylsulfonyl fluoride (PMSF), pepstatin, leupeptin, aprotinin, sodium fluoride (NaF), Sodium orthovanadate (Na_3VO_4) and Nonidet P-40 (NP-40) were obtained from BioShop Inc. (Burlington, ON, Canada). Glutathione-agarose beads were acquired from Sigma-Aldrich (Oakville, Ontario, Canada) and Pierce Protein G magnetic beads were acquired from ThermoFisher Scientific Inc. (Rockford, Illinois, USA). Polyvinylidene

fluoride membranes, Bio-Rad Protein Assay Dye Reagent Concentrate (used for Bradford Assays) and Clarity Western ECL substrate were purchased from Bio-Rad (Mississauga, Ontario, Canada). Crystal violet was purchased from Sigma-Aldrich (Oakville, Ontario, Canada).

Cloning and bacterial work reagents

Restriction enzymes were purchased from New England Biolabs Inc. (Ipswich, Massachusetts, USA) and Fermentas Thermo Fisher Inc. (Waltham, Massachusetts, USA). KOD hot start DNA Polymerase was purchased from EMD Millipore Corporation (Billerica, Massachusetts, USA). Primers were purchased from Integrated DNA Technologies Inc. (Coralville, Iowa, USA), UWO Oligo Factory (London, Ontario, Canada) and Sigma-Aldrich (Oakville, Ontario, Canada). Isopropyl β-D-1-thiogalactopyranoside (IPTG) was purchased from BioShop Inc. (Burlington, ON, Canada).

2.2 Antibodies

Primary Antibodies

Ku70 (N3H10) and GST (B-14) antibodies were purchased from Santa Cruz Biotechniology Inc. (Santa Cruz, California, USA). The GFP antibody (A6455) was purchased from Life Technologies, ThermoFisher Scientific Inc (Rockford, Illinois, USA). The rabbit phosphoserine 139 H_2AX (20E3) antibody was purchased from Cell Signalling (Beverly, Massachusetts, USA). Mouse HA (H9658) and Mouse Anti-polyHistidine (H1029) antibodies were purchased from Sigma-Aldrich (Oakville, Ontario, Canada). Mouse phosphoserine 139 H_2AX (953) was purchased from Abcam Inc. (Cambridge, Massachusetts, USA). Table 2-1 summarizes primary antibody dilutions used in this work.

Table 2-1: Summary of primary antibodies used herein. Primary antibodies used for experiments are indicated along with the dilution at which they were used and the applications that they were used for.

Antibody	Species	Application	Dilution
Ku70 (N3H10)	Mouse	Western Blot	1:200-1:500
Ku70 (N3H10)	Mouse	Immunofluorescence	1:100
GST (B-14)	Mouse	Western Blot	1:500
GFP (A6455)	Rabbit	Western Blot	1:100000
Phosphoserine 139 H_2AX (20E3)	Rabbit	Immunofluorescence	1:1000
Phosphoserine 139 H_2AX (953)	Mouse	Immunofluorescence	1:1000
PolyHistidine, Clone HIS-1 (H1029)	Mouse	Western Blot	1:5000

Secondary Antibodies

For Western blot analyses, secondary antibodies used were Peroxidase-conjugated AffiniPure Goat anti-Mouse IgG (H+L) (Jackson ImmunoResearch Laboratories Inc., West Grove, Pennsylvania, USA) and Blotting Grade Goat anti-Rabbit IgG (H+L) (Human IgG Adsorbed) Horseradish Peroxidase Conjugate (Bio-Rad Laboratories Inc., Mississauga, Ontario, Canada). These were used at a 1:5000 dilution. For immunofluorescence, anti-mouse 488, anti-mouse 647, anti-rabbit 488, or anti rabbit 647 Alexa antibodies (ThermoFisher Scientifc Inc., Rockford, Illinois USA) were used at a 1:1000 dilution.

2.3 Cloning and plasmids

Restriction enzymes were used as directed in the manufacturers' protocols. To generate Ku70 K182R/K189R in pMSCV Puro, a Ku70 K182R substitution was introduced to wild-type Ku70 in pEGFP-C1 using the KOD hot start DNA Polymerase (EMD Millipore Corporation, Billerica, Massetuches, USA) in accordance with the manufacturer's protocol with forward (**5'**CAATGACAGTGCCAGAGCCAGCCGGG**3'**) and reverse primers (**5'**CCCGGCTGGCTCTGGCACTGTCATTG**3'**). A K189R substitution was then introduced to the same DNA with KOD hot start DNA polymerase and forward (**5'**GGCCAGGACCAGAGCCGGTGATCTC**3'**) and reverse (**5'**GAGATCACCGGCTCT GGTCCTGGCC**3'**) primers. The pMSCV-Puro vector containing wild-type Ku70 was cut with XhoI and PsiI, removing the Ku N-terminus from the vector. It was then replaced by Ku70 K182R/K189R isolated from pEGFP-C1 with the same enzymes. Ku70 (1-219) was isolated from pEGFP-C1 using BamHI and EcoRV and then introduced to the BamHI and SmaI sites of pGEX-4T-1 to generate Ku70 (1-219) in pGEX-4T-1. Ku70 D192A/D195R (1-219) in pGEX-4T-1 was generated from this plasmid using site-directed mutagenesis with the forward primer **5'**CCAAAGCCGGTGCTCTCCGACGTA CAGGCATCTTCC**3'** and the reverse primer **5'**GGAAGATGCCTGTACGTCGGAGAG CACCGGCTTTGG**3'**. GST-Ku70 (1-252) and GST-Ku70 D192A/D195R (1-252) in pGEX-4T-1 were generated through PCR amplification of residues 1-252 of Ku70 in pEGFP-C1 or Ku70 D192A/D195R in pEGFP-C1. The forward primer (**5'**CGAATTCTGCAGTCGACGGTAC**3'**) included the BamHI site in pEGFP-C1 and

reverse primer (**5'**GCTTATCTCGAGTTACCTGGTCTCCTTGGCGCGAA**3'**) was designed to introduce a stop codon at residue 252 followed by a XhoI site. The amplified region was digested with BamHI and XhoI and ligated into BamHI and XhoI-digested pGEX-4T-1. Sequences of these plasmids were verified by DNA sequencing at the London Regional Genomics Center, (London, Ontario, Canada).

Wild-type Ku70, Ku D192A/D195R, Ku70 K182A, and Ku70 K189A in pMSCV were generated in our lab by Victoria Fell and Jorge Georgakopoulous. GFP-XRCC4 was obtained from A. Yasui (Institute of Development, Aging and Cancer, Tohoku University, Sendai Japan). Parp1-GFP was obtained from M. J. Hendzel (Department of Oncology, University of Alberta, Edmonton, Alberta, Canada). EGFP-Ku80 and EGFP-DNA Ligase IV were obtained from D. van Gent (Department of Genetics, Erasmus MC, Rotterdam, the Netherlands). GFP-NPM1 was received from P. Hordjik (Sanquin Blood Supply, Department of Molecular Cell Biology, Amsterdam, the Netherlands). YFP-XLF was obtained from D. Chen (Department of Radiation Oncology, UT Southwestern Medical Center, Dallas Texas). His-PAXX was provided by M. Junop (Department of Biochemistry, Western University, London, Ontario, Canada) in collaboration with M. Modesti (Centre de Recherche en Cancérologie de Marseille, Marseille, France). GFP-Aurora B was provided by G. Pfeifer (Beckman Research Institute, City of Hope, Duarte California).

Sequences of plasmids cloned in our lab and the plasmids containing GFP-DNA ligase IV and EGFP-Aurora B respectively were verified by DNA sequencing at the London Regional Genomics Center, (London, Ontario, Canada). For other GFP-repair protein containing plasmids received from collaborators, protein identity was confirmed by Western blotting with a GFP antibody that also recognizes YFP (see Appendix A, Figure A-1).

2.4 Cell culture and treatments

All cell lines used were cultured at 37°C in 5% CO_2 in Dulbecco's modified Eagle's Medium (DMEM) supplemented with 10% fetal bovine serum, 1% sodium pyruvate and

1% glutamine. Cell lines expressing Ku70 via retroviral infection were maintained in media supplemented with 2.5μg/mL puromycin.

A Faxitron RX-650 X-ray cabinet (Faxitron X-ray LLC, Lincolnshire, IL, USA) was used for X-ray irradiation treatments. The machine's dose rate was 1.42 Gy per minute.

Transfections were conducted with JetPrime transfection reagent (PolyPlus Transfection, Illkrich, France) according to the manufacturer's protocol. To encourage uniform transfection in microirradiation experiments, the vector pBS-SK (Agilent Technologies, Santa Clara, CA, USA) was transfected along with DNA used for experiments with a 1:3 ratio of pBS-SK DNA to experimental DNA. pBS-SK was not used with GFP-Ku80.

2.5 Retroviral infection to generate stable cell lines

Phoenix Ampho retroviral packaging cells were transfected with 8-10μg of pMSCV Puro vector alone or containing the various mutated forms of Ku discussed herein using calcium phosphate transfection with 0.13M $CalCl_2$ in HBS (140mM NaCl, 0.75mM Na_2HPO_4, 6mM Dextrose, 5mM KCl, 25mM HEPES pH 7.4). Viral medium was harvested 48 hours after transfection, filtered with a 0.45μm filter, and used to infect Ku70 knockout MEFs obtained from S. Matsuyama (Case Western, Cleaveland USA). Cells infected with pMSCV Puro were selected in media supplemented with 2.5μg/mL puromycin. Expression of retrovirally-introduced proteins was confirmed by Western blotting (see Appendix A, Figure A-2).

2.6 Clonogenic cell survival assays

Ku70 knockout MEFs expressing wild-type Ku70, Ku70 K182A, Ku70 K189A, Ku70 K182R/K189R, or the pMSCV empty vector respectively were seeded to single-cell density on 6cm plates (approximately 1000-3000 cells per plate). When cells had adhered to the plate, they were treated with 0, 2, 4, 6, or 10 Gy of IR (see 2.5). Six to nine days after irradiation (when colonies had grown), cells were fixed and stained with 0.5% crystal violet in 20% methanol. Colonies were counted manually. Plates were seeded, treated, and fixed in triplicate such that three sets of colonies were counted per IR dose for each experiment.

2.7 Extracts

2.7.1 Nuclear extracts

Nuclear extracts were prepared as previously described[106]. Briefly, cells were lysed in Buffer A (10mM Hepes pH 7.9, 1.5mM $MgCl_2$, 10mM KCl, 0.5mM DTT, 0.2mM PMSF, and 0.2% NP-40). Nuclei were then pelleted and lysed in Buffer C (20mM Hepes pH 7.9, 25% glycerol, 450mM NaCl, 1.5mM $MgCl_2$, 0.2mM EDTA, 0.5mM DTT, 0.2mM PMSF supplemented with 2µg/mL leupeptin, 1µg/mL pepstatin, 10µg/mL aprotonin, 1mM NaF, and 1mM Na_3VO_4). Lysed nuclei were centrifuged and the recovered supernatant served as a nuclear extract for experimental purposes. Nuclear extracts were quantified using a Bradford assay.

2.7.2 Bacterial protein expression and extracts

For bacterial protein expression, constructs were transformed into *E. coli* BL21DE3. Transformants were grown in Luria Bertani (LB) medium for 16 hours and then diluted 1:100 in fresh LB. Depending on the construct and the protein's tendency to precipitate in bacterial extracts, cells were grown to an appropriate OD_{600} and then induced with IPTG in amounts that, again, varied with the construct. Table 2-2 summarizes that OD_{600} for induction, the concentration of IPTG used for induction, the induction temperature, and the duration of induction for each construct used in this thesis.

Following induction, cells were centrifuged at 4000rpm for 20 minutes at 4°C and then suspended in 1mL of Lysis buffer (10mM KCl, 25mM HEPES pH 7.4, 2mM EDTA, 20% glycerol, and 0.1% NP-40 with 10 µg/mL aprotinin, 2µg/mL leupeptin, 2.5µg/mL pepstatin, 1mM DTT, 2mM NaF, 2mM Na_3VO_4, and 0.1mM PMSF) for every 50mL of culture volume prior to centrifugation. They were then sonicated up to six times on ice, until the suspension became translucent, for five seconds using a Sonic Dismembrator Model 100 (ThermoFisher Scientifc Inc., Rockford, Illinois USA). To remove cellular debris, the sonicated samples were centrifuged at 13000rpm for 10 minutes at 4 degrees Celsius. Supernatant extracts were then collected and stored at -80 degrees Celsius prior to experimental use. Expression of each protein was assessed by Western blotting with a GST antibody for GST and GST-tagged proteins and a His tag for His-PAXX.

Table 2-2: Conditions for bacterial protein expression. Conditions for expression of proteins isolated from bacterial extracts for this work are outlined.

Protein	OD at Induction	[IPTG] for Induction	Induction Temperature (degrees Celsius)	Duration of Induction
GST	0.3-0.4	0.1mM	37	2h
GST-Ku70 (1-219)	0.3-0.4	0.05mM	23	4h
GST-Ku70 D192A/D195R (1-219)	0.3-0.4	0.05mM	23	4h
GST-Ku70 (1-252)	0.3-0.4	0.1mM	23	4h
GST-Ku70 D192A/D195R (1-252)	0.3-0.4	0.1mM	23	4h
His-PAXX	0.3-0.4	1mM	37	4h

2.8 Binding GST-tagged proteins to glutathione-agarose beads

Glutathione-Agarose beads were washed three times with binding buffer (15mM HEPES pH 7.4, 6mM KCl, 1.2mM EDTA, and 12% glycerol) supplemented with 0.1% NP-40 with 10 μg/mL aprotinin, 2μg/mL leupeptin, 2.5μg/mL pepstatin, 1mM DTT, 2mM NaF, 2mM Na_3VO_4, and 0.1mM PMSF. Bacterial extracts containing GST-tagged proteins in binding buffer (15mM HEPES pH 7.4, 6mM KCl, 1.2mM EDTA, and 12% glycerol) supplemented with 0.1% NP-40 with 10 μg/mL aprotinin, 2μg/mL leupeptin, 2.5μg/mL pepstatin, 1mM DTT, 2mM NaF, 2mM Na_3VO_4, and 0.1mM PMSF were then added to the beads and rotated for two hours at 4°C. Following rotation, the beads were washed three times in binding buffer and a small fraction of the beads was subjected to SDS-PAGE and staining with Coomassie Blue stain (0.25% Coomassie Blue R-250, 50% methanol, 10% Glacial Acetic Acid, 40% H_2O) in parallel with 200ng, 500ng, or 1μg of BSA. Densitometry was performed with reference to BSA with Image Lab Software (Bio-Rad, Mississauga, Ontario, Canada) to calculate the approximate amount of GST-tagged protein present per microliter of glutathione-agarose beads.

2.8.1 GST pulldowns

GST pulldown for Ku tetramerization with HeLa extracts

GST, GST-Ku70 (1-219), and GST-Ku70 D192A/D195R (1-219) respectively were bound to glutathione-agarose beads and protein bound to the beads was quantified (see 2.11.1). HeLa cells were treated with 10Gy of IR and incubated for 30 minutes at 37°C. Nuclear extracts were then harvested. 1.25μg of each GST-tagged protein bound to beads was then incubated with 750μg of the nuclear extracts in Nuclear Extract Pulldown Buffer (20mM Hepes pH 7.9, 1.5mM $MgCl_2$, 0.2mM EDTA, 112.5mM NaCl, and 6.25% glycerol supplemented with 0.5mM DTT, 0.2mM PMSF, 2μg/mL leupeptin, 1μg/mL pepstatin, 10μg/mL aprotonin, 1mM NaF, and 1mM Na_3VO_4). Beads were then washed three times with binding buffer (15mM HEPES pH 7.4, 6mM KCl, 1.2mM EDTA, and 12% glycerol) and analyzed by SDS-PAGE followed by Western blotting for GST and Ku70.

Ku70 N-terminus-NPM1 GST pulldown

HeLa cells were grown on 10cm plates to 60-80% confluence and then transfected with 2.25µg of GFP-NPM1 DNA and 0.75µg of PBS-SK plasmid carrier DNA. Twenty-four hours later, nuclear extracts were isolated from transfected cells. GST, GST-Ku70 (1-252), and GST-Ku70 D192A/D195R (1-252) respectively were bound to glutathione-agarose beads and protein bound to the beads was quantified (see 2.11.1). 200µg of HeLa extract in Nuclear Extract Pulldown Buffer (20mM Hepes pH 7.9, 1.5mM $MgCl_2$, 0.2mM EDTA, 112.5mM NaCl, and 6.25% glycerol) supplemented with 0.5mM DTT, 0.2mM PMSF, 2µg/mL leupeptin, 1µg/mL pepstatin, 10µg/mL aprotonin, 1mM NaF, and 1mM Na_3VO_4 was pre-cleared with glutathione-agarose beads and then rotated with 1 µg of glutathione-agarose-bound GST peptides and the molecular equivalent of GST for two hours at 4°C. Beads were then washed three times with binding buffer (15mM HEPES pH 7.4, 6mM KCl, 1.2mM EDTA, and 12% glycerol) and analyzed by SDS-PAGE followed by Western blotting for GST and GFP.

GST pulldown for Ku tetramerization with MEF extracts

GST, GST-Ku70 (1-252), and GST-Ku70 D192A/D195R (1-252) respectively were bound to glutathione-agarose beads and protein bound to the beads was quantified (see 2.11.1). Nuclear extracts were isolated from Ku70 knockout MEFs expressing wild-type Ku70 or Ku70 D192A/D195R. 1µg of each GST-tagged protein and the molecular equivalent of GST was bound to beads was then incubated with 250µg of the nuclear extract in Nuclear Extract Pulldown Buffer (20mM Hepes pH 7.9, 1.5mM $MgCl_2$, 0.2mM EDTA, 112.5mM NaCl, and 6.25% glycerol) supplemented with 0.5mM DTT, 0.2mM PMSF, 2µg/mL leupeptin, 1µg/mL pepstatin, 10µg/mL aprotonin, 1mM NaF, and 1mM Na_3VO_4. Beads were then washed three times with binding buffer (15mM HEPES pH 7.4, 6mM KCl, 1.2mM EDTA, and 12% glycerol) and analyzed by SDS-PAGE followed by Western blotting for GST and Ku70.

GST pulldown assessing the Ku-PAXX interaction

GST, GST-Ku70 (1-219), and GST-Ku70 D192A/D195R (1-219) respectively were bound to glutathione-agarose beads and protein bound to the beads was quantified (see 2.11.1). Bacterially expressed His-PAXX was quantified from bacterial extracts through comparison with known amounts of BSA using densitometry. 1µg His-PAXX was diluted to 15mM HEPES pH 7.4, 6mM KCl, 1.2mM EDTA, and 12% glycerol and supplemented with 0.1% NP-40 with 10 µg/mL aprotinin, 2µg/mL leupeptin, 2.5µg/mL pepstatin, 1mM DTT, 2mM NaF, 2mM Na_3VO_4, and 0.1mM PMSF and then combined with 1µg GST-Ku70 (1-252), GST-Ku70 D192A/D195R (1-252), or the molecular equivalent of GST bound to glutathione-agarose beads. The mixture was rotated for two hours at 4°C and then washed with binding buffer (15mM HEPES pH 7.4, 6mM KCl, 1.2mM EDTA, and 12% glycerol). This was followed by analysis by SDS-PAGE and Western blotting for GST and His tags.

Large-scale GST pulldown

17.5µg of GST, GST-Ku70 (1-219), and GST Ku70 D192A/D195R (1-252) bound to glutathione-agarose beads was quantified (see 2.11.1) and added to 4mg of nuclear extracts from Ku70 knockout MEFs expressing wild-type Ku70 that had been irradiated with 10 Gy IR and then incubated at 37 degrees for 30 minutes. The mixture was incubated for two hours at 4°C in 20mM Hepes pH 7.9, 1.5mM $MgCl_2$, 0.2mM EDTA, 112.5mM NaCl, and 25% glycerol and then washed in binding buffer (15mM HEPES pH 7.4, 6mM KCl, 1.2mM EDTA, and 12% glycerol). Results were analyzed by SDS-PAGE followed by silver staining. Proteins of interest were then identified by Maldi-TOF/TOF mass spectrometry at the London Regional Proteomics Center (London, ON) with an AB Sciex 5800 TOF/TOF System, (Sciex, Framingham, MA, USA).

2.9 Immunoprecipitation and binding of Ku to His-PAXX

HeLa nuclear extracts in IP buffer (20mM HEPES pH 7.9, 150mM NaCl, and 10% glycerol supplemented with 0.5mM DTT, 0.5% Trition X-100, 0.2mM PMSF, 2µg/mL leupeptin, 1µg/mL pepstatin, 10µg/mL aprotonin, 1mM NaF, and 1mM Na_3VO_4) were

pre-cleared with Pierce Protein G magnetic beads. 200µg of extract was incubated with 2µg of a mouse anti-Ku70 antibody overnight and 200µg of extract was incubated with 2µg mouse IgG in parallel, as a control. The incubated mixtures were then bound to Pierce Protein G magnetic beads for thirty minutes. Beads were washed with IP buffer and then incubated for two hours with 1mg of bacterial extract containing His-PAXX diluted in IP buffer supplemented with 0.5% NP-40, 0.5% Triton X-100, 10 µg/mL aprotinin, 2µg/mL leupeptin, 2.5µg/mL pepstatin, 1mM DTT, 2mM NaF, 2mM Na_3VO_4, and 0.1mM PMSF for two hours at 4°C. Beads were washed three times in IP buffer and results were analyzed by Western blotting.

2.10 Western blotting

For Western blot experiments, proteins were subjected to SDS-PAGE on 8-12.5% polyacrylamide gels, depending on protein size and desired resolution of proteins. They were then transferred to polyvinylidine difluoride (PVDF) membranes, blocked in 5% milk in TBS-T, and hybridized with appropriate antibodies overnight at 4°C Celsius of for one hour at room temperature, depending on antibody hybridization efficiency. Membranes were then washed in PBS, hybridized with secondary antibody for one hour at room temperature, washed, and developed using the Clarity Western ECL substrate. A Molecular Imager ChemiDoc TM XRS system (Bio-Rad, Mississauga, Ontario, Canada) was used to image the blots.

2.11 Immunofluorescence

Cells were grown on 22 by 22mm 1.5 thickness coverslips in 6-well plates. Following experimental treatments (for example, IR), they were washed three times in phosphate buffered saline (PBS) and then fixed with 4% paraformaldehyde for 10-15 minutes at 4°C. Again, cells were washed in PBS, permeablized in 0.5% Triton X-100, then washed. Samples were blocked in 5% fetal bovine serum (FBS) for at least one hour and then incubated overnight with primary antibodies at dilutions given in Table 2-1. Hybridized samples were washed with PBS and hybridized with Alexa secondary antibodies, followed by mounting to slides with ProLong Gold Antifaide 4′,6′-diamidino-2-phenylindole (DAPI)-containing mounting medium. For microirradiation experiments

involving immunofluorescence, DAPI-free medium was used for mounting as microirradiated nuclei contained Hoechst 33342, which acts as a nuclear stain as well as a sensitizing agent for microirradiation.

For analysis of samples where CSK+R pre-extraction was performed, cells were treated with 10 Gy of IR, incubated for five minutes at room temperature, and then washed three times with PBS. They were then treated with CSK+R (10mM Pipes pH 7.0, 100mM NaCl, 300mM sucrose, 3mM $MgCl_2$, 0.7% Triton X-100, and 0.3mg/mL RNase A) twice for three minutes[97]. They were then washed three times and fixed in 2% PFA in CSK (10mM Pipes pH 7.0, 100mM NaCl, 300mM sucrose, and 3mM $MgCl_2$). This was followed by permeablization in 0.2% Triton X-100 in PBS for five minutes at room temperature, blocking with 5% FBS, and hybridization with antibodies as described in the previous paragraph.

2.12 Microscopy

2.12.1 Confocal microscopy

Confocal images were acquired with a Zeiss Axiovert 200 Motorized LSM 510 META NLO confocal microscope with AIM 4.2 software (Zeiss, Oberkochen, Germany) for microirradiation and a Zeiss LSM 510 META microscope with the Zen software (Zeiss, Oberkochen, Germany) for foci experiments. Images for microirradiation were acquired with a 488nm Argon laser (Zeiss, Oberkochen, Germany) with a 505nm long-pass filter. Images for foci experiments were obtained using a 405nm Diode laser (Lasos, Jena, Germany) with a BP 420-480 filter, a 488nm Argon laser (Zeiss, Oberkochen, Germany) with a BP 505-530 filter, and a 633nm HeNe2 laser (Lasos, Gena, Germany) with an LP 650 filter.

2.12.2 Fluorescence microscopy

Fluorescence microscopy images were acquired with an Olympus BX51 microscope (Olympus Corporation, Tokyo, Japan) at 40X magnification with Image-Pro Plus software (Media Cybernetics, Rockville, Maryland, USA).

2.13 Laser microirradiation

Cells were grown to 60-80% confluence on 22mm by 22mm 1.5 thickness coverslips in a six-well plate and transfected with plasmids containing each fluorescently-tagged repair protein. Twenty-four hours after transfection, cells were sensitized with 1μg/mL Hoechst 33342. Microirradiation was conducted in a magnetic chamber (Chamlide, Seoul, South Korea) containing 1mL of media and set on a 37°C heated stage (Zeiss, Jena, Germany) on a with a Zeiss Axiovert 200 Motorized LSM 510 META NLO confocal microscope with a 63X Plan-Apochromat oil objective. (A 40X C-Apochromat W objective was used during optimization, but the 63X objective was later employed for NHEJ factor recruitment experiments because it allowed improved resolution and visualization of factors that were recruited at low levels).

For live imaging experiments nuclei were microirradiated with a 750nm titanium-sapphire laser (Coherent, Santa Clara, California, USA) with 20% power and 20 iterations. Imaging zoom was set to 2.9 such that 10 pixels in a 1024 X 1024 pixel image corresponded to 0.5μm. This allowed use of consistent parameters when defining a region to be damaged. For experiments with GFP-tagged proteins, damage was induced in 0.5 X 24μm rectangles across target nuclei. The same rectangle size was used for every nucleus treated as this kept damage time consistent from cell to cell and ensured that imaging of protein recruitment to laser tracks began at the same time point following damage. For γ-H_2AX immunofluorescence experiments, it was important to damage as many cells as possible and multiple 0.5μm-wide rectangles were defined across the length of the entire field of view and then microirradiated under the same conditions described above. Within 10 minutes of microirradiation, the treated cells were subjected to immunofluorescence staining for γ-H_2AX and imaged with fluorescence microscopy.

2.14 Construction of X-Ray irradiation standard curve and calculation of DSB equivalence of microirradiation

Ku70 knockout MEFs expressing wild-type Ku70 were irradiated with 0, 2, 4, 6, or 10 Gy of IR, immunostained for γ-H_2AX, and imaged with fluorescence microscopy. Corrected total nuclear fluorescence of γ-H_2AX in cells treated with each IR dose was

then computed in the same manner as corrected total cell fluorescence, which has been described previously, but with only nuclear fluorescence measured using ImageJ software (ImageJ, U. S. National Institutes of Health, Bethesda, Maryland, USA)[107]. To account for non-specific primary antibody background, corrected total nuclear fluorescence at 0 Gy was subtracted from the fluorescence value at each IR dose. The corrected values were plotted (see Figure 3-10 in Results) and an equation for the linear relationship between γ-H_2AX fluorescence and IR dose was determined:

$$y = 321282x + 446147 \quad (1)$$

Where y is the corrected total nuclear γ-H_2AX fluorescence and x is the IR dose in Gy.

Corrected total nuclear fluorescence of three microirradiated cells fixed and immunostained for γ-H_2AX within 10 minutes of microirradiation was measured and averaged. Only cells containing one laser "line" of damage were considered in this calculation. Again, the average corrected total nuclear fluorescence of 20 non-microirradiated cells in the same field of view was subtracted from the average corrected total nuclear fluorescence of the microirradiated cells to account for antibody background. The normalized corrected total nuclear fluorescence value was substituted into Equation 1 to calculate the gray equivalence of damage.

2.15 Statistical analyses

Graphed data are represented by the mean of all experimental n's with error bars representing the standard error of the mean (SEM). Graphs with error bars were generated using Microsoft Excel for Mac Version 14.2.0 (Microsoft Corporation, USA) and GraphPad Prism software (GraphPad Software Inc., La Jolla, California USA). One-way analysis of variance (ANOVA) and post-hoc Tukey HSD (Honest Significant Differences) analyses were conducted with SPSS software (IBM, USA).

CHAPTER 3: RESULTS

3.1 Integrity of K182 and K189 within helix five of the Ku70 vWA domain is not necessary for cell survival after IR

K182 and K189 within helix five of the Ku70 vWA domain display high conservation in mammals and a mass spectrometry study has implicated K182 as a ubiquitination target[84]. Additionally, there is evidence that Ku function is regulated by lysine modification[43,85]. This led us to believe that these residues may contribute to the function of helix five in NHEJ. To evaluate the roles of K182 and K189 in NHEJ, we first introduced Ku70 K182A and K189A mutant Ku70 in Ku70 knockout MEFs using a pMSCV retroviral method used previously to characterize the D192A/D195R mutant's repair defect[61]. This yielded Ku70 knockout cells re-expressing retrovirally-introduced Ku70. Therefore, there was no endogenous Ku70 background present in this system and we could study the effects of the K182 and K189 mutations without interference from endogenous wild-type Ku70. Cells were irradiated and subjected to clonogenic survival assays alongside wild-type and empty retroviral vector controls to determine survival at various IR doses. Comparison of survival curves for wild-type, mutant, and Ku-deficient cells by one-way analysis of variance (ANOVA) indicated that the survival of K182A and K189A mutants was not significantly different ($p>0.05$) than that of wild-type at each IR dose (Figure 3-1). Conversely, Ku-deficient cells displayed impaired survival as compared to cells expressing wild-type and mutant forms of the protein and this was significant at each IR dose ($p<0.031$). An exception was at 10Gy, when the K189A mutant's survival was not significantly different than that of Ku-deficient cells ($p<0.044$) but was significantly different than the survival of the wild-type and other mutant cell lines ($p>0.05$). However, this could be attributed to low amounts of colonies present after 10Gy of irradiation, which was the highest IR dose used in this assay. The D192A/D195R mutant's survival had been similar to that of Ku-deficient cells in previous work[61]. Clearly, the K182A and K189A substitutions did not confer the same profound effect on cell survival as the D192/D195R mutation.

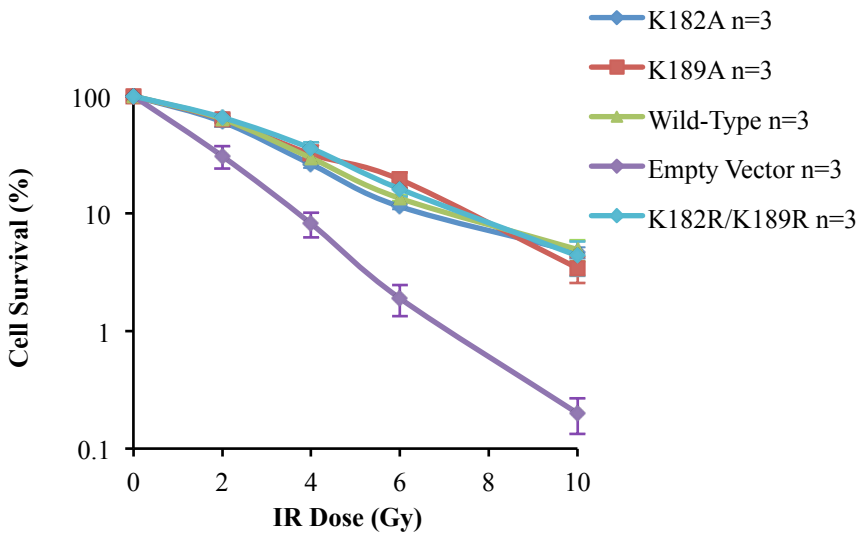

Figure 3-1: Mutation of K182 and K189 of helix five of the Ku70 vWA domain does not impact cell survival in response to IR. Ku70 knockout MEFs stably expressing wild-type Ku70, Ku70 K182A, Ku70 K189A, Ku70 K182R/K189R, or the empty pMSCV Puro vector were subjected to clonogenic cell survival assays. Cell survival is plotted as a function of IR dose. Data is plotted with a logarithmic scale with error bars representing the standard error of the mean (SEM). Experiments were performed in triplicate with n=3. One-way analysis of variance (ANOVA) analysis and post-hoc Tukey HSD (Honest Significant Differences) was used to identify differences between wild-type Ku70, Ku70 K182A, Ku70 K189A, Ku70 K182R/K189R, and pMSCV Puro expressing cells' survival at each IR dose.

As K182 and K189 are close together, we considered the possibility that the two residues could have an interchangeable role in helix five's function (ie. if one lysine were mutated, the other could take its place in acting to mediate the helix's function). We therefore repeated experiments with a Ku70 K182R/K189R double mutant in which both residues were substituted. Again, mutation of the lysines in helix five did not impair cell survival in response to IR and mutant cell survival did not significantly differ from wild-type ($p>0.05$) while survival of Ku-deficient cells was significantly lower than that of the mutant ($p>0.044$). These results suggest that K182 and K189 in helix five, alone or together, do not affect sensitivity to radiation and overall this implied that helix five's repair function is independent of K182 and K189.

3.2 Helix five of the Ku70 vWA domain alone is not sufficient for Ku tetramerization in a GST pulldown system

Some evidence has suggested that helix five of the Ku70 vWA domain allows Ku tetramerization and that this could bridge the DNA ends in NHEJ[52]. To evaluate the ability of helix five to mediate Ku tetramerization, we conducted two experiments using a GST pulldown system. We began by comparing the ability of Ku70 from irradiated and non-irradiated HeLa cell extracts to bind GST-tagged Ku70 (1-219) and GST-Ku70 D192A/D195R (1-219) using a GST pulldown. This region comprises the majority of the Ku N-terminus. The pulldown was analyzed by SDS-PAGE followed by Western blotting for Ku70 and GST. Minimal association occurred between the GST-tagged Ku N-termini and HeLa Ku70, regardless of whether cells had been irradiated and whether the D192A/D195R mutation was present (Figure 3-2A). Although Ku signal could be observed under high exposures on the Western blot, levels were much lower than in a 0.05% HeLa nuclear extract input control, suggesting that this interaction was non-specific and that Ku70 could not bind the GST-tagged Ku70 N-termini.

We performed a similar experiment to determine whether Ku tetramerization would occur with nuclear Ku from Ku70 knockout MEFs expressing wild-type Ku70 or Ku70 D192A/D195R. The ability of wild-type Ku70 from nuclear extracts to bind to the wild-type Ku N-terminus was assessed, as was the ability of Ku70 D192A/D195R from nuclear extracts to bind the D192A/D195R mutant N-terminus. For these experiments, a

GST-Ku70 N-terminus peptide, which contained the entire N-terminus (1-252), was generated to decrease the likelihood that our negative results arose form misfolding of the Ku N-terminus. Again, we did not observe evidence of nuclear extract Ku binding to bacterially-expressed GST-Ku70 (1-252), despite clear presence of Ku in 5% inputs (Figure 3-2B). These results indicate that the Ku N-terminus peptides alone were not sufficient for Ku tetramerization, regardless of whether helix five was mutated.

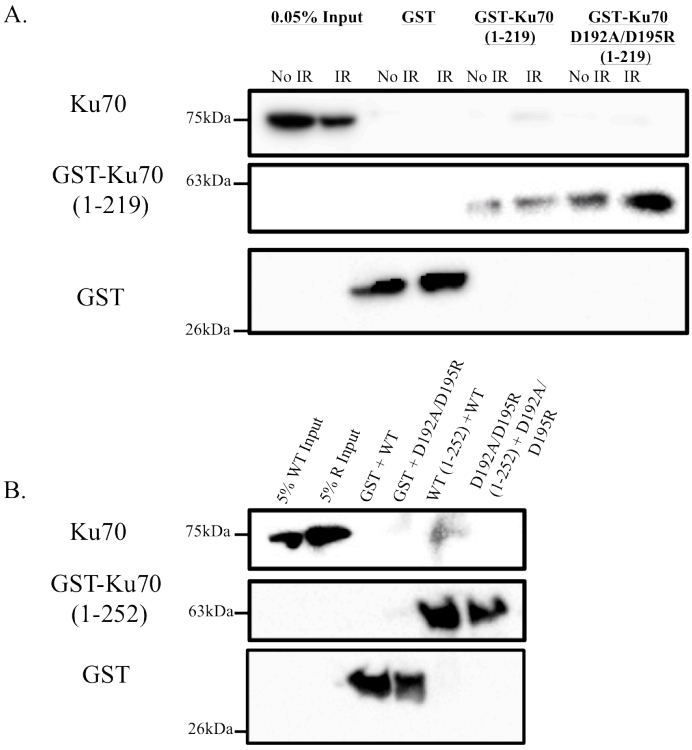

Figure 3-2: Helix five of the Ku70 vWA domain alone is not sufficient for Ku tetramerization. A.) GST, GST-Ku70 (1-219), and GST-Ku70 D192A/D195R (1-219) were bound to glutathione-agarose beads. The bead-bound GST and GST-tagged peptides were then incubated with irradiated (IR) or non-irradiated (no IR) HeLa cell extracts. The ability of full-length Ku from the HeLa extracts to bind to each GST peptide was assayed by SDS-PAGE and Western blotting with Ku70 and GST antibodies. The Ku70 antibody does not recognize the GST-tagged Ku N-terminus, so Ku70 signal corresponds to full-length nuclear Ku70 from HeLa extracts. Representative experiment is shown, n=3. **B.)** GST, GST-Ku70 (1-252), and GST-Ku70 D192A/D195R (1-252) were bound to glutathione-agarose beads and incubated with nuclear extracts from Ku70 knockout MEFs stably expressing wild-type Ku70 (GST+WT and WT (1-252)+WT) or nuclear extracts from Ku70 knockout MEFS stably expressing Ku70 D192A/D195R (GST+D192A/D195R) and (D192A/D195R (1-252)+D192A/D195R). Ability of full-length Ku from the nuclear extracts to associate with the GST-tagged Ku peptides was analyzed with SDS-PAGE and Western Blotting for Ku70 and GST. Representative experiment is shown, n=3.

3.3 Assessment of PAXX's interaction with the Ku70 vWA domain

The recently identified NHEJ factor PAXX has been shown to interact with Ku[29], but the region of Ku70 required for this interaction has yet to be identified. We tested the possibility that the PAXX-Ku interaction is mediated by helix five of the Ku70 vWA domain. Bacterially expressed, His-tagged, PAXX was subjected to a GST pulldown with GST-tagged Ku70 (1-252) and Ku70 D192A/D195R (1-252). Results were analyzed with SDS-PAGE followed by Western blotting. These analyses did not present evidence of interaction between PAXX and the Ku70 N-terminus, as His-PAXX was not pulled down with the Ku70 N-terminus regardless of whether D192 and D195 were mutated (Figure 3-3). This suggests that if involved at all, the Ku70 N-terminus is not sufficient for the Ku-PAXX interaction.

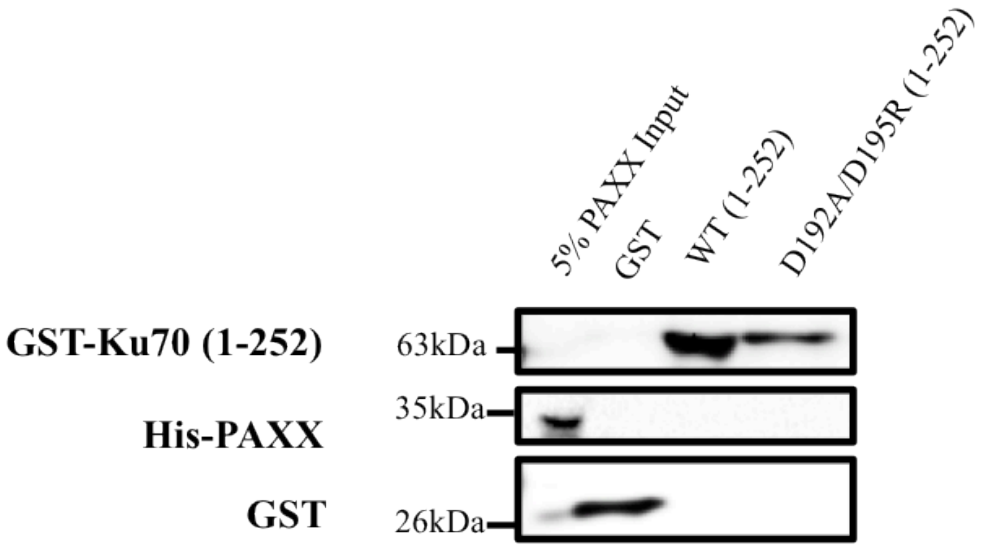

Figure 3-3: The Ku70 N-terminus is not sufficient for binding PAXX. GST, GST-Ku70 (1-252), and GST-Ku70 D192A/D195R (1-252) bound to glutathione-agarose beads and incubated with bacterial extracts from cells expressing His-PAXX. Western blot analysis with antibodies for GST and a His tag was used to evaluate the ability of bacterially expressed PAXX to interact with the GST-tagged Ku peptides or with a GST control. Representative image is shown, n=3.

To confirm that the bacterially expressed PAXX used herein could bind to Ku, we immunoprecipitated Ku from HeLa cells and incubated the immunoprecipitated Ku with bacterial extracts containing His-PAXX (Figure 3-4). Indeed, His-PAXX bound Ku, supporting the idea that while Ku can interact with PAXX, a region of Ku beyond the Ku70 vWA domain is needed for this interaction to occur.

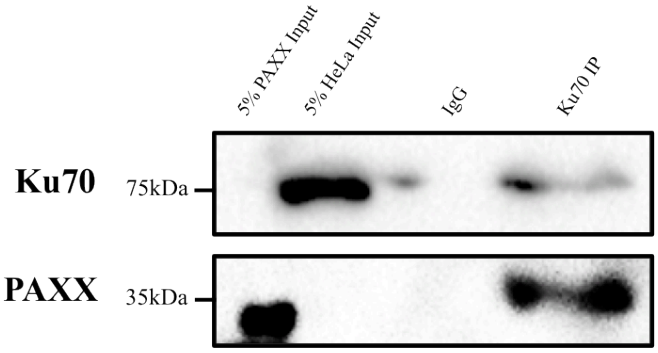

Figure 3-4: Bacterially-expressed histidine-tagged PAXX binds to human Ku. Ku70 was immunoprecipitated from nuclear extracts of HeLa cells (IP denoted as "Ku70 IP" with a 5% input from the immunoprecipitation denoted as "5% HeLa Input") alongside an IgG control (IgG). Immunoprecipitated protein on beads was incubated with bacterially expressed His-PAXX (5% input from binding is shown, denoted as "5% PAXX Input") and washed. Results were analyzed by Western blotting for Ku70 and a histidine tag (to detect His-PAXX). Representative experiment, n=3.

3.4 Identifying novel factors that interact with the Ku N-terminus

We next examined the possibility that a yet unknown NHEJ factor could interact with helix five of the Ku70 vWA domain. To identify such a factor, we performed a large-scale GST pulldown. GST-Ku70 (1-219) and GST-Ku70 D192A/D195R (1-219) peptides were expressed in bacteria. Expression of GST-tagged Ku70 N-termini was confirmed by Western blotting (Figure 3-5A). Coomassie Blue staining of GST-Ku70 (1-219) and GST-Ku70 D192A/D195R (1-219) extracts from bacteria that had been grown and induced in parallel did not show an obvious difference in stability or expression levels of GST-Ku70 D192A/D195R (1-219) as compared to wild-type GST-Ku70 (1-219) (Figure 3-5B). Nuclear extracts of irradiated Ku70 knockout MEFs expressing wild-type Ku70 were incubated with GST-Ku70 (1-219) and GST-Ku70 D192A/D195R (1-219) respectively on glutathione-agarose beads. Upon completion of the pulldown, proteins bound to the Ku70 N-termini were subjected to SDS-PAGE and silver staining (Figure 3-5C). This allowed comparison of proteins pulled down for the wild-type and mutant Ku70 N-termini. Bands of interest on the silver stained gel were identified by Maldi TOF/TOF mass spectrometry with an AB Sciex 5800 TOF/TOF System (Sciex, Framingham, MA, USA). See Appendix B for analysis.

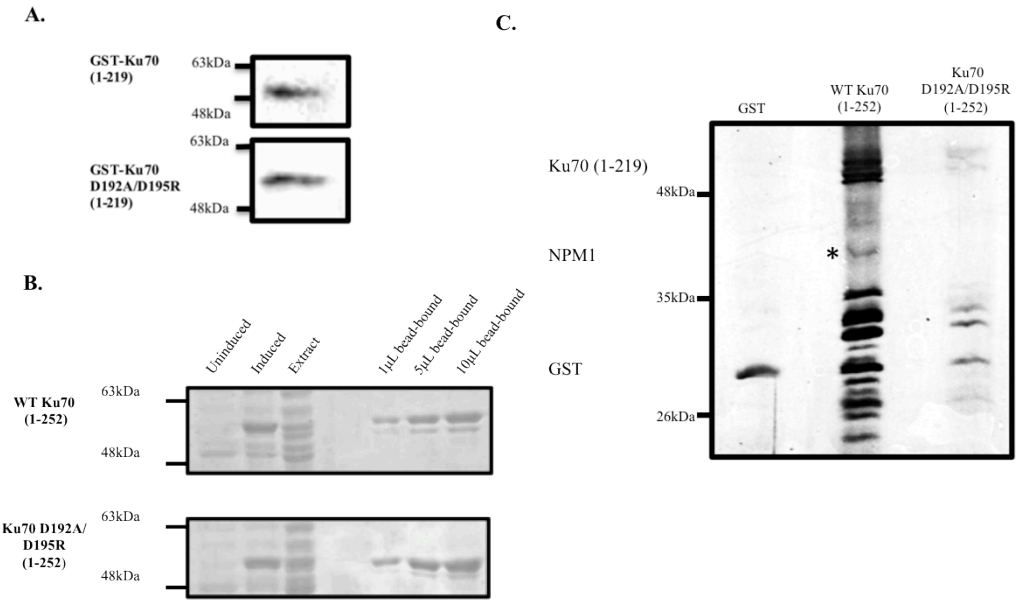

Figure 3-5: GST pulldown comparing protein-protein interactions between the wild-type and D192A/D195R mutant Ku70 N-termini. Expression of the GST-tagged Ku N-termini (1-219) was confirmed by Western blotting (A) and GST-Ku70 (1-252) and GST Ku70 D192A/D195R (1-252) stability was assessed by Coomassie Blue staining (B). Cells expressing the two constructs were grown and induced in parallel and then lysed before induction (labeled "Uninduced") and after induction ("Induced") for SDS-PAGE analysis. Extracts isolated from the cells (labeled "Extract") were bound to glutathione-agarose beads. 1, 5, and 10μL of isolated protein bound to beads were subjected to SDS-PAGE. A large-scale GST pulldown was then performed with GST-tagged wild-type Ku70 (1-219) and GST-Ku70 D192A/D195R (1-219) respectively incubated with nuclear extracts from Ku70 knockout MEFs expressing wild-type Ku70 that had been irradiated with 10Gy IR. Bound proteins were resolved by SDS-PAGE with silver staining (C). Proteins that appeared to bind uniquely to the wild-type Ku N-terminus were identified with Maldi TOF/TOF mass spectrometry. Of particular interest was nucleophosmin (NPM1) which is indicated with an asterisk in (C).

The initial intent of this pulldown was to identify factors that associate with the wild-type Ku70 N-terminus, but not the Ku70 D192A/D195R N-terminus. However, the experiment showed uneven levels of GST-Ku70 (1-219) as compared to GST-Ku70 D192A/D195R (1-219), with a lower amount of protein present in the mutant N-terminus pulldown (Figure 3-5C). Since the wild-type and mutant N-terminus were expressed at similar levels (Figure 3-5B), we attributed the relatively low levels of the GST-tagged mutant N-terminus in the pulldown to a loading error in the experiment, rather than a stability issue that could arise from the D192A/D195R mutation. Due to this loading problem, it was difficult to compare proteins that pulled down with the wild-type and mutant N-termini.

However, we observed a band on the silver stained gel that appeared to be specific to the wild-type Ku70 N-terminus as compared to the GST control and this was identified as nucleophosmin (NPM1) with a score of 52 where a score of 65 is significant ($p<0.05$) (see Appendix B). While the score was below the threshold for significance, the protein ran at the appropriate size of NPM1 and relatively low abundance of the protein on the gel suggested that perhaps the low score was due to a small amount of protein in the sample, rather than a poor identity match. We thus considered nucleophosmin a candidate binding partner for the Ku N-terminus and possibly helix five.

To assess whether the interaction between the Ku N-terminus and NPM1 was legitimate, and not an artifact of the large-scale pulldown, we performed a small-scale pulldown with GST-Ku70 (1-252) and GST-Ku70 D192A/D195R (1-252) respectively and nuclear extracts of HeLa cells transfected with GFP-NPM1. Initially, GFP-NPM1 appeared to interact with GST, GST-Ku70 (1-252) and GST-Ku70 D192A/D195R (1-252). The GST-NPM1 interaction was likely indicative of non-specific binding between NPM1 and the glutathione-agarose beads used for the pulldown. Upon pre-clearing HeLa extracts with glutathione-agarose beads, such that non-specific binding with beads was minimized, GFP-NPM1 was not pulled down with the Ku N-terminus, as indicated by Western blot analysis (Figure 3-6). This suggested that the NPM1 identified in the large-scale pulldown was a non-specific artifact, rather than a true binding partner for the Ku N-terminus.

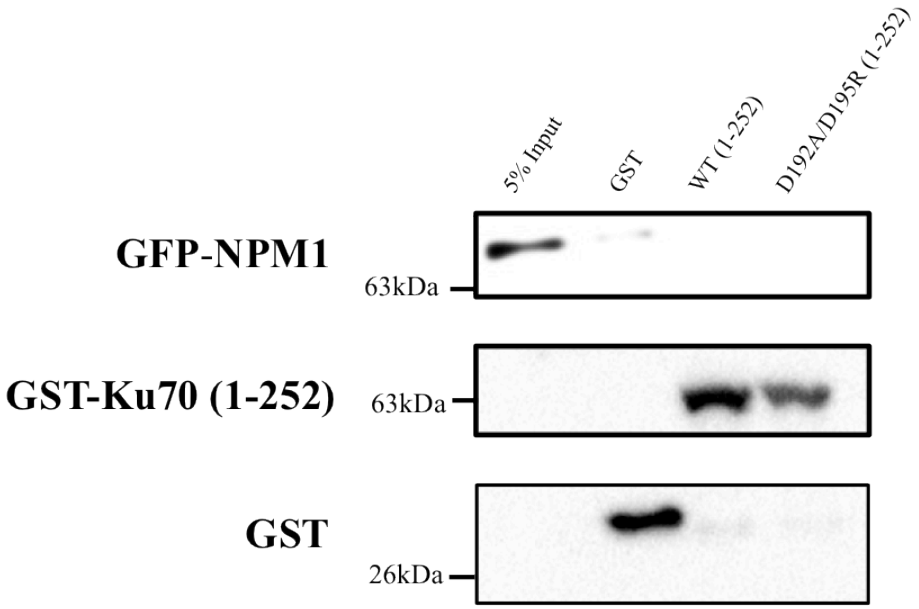

Figure 3-6: The Ku70 vWA domain does not interact with NPM1 in an in vitro binding assay. Extracts of HeLa cells transfected with GFP-NPM1 were subjected to a GST-pulldown with GST, GST-tagged Ku70 (1-252), and GST-Ku70 D192A/D195R (1-252). Samples were analyzed by Western blotting with antibodies for GST and GFP. Representative image is shown, n=3.

Overall, use of a large-scale pulldown to identify factors that interact with helix five was limited in that it was highly time-consuming and resource-intensive. Furthermore, there was no guarantee of outcome from this type of experiment. Thus, we chose to instead pursue a targeted approach for comparing factor recruitment in wild-type Ku70 and Ku70 D192A/D195R expressing cells.

3.5 Developing a targeted approach for assaying factor recruitment in wild-type and D192A/D195R expressing cells

We postulated that mutation of helix five of the Ku70 vWA domain could result in a defect in NHEJ complex formation. To test known NHEJ factors' recruitment to DSBs in wild-type and D192A/D195R expressing cells, we used two methods for observing Ku recruitment to DNA damage. While many proteins accumulate in large amounts at sites of damage and some form foci that can be visualized by indirect immunofluorescence and microscopy, NHEJ factors do not. To surpass this issue, we employed two methods for assaying Ku recruitment to DSBs in cells: a newly developed pre-extraction approach and the more established approach of laser microirradiation. These are discussed herein.

3.5.1 The CSK + R pre-extraction approach to observing repair protein foci is not a reliable method for the purposes of our experiments

The first method we explored for testing NHEJ factor recruitment to sites of DNA damage was a recently developed pre-extraction technique[97]. Briefly, X-ray irradiated cells are treated with a mixture of detergent, sucrose, and RNAse A (CSK+R) prior to fixing and immunofluorescence. Presumably, CSK+R removes non-DSB bound Ku and Ku associated with chromatin via RNA, leaving only Ku bound to DSBs for immunostaining in the nucleus. Ku foci can then be resolved by microscopy.

We tested this method in Ku70 knockout MEFs stably expressing wild-type Ku70. Irradiated and non-irradiated cells were subjected to pre-extraction and indirect immunofluorescence with antibodies for Ku70 and the DNA damage marker γ-H_2AX. Cells were then imaged with confocal microscopy. CSK+R removed a large amount of Ku from the nucleus and surrounding area, as indicated by a decrease in Ku staining after

CSK+R treatment in both irradiated and non-irradiated cells (Figure 3-7A). The small amount of staining that remained occurred in small, punctate structures fitting the description of Ku foci. However, these structures only partially localized with γ-H_2AX after IR and several Ku "foci" were not in close proximity to γ-H_2AX at all, suggesting that they did not occur at sites of DNA damage. Furthermore, amounts of Ku "foci" did not increase greatly in irradiated cells as compared to non-irradiated cells, leading us to question whether the signal we observed truly represented Ku bound to DNA DSBs.

To determine whether Ku "foci" were an artifact of immunostaining, we immunostained irradiated Ku70 knockout MEFs that had been treated with CSK+R pre-extraction or conventional immunofluorescence for Ku70 and γ-H_2AX (Figure 3-7B) and ran no primary antibody controls for both wild-type Ku70-expressing cells and Ku-deficient cells (Figure 3-7A and B). While secondary antibody background was low, as indicated by absence of staining in the no primary antibody controls, a small amount of non-specific signal appeared in Ku-deficient cells hybridized with the Ku70 antibody. This was indicative of non-specific binding of the Ku antibody to structures within the cells. While CSK+R pre-extraction greatly reduced the non-specific signal, some staining was still present and this signal took the form of punctate, spherical structures in the nucleus similar to foci. There did appear to be a reduction of Ku staining in the CSK+R-treated Ku-deficient control, as compared to CSK+R-treated cells expressing wild-type Ku70, but distinguishing non-specific signal and noise in the image from foci was not possible because both non-specific and foci signals appeared as small spheres within the nucleus.

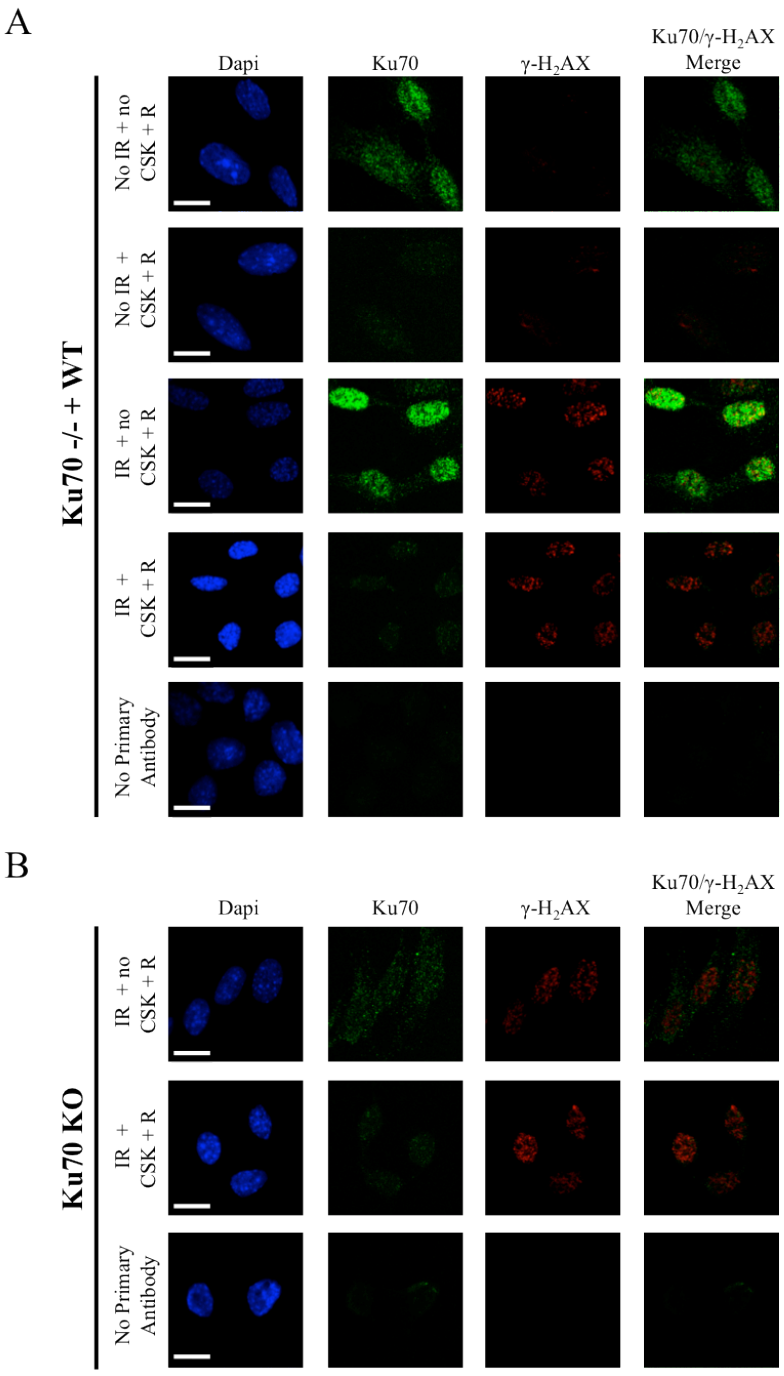

Figure 3-7: Ku and γ-H_2AX staining by CSK+R pre-extraction removes background Ku but does not generate convincing Ku foci. Irradiated and non-irradiated Ku70 knockout MEFs expressing wild-type Ku70 were subjected to immunofluorescence with CSK+R pre-extraction, conventional immunofluorescence, or CSK + R pre-extraction with a no primary antibody control (A). Irradiated Ku70 knockout MEFs treated with or without CSK+R were immunostained along with a no primary antibody control (B). Scale bars=10μm.

Overall, we anticipated difficulty in distinguishing NHEJ factor foci from antibody background when using this method for visualizing Ku recruitment to breaks, particularly when immunostaining for factors with poor-quality antibodies. Background staining could easily create false positives in experiments comparing NHEJ factor recruitment in wild-type and D192A/D195R-expressing cells. Furthermore, NHEJ factors are known to be recruited rapidly, within one minute, to DSBs[104]. As the pre-extraction process lasts 6 minutes before fixing, using this technique would not allow us to observe NHEJ factor recruitment at the time when it is expected to peak (one minute). Because of these limitations, as well as knowledge that this technique is not yet well established in the community, we turned our attention to the more common method for analyzing NHEJ factor recruitment, microirradiation.

3.5.2 Optimizing microirradiation with a multiphoton NIR laser system

Microirradiation was performed with a 750nm infrared laser coupled to a Zeiss LSM 510 Meta NLO confocal microscope. A microirradiation protocol provided by the Hendzel lab (University of Alberta, Canada) was optimized with Ku70 knockout MEFs expressing wild-type Ku70. 24 hours prior to microirradiation, cells were transfected with PARP1-GFP (provided by Dr. M. Hendzel, University of Alberta). This protein is known to be recruited to laser-induced DNA damage and the confocal microscope to which the infrared laser was coupled could be used to image PARP1-GFP directly after damage. As a result, a "trial and error" approach could be used to optimize the system and damage formation could be observed immediately after laser treatment. Overall, this greatly simplified optimization of the system.

We began using the system with a 40X objective. Prior to microirradiation, zoom was set in the confocal software such that one pixel in the acquired image corresponded to 0.05 μm. The zoom was kept constant, allowing the user to specify regions of interest (ROI's) for microirradiation corresponding to a known size. The level of damage induced by the laser could be adjusted by changing the laser power and the number of iterations (or repetitions) of the laser pulses. Strong recruitment of PARP1-GFP was evident at 20% power with 20 iterations in a 0.5 μm-wide region (Figure 3-8A).

PARP1 can respond to multiple types of DNA damage. To confirm that the described conditions were truly stimulating DSB formation, microirradiated cells were subjected to immunofluorescence staining for the DSB marker γ-H_2AX within 10 minutes of damage induction. γ-H_2AX foci accumulated along laser tracks implying DSB formation (Figure 3-8B). Finally, stimulation of NHEJ DNA repair under these conditions was confirmed by monitoring recruitment of GFP-Ku80 to laser-induced damage (Figure 3-8C). Presence of GFP-Ku80 at the laser line indicated that NHEJ proteins responded to laser-induced damage and suggested that repair was active. Overall, we had reasonable evidence to conclude that the system was effective in stimulating both DSBs and NHEJ.

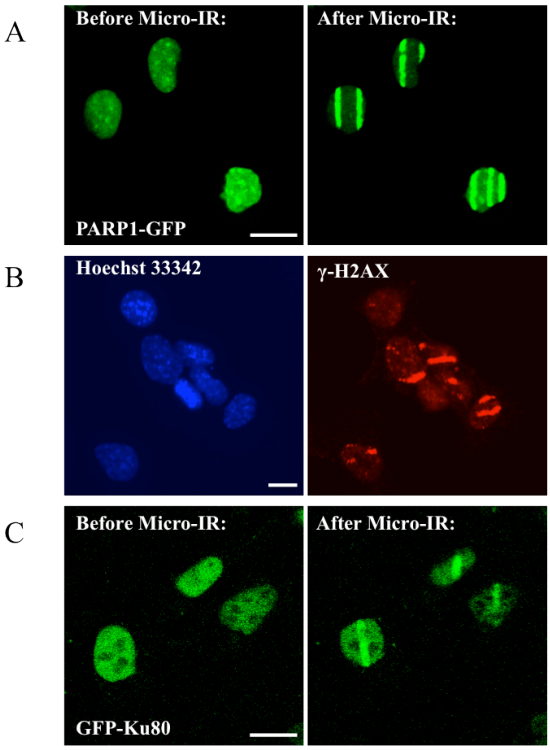

Figure 3-8: Optimization and validation of a near infrared laser system for microirradiation. Conditions for microirradiation with a 750nm NIR laser were optimized in Ku70 knockout MEFs re-expressing wild-type Ku70 and transfected with PARP1-GFP. PARP1-GFP's recruitment to laser lines immediately after damage was imaged using the confocal microscope to which the damage-inducing NIR laser was coupled (A). Damage was induced at 40X magnification with 0.5μm-wide rectangles defined across the length of each cell with 20% laser power and 20 iterations. Formation of DSBs was confirmed by γ-H_2AX immunostaining and fluorescence microscopy (B). Activation of NHEJ was assessed by observing GFP-Ku80 recruitment to laser tracks (C). GFP-Ku80 was imaged with the same microscope coupled to the laser used for inducing DNA damage. In C, Ku80 recruitment was visualized after only 4 laser iterations at 20% laser power. Scale bars=10μm.

While these conditions were effective for inducing damage and stimulating Ku recruitment, visualizing other fluorescently tagged repair factors' recruitment proved to be surprisingly difficult under a 40X objective. While GFP-Ku80 recruitment was easily visualized, it was more difficult to observe recruitment of GFP-XRCC4, GFP-DNA Ligase IV, and YFP-XLF, possibly because endogenous versions of each protein in the cells outcompeted the heavier fluorescently tagged proteins used in these experiments. To improve resolution of these proteins' recruitment, we increased the mean scan number of the microscope to improve image quality and also moved from a 40X objective to the 63X objective. The zoom was adjusted such that 0.05 μm corresponded to one pixel. This allowed visualization of each protein's recruitment in microirradiated cells (Figure 3-9).

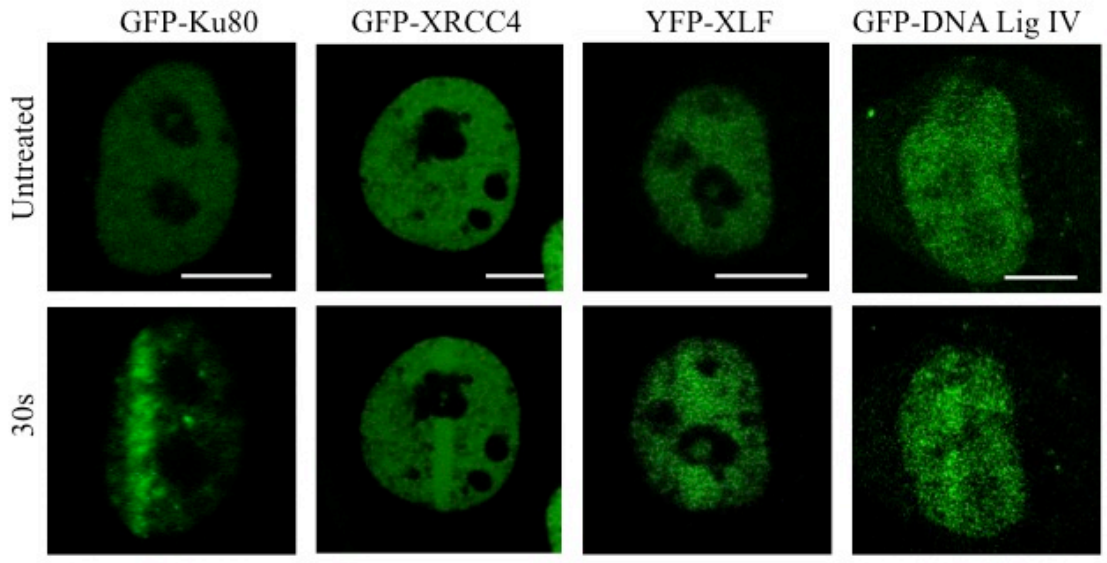

Figure 3-9: EGFP-Ku80, GFP-XRCC4, YFP-XLF, and EGFP-DNA Ligase IV are recruited to laser-induced DNA damage. Ku70 knockout MEFs stably expressing wild-type Ku70 were transfected with EGFP-Ku80, GFP-XRCC4, YFP-XLF, and EGFP-DNA Ligase IV. They were then microirradiated with a 750nm NIR laser with 20% power and 20 iterations at 63X magnification. Fluorescently tagged protein recruitment was imaged within 30 seconds of damage using an Argon laser coupled to the same microscope. Cells are shown before and after microirradiation. Representative images are shown, n=10. Scale bars=5μm.

With the system at optimal settings for visualizing all of the repair proteins we intended to observe, we next sought to determine a quantitative amount of damage induced by our system. To approximate the amount of DSBs induced by microirradiation, we measured corrected total nuclear fluorescence in cells treated with various doses of IR and immunostained for the DNA damage marker γ-H_2AX[107]. The linear relationship between IR dose and γ-H_2AX fluorescence was plotted to generate a line of best fit (Figure 3-10) expressed by Equation 1 (see Methods).

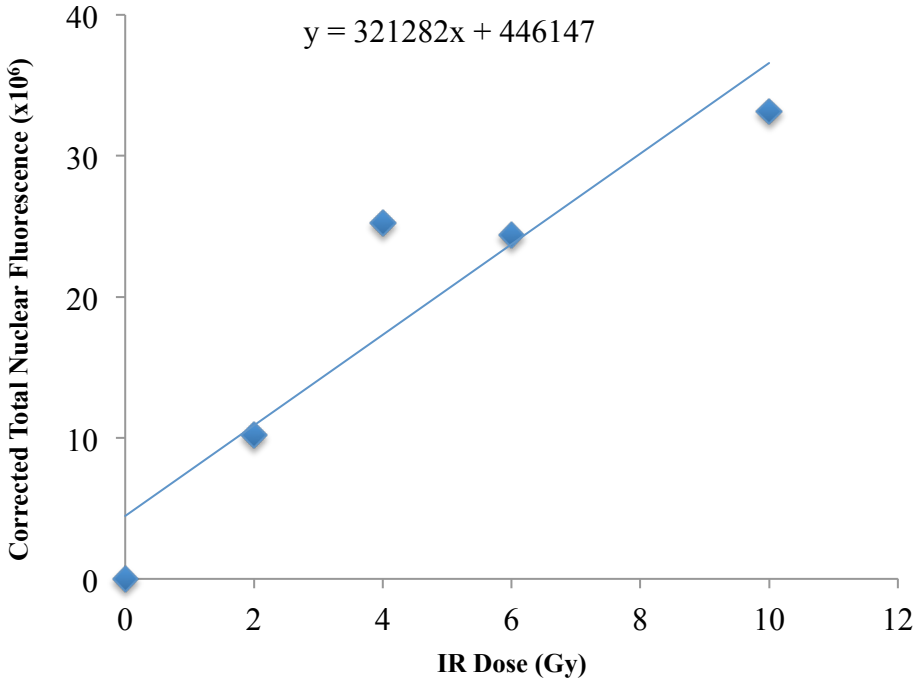

Figure 3-10: Standard curve used for calculating IR dose equivalence of laser-induced DNA damage. Ku70 knockout MEFs expressing wild-type Ku70 were irradiated with X-rays at various doses and then immunostained for γ-H_2AX. γ-H_2AX was imaged with fluorescence microscopy. Corrected total nuclear fluorescence of γ-H_2AX at each IR dose was quantified from these images. For each data point, n=20 cells.

Total γ-H_2AX fluorescence was then measured in nuclei of microirradiated cells containing one laser line of microirradiated damage. The average γ-H_2AX fluorescence of microirradiated cells was substituted into Equation 1. Solving for x, we found that the level of γ-H_2AX fluorescence generated from one line of microirradiated damage in a cell corresponded to the amount of γ-H_2AX fluorescence generated by approximately 5.28Gy of IR. As 1Gy of IR corresponds to about 35 DSBs, we estimate that in this study a microbeam spanning the length of a nucleus yields approximately 185 DSBs[108].

With an effective system for visualizing repair protein recruitment to damage, we began experiments comparing factor recruitment in Ku70 knockout MEFs expressing WT Ku70 and Ku70 D192A/D195R respectively, as well as Ku70-deficient control MEFs.

3.6 The Ku70 D192A/D195R mutation does not impair Ku recruitment to DNA DSBs

Before we could compare the recruitment of NHEJ factors expected to associate with helix five of the Ku70 vWA domain to laser-induced DNA damage in WT Ku70 and Ku70 D192A/D195R-expressing cells, it was first important to confirm that the Ku70 D192A/D195R mutation does not impair recruitment of Ku itself to laser-induced DNA damage. We thus performed a control experiment with GFP-tagged Ku80-transfected cells assaying recruitment of GFP-Ku80 to laser-induced DNA damage in cells expressing wild-type Ku70, cells expressing Ku70 D192A/D195R, and Ku-deficient cells. Ku70/80 binds DSBs as a heterodimer and is not functional in absence of either member of the heterodimer[49,50], so recruitment of Ku80 is dependent on Ku70 expression. The GFP-Ku80 construct used in these experiments yielded protein that had been recruited to laser-induced damage in a previous study and thus we were confident that it was able to associate with damage[92].

Both wild-type Ku70 and Ku70 D192A/D195R expressing cells displayed GFP-Ku80 recruitment to microirradiated sites, indicating that the D192A/D195R mutation does not prevent Ku recruitment to DSBs (Figure 3-11). Conversely, Ku70-deficient cells, which lack Ku heterodimer function due to the absence of Ku70 did not display GFP-Ku80 recruitment to damage, as expected. These results suggest that our laser-induced DNA

damage method triggers specific recruitment of NHEJ factors and that D192A/D195R mutant Ku70 can be recruited normally to DNA damage.

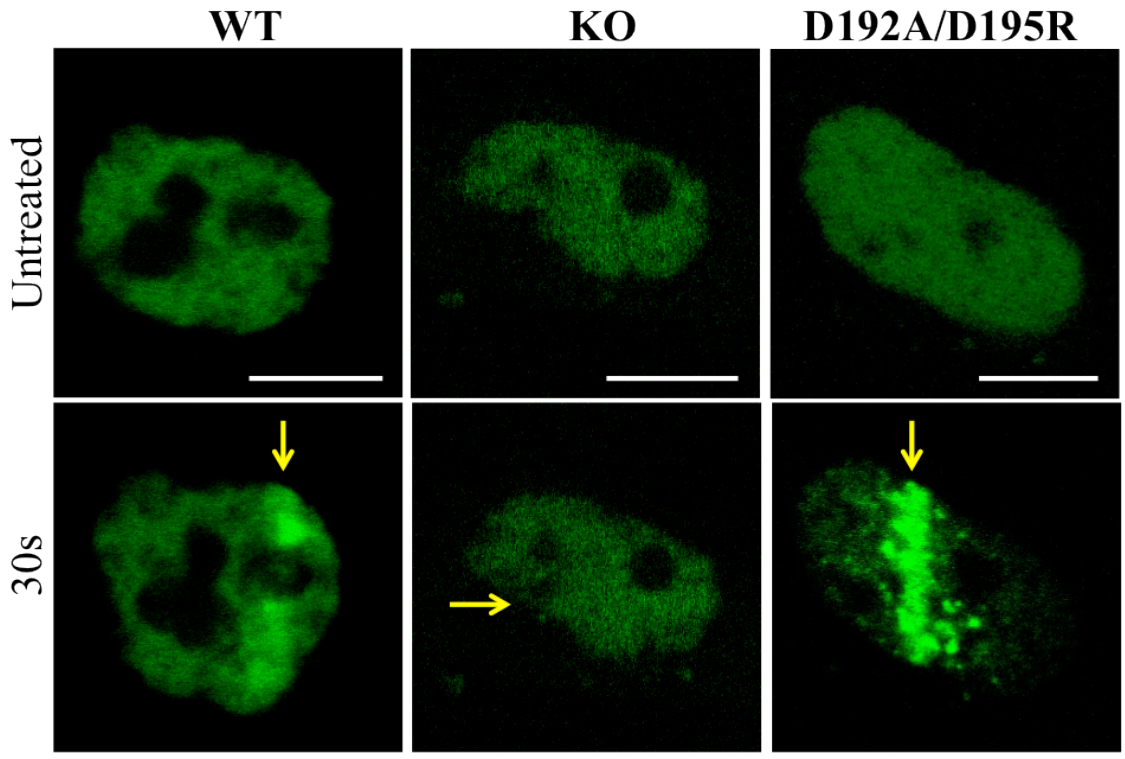

Figure 3-11: D192A/D195R mutation does not affect Ku recruitment to laser-induced DNA damage. Ku70 knockout MEFs (KO), Ku70 knockout MEFs expressing wild-type Ku70 (WT), and Ku70 knockout MEFs expressing Ku70 D192A/D195R (D192A/D195R) transfected with GFP-Ku80 were microirradiated. GFP-Ku80 recruitment to breaks was observed by live imaging. Scale bars=5μm.

3.7 Members of the XRCC4-XLF-DNA Ligase IV complex are recruited to laser-induced DNA damage in Ku70 D192A/D195R-expressing cells

Having shown that the Ku70 D192A/D195R mutant can be recruited to DNA damage, we next assayed recruitment of EGFP-DNA Ligase IV, GFP-XRCC4, and YFP-XLF in Ku70 knockout MEFs expressing wild-type Ku70 and Ku70 knockout MEFs expressing Ku70 D192A/D195R. All tagged proteins used in these experiments had been shown to be recruited to laser-induced damage in previous studies[92,109,110]. XRCC4, XLF, and DNA Ligase IV form a complex responsible for rejoining the broken DNA ends in the final step of repair[27]. It was expected that if one of these factors' or an upstream factor's recruitment were perturbed by the Ku70 D192A/D195R mutation, at least one member of the complex would not be recruited in the repair mutant. Surprisingly, all three NHEJ factors were recruited similarly in wild-type and mutant cells (Figure 3-12). Recruitment of XLF and DNA Ligase IV was Ku-dependent, as indicated by their absence at laser tracks in Ku70 knockout MEFs, although in some cases GFP-XRCC4 recruitment was observed in the absence of Ku, likely as an artifact of overexpression. Overall, these results suggested that mutation of helix five did not abolish recruitment of the XRCC4-XLF-DNA Ligase IV complex to the DSB.

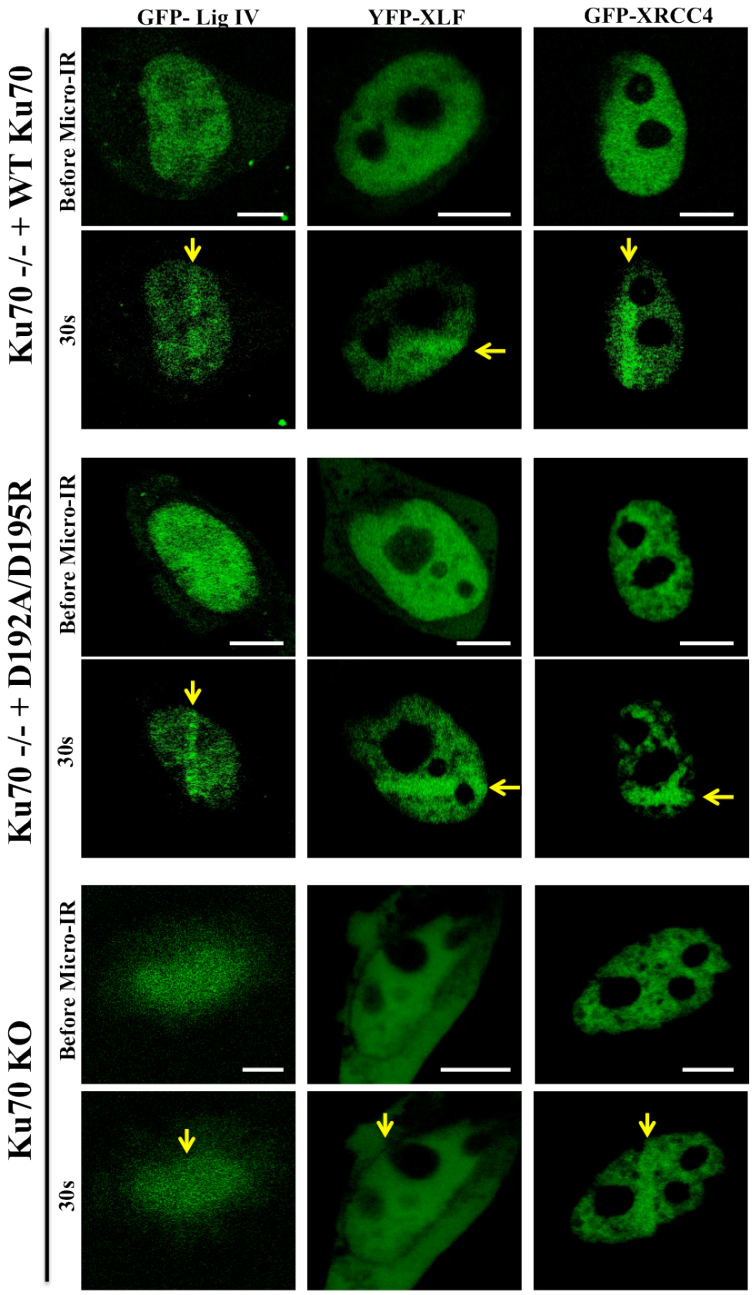

Figure 3-12: Members of the ligation complex are recruited to laser-induced DNA damage in the D192A/D195R repair mutant. Ku70 knockout MEFs (labeled "Ku70 KO") and Ku70 knockout MEFs expressing wild-type Ku70 ("Ku70-/- + WT") and Ku70 D192A/D195R ("Ku70-/- + D192A/D195R") respectively were transfected with GFP-XRCC4, GFP-DNA Ligase IV, or YFP-XLF and then microirradiated with an NIR laser. Fluorescently tagged factors were imaged before and after microirradiation with the confocal microscope to which the NIR laser was coupled. Representative images are shown, n=10 for each. Scale bars=5μm.

3.8 Use of microirradiation to demonstrate recruitment of a previously uncharacterized NHEJ factor to DNA damage

In addition to using microirradiation for characterizing the role of helix five of the Ku70 vWA domain in NHEJ factor recruitment, we employed laser microirradiation to evaluate recruitment of the Aurora B kinase to DSBs. Work in our lab has indicated that Aurora B is regulated via S155 of the Ku70 vWA domain[62]. Following DNA damage, phosphorylation of this residue inhibits Aurora B's activity in stimulating mitosis and cell cycle progression such that, presumably, cells will be given ample time to repair their DNA prior to mitosis. Using microirradiation we showed that Aurora B is recruited to sites of laser-induced DNA damage in both HeLa cells and wild-type Ku70 expressing cells (Figure 3-13A). Quantification of Aurora B recruitment indicated rapid recruitment of the protein to DNA damage within 15 seconds (Figure 3-13B). This is the first demonstration of Aurora B recruitment to damage in living cells and illustrates the utility of microirradiation in assaying recruitment of uncharacterized factors to damage.

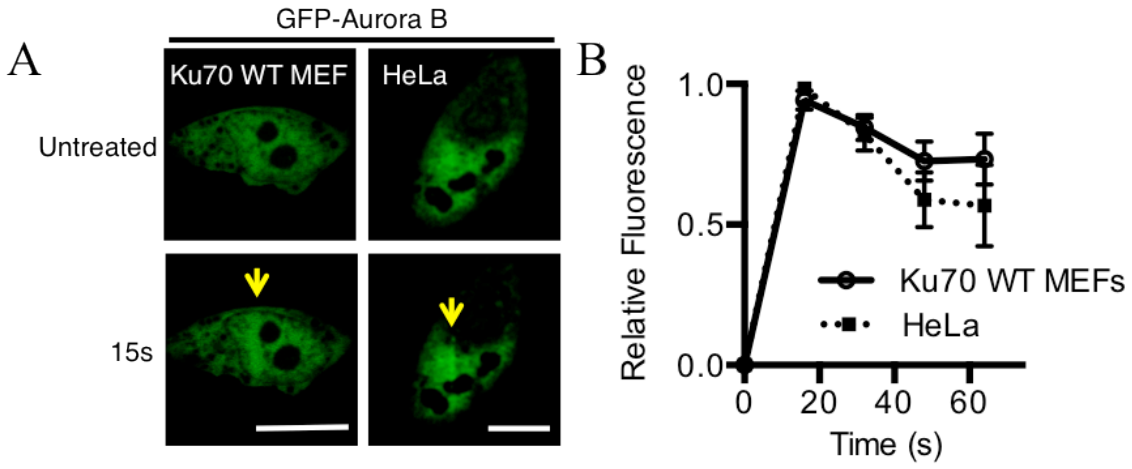

Figure 3-13: Aurora B is recruited to laser-induced DNA damage. Microirradiation was used to illustrate the recruitment of GFP-Aurora B, a kinase implicated by work in our lab to be involved in DNA damage signaling, to DNA damage in HeLa cells (n=5) and Ku70 knockout MEFs expressing wild-type Ku70 (n=10) that had been transfected with GFP-Aurora B DNA. Representative images are shown in A. Scale bars=10μm. Relative intensity of fluorescence at microirradiated sites, calculated as previously described[111], is plotted for both cell lines in B.

CHAPTER 4: DISCUSSION

4.1 Summary of results

We sought to characterize the function of helix five of the Ku70 vWA domain in non-homologous end joining, with the hypothesis that it is involved in mediating a protein-protein interaction. Within this, we explored the possibilities that helix five mediates an interaction via K182 and K189, that the helix mediates Ku tetramerization, that it is involved in the PAXX-Ku interaction, or that it directly interacts with another NHEJ factor.

Clonogenic cell survival assays indicated that K182 and K189 of helix five were not essential for DNA repair. Unlike the D192A/D195R mutant, which displays a profound survival defect as compared to wild-type Ku70-expressing cells when treated with IR[61], K182A, K189A, and K182R/K189R mutant expressing cells had similar survival after IR to cells expressing wild-type Ku70. This led us to reject the hypothesis that helix five's repair function is dependent on the two lysine residues and the remainder of our work focused on the possibility that helix five mediates a direct protein-protein interaction.

Two major candidates for interacting with helix five were the newly identified NHEJ factor PAXX and Ku itself, with the latter possibility being that Ku could tetramerize via helix five as previously suggested[52]. These sub-hypotheses were tested in a GST pulldown system. Neither PAXX nor Ku70 were pulled down with the Ku N-terminus, regardless of whether helix five was mutated. This suggested that these interactions occur independently of helix five and the Ku N-terminus or may require additional regions of the Ku heterodimer to occur.

We next considered the possibility that helix five of the Ku70 vWA domain interacts with yet unidentified NHEJ factors. To identify such factors, we performed a large-scale GST pulldown with GST-tagged wild-type and mutant Ku70 N-termini and nuclear extracts from irradiated cells. This pulldown identified few candidate binding partners for the Ku N-terminus or helix five. The exception was nucleophosmin, NPM1 and this result could not be reproduced in pulldown experiments followed by Western blotting. Having had

little success in our non-targeted approach, we moved on to a targeted approach of assaying NHEJ factor recruitment in cells.

We tested two methods for observing NHEJ factor recruitment. The first method was a newly developed technique for resolving Ku foci at sites of laser-induced damage. While this appeared to be somewhat effective, in that it removed a large amount of Ku from the nucleus and left behind small, spherical, focus-like structures, there were several uncertainties in its use. Ku and γ-H_2AX foci did not colocalize and there was not a large difference in the appearance of Ku staining in irradiated and non-irradiated cells, leading us to question whether what we observed was truly Ku associated with damage, rather than antibody background. As the technique requires treatment of cells with pre-extraction solution prior to fixing, it limits the scope of kinetic studies, especially as Ku is known to be recruited at maximal levels within one minute of damage[104]. For this reason, we explored a more established technique, laser microirradiation.

We optimized a microirradiation system to observe recruitment of GFP-tagged NHEJ factors to sites of laser-induced DNA damage using a near infrared laser system coupled to a confocal microscope. We showed that our system was effective in stimulating DSBs and NHEJ and calculated the approximate amount of DSBs formed by our system. We confirmed that Ku is recruited to damage in both wild-type and Ku70 D192A/D195R expressing cells using GFP-Ku80 and then observed recruitment of members of the ligation complex: XRCC4, XLF, and DNA ligase IV. We expected that if the D192A/D195R mutant were defective in recruiting an NHEJ factor, the ligation complex, which is the last player in NHEJ, would not be recruited for repair in the mutant. Surprisingly, XRCC4, XLF, and DNA Ligase IV each displayed recruitment in microirradiated cells. This led us to conclude that despite its repair defect, the Ku70 D192A/D195R mutant is able to recruit NHEJ factors involved in end ligation. Finally, we employed microirradiation to show that Aurora B, which our lab showed was involved in mediating DNA damage signaling, is recruited to laser-induced DNA damage.

4.2 Role of K182 and K189 in NHEJ

We had considered the possibility that K182 and K189 within helix five of the Ku70 vWA domain are important for the helix's repair function. To evaluate this, we substituted the residues and assayed cell survival in response to IR using clonogenic survival assays. These indicated that Ku70 knockout MEFs expressing Ku70 K182A, K189A, or K182R/K189R did not display impaired survival after IR, as compared to wild-type expressing cells. Past work has shown that the D192A/D195R mutation in helix five of the Ku70 vWA domain led to impaired cell survival after IR[61], so had K182 and K189 been important for repair, we would have expected the K182A, K189A, and K182R/K189R mutations to lead to decreased cell survival, as well. Overall, our results suggest that K182 and K189 do not affect cell survival after IR, which implies that they do not affect DNA repair.

We used a K182R/K189R double mutant to ensure that K182 and K189 did not have an interchangeable function. However, we cannot completely rule out the possibility that other lysines could play an interchangeable role with K182 and K189 or act independently to signal in the function of helix five of the Ku70 vWA domain. The nearest lysines, apart from K182 and K189, to D192 and D195 are residues 164 and 206, which are both beyond the structural boundaries of helix five. K206 is located on the side of helix five opposite to D192 and D195 and its side chain faces the opposite direction to those of D192 and D195, making it unlikely that this residue's integrity is important for helix five's function. However, K164, which is located within a beta sheet in close proximity to helix five is fairly close to D192 and D195, with a side chain extending towards D192 and D195 (Figure 4-1). This conserved residue could act interchangeably with K182 and K189, or alone to mediate the function of helix five and its role should be investigated. Additionally, recent work showed that two lysines in the Ku70 vWA domain at positions 31 and 160 confer lyase activity of Ku[31]. This function allows removal of abasic sites from DNA lesions. K31 is not a part of the known crystal structure of Ku70, but K160 is within close proximity to helix five of the Ku70 vWA domain (Figure 4-1) and we cannot rule out the possibility that the Ku70 vWA domain's repair function is also related to the protein's lyase activity, even if K182 and K189 are

not important in this function. As outlined in the introduction, lysine signaling via ubiquitination, acetylation, and neddylation has been implicated in several Ku functions and further study is needed for a complete understanding of these signals and their overall effects on DNA repair[43,44,85].

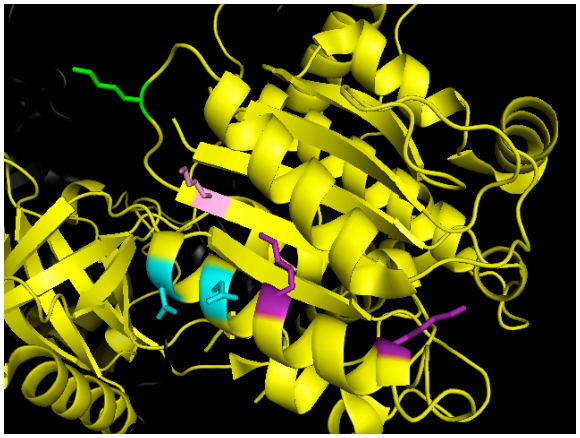

Figure 4-1: Structural representation D192, D195, and surrounding lysine residues within helix five of the Ku70 vWA domain. K182 and K189, which were studied, are indicated in purple. K164 (pink) is located beyond helix five of the Ku70 vWA domain. However, it is located within close physical proximity to D192 and D195 (blue), based on the protein's crystal structure. K160 (green) has been implicated in Ku's lyase activity and is somewhat close to D192 and D195, as well. Images are adapted from the crystal structure solved by Walker *et al*. using the PyMOL Molecular Graphics System Version 1.3 (Schrödinger LLC, USA)[72]. (Adapted with permission from Macmillan Publishers Ltd: [**N**ature] ([72]), copyright 2001). (See Appendix C).

While K182 and K189 alone do not appear to play an apparent role in NHEJ, we cannot conclude that signaling via these residues is not important for Ku function, especially beyond repair. As outlined in the introduction, several studies have pointed to lysine modifications in various functions of Ku, particularly its removal from the break[43,44]. K182 and K189 may be modified not for repair, but for Ku removal as part of the aftermath of repair. However, prolonged Ku retention leads to impaired NHEJ, so we do not expect that K182 and K189 are involved in Ku retention[43].

Overall, our work has shown that lysines 182 and 189 in helix five of the Ku70 vWA domain, alone or together, do not play a role in conferring cell survival after IR. However, we do not rule out the possibility that these lysines act interchangeably with additional residues or function beyond repair.

4.3 Imaging Ku: A review of two techniques

To assay recruitment of NHEJ factors to DNA damage, we considered two techniques. The first technique involved pre-extraction of background Ku from the nuclei of X-ray treated cells with a solution of sucrose, detergent, and RNase A (CSK+R)[97]. This was thought to remove free protein in the nucleus as well as protein associated with chromatin via RNA, leaving behind only Ku associated with damage. The authors of the study where the technique was first demonstrated utilized the technique to visualize GFP-Ku70, GFP-XRCC4, Nijmegen breakage syndrome protein 1 (Nbs1), and untagged Ku70 foci through immunofluorescence. It was shown to be effective in the context of DSBs induced by nucleases, chemicals, X-rays, and microirradiation. However, concern was expressed in the publication regarding the presence of fewer foci than theoretical amounts of breaks at a given IR dose, suggesting that there were limitations to the pre-extraction technique.

When replicating this method, we found that we were able to see nuclear staining of structures fitting the description of Ku foci following CSK+R pre-extraction. There was an obvious difference in pre-extracted and non-pre-extracted cells, with the majority of Ku removed from CSK+R treated cells. However, it was not clear that what was left behind following pre-extraction was truly Ku bound to DSBs. γ -H_2AX staining and

Ku70 staining did not fully colocalize despite the fact that γ-H_2AX is a known DSB marker[112]. Britton *et al*. also observed this using the CSK+R pre-extraction technique[97]. They argue that Ku and γ-H_2AX do not colocalize because γ-H_2AX is a histone modification and histones are not present directly at the DSB while Ku associates directly with broken DNA ends. However, we observed foci far from any γ-H_2AX staining and even if γ-H_2AX foci were truly forming at the periphery of Ku foci, rather than directly colocalizing with them, we would have expected to see some degree of localization to the same region of the nucleus. Furthermore, previous reports indicate that phosphorylated DNA-PK foci, which would be present directly at DSBs, colocalize with γ-H_2AX foci and therefore Ku foci would be expected to do the same[113].

The low difference in Ku signal between non-irradiated and irradiated cells, despite a clear signal difference in the DNA damage marker γ-H_2AX between non-irradiated and irradiated cells suggested that much of what was observed was simply antibody background or noise that occurs during image acquisition, rather than IR-induced foci. Due to the fact that non-specific immunostaining is inherent to many antibodies in immunofluorescence, this places a great limitation to the pre-extraction technique. This can be surpassed if pre-extraction is performed in conjunction with microirradiation, which was shown to be possible in the original study by Britton *et al*.[44,97]. Microirradiation would restrict foci to a defined pattern along a laser track in the nucleus, rather than dispersing the foci throughout the cell like X-rays. Thus, it could be easier for an observer to distinguish foci from non-specific signal in microirradiated cells.

To truly validate that Ku and other NHEJ factors localize to foci resolvable by pre-extraction, CSK+R pre-extraction would need to be carried out with GFP-tagged proteins. This would eliminate concerns of antibody background. While Britton *et al*. used GFP-tagged Ku and XRCC4 in some pre-extraction experiments, they used a GFP antibody and immunofluorescence to strengthen their signal[97]. Even with GFP-tagged protein, it could be difficult to prove definitively that the sites to which proteins have localized truly correspond to DSBs. Colocalization experiments with cotransfected fluorescently-tagged repair proteins known to interact only at the break (with tags that are excited at non-overlapping wavelengths) would be an effective means of confirming this.

Assuming that the limitations of non-specific staining could be overcome in the use of CSK+R pre-extraction, the technique still poses a major limitation in kinetic studies. Ku is recruited rapidly to DNA damage and recruitment is thought to peak within one minute of damage induction[104]. However, CSK+R pre-extraction takes six minutes to perform before cells are fixed[97]. Thus, recruitment of Ku and other NHEJ factors cannot be observed within critical recruitment time points using this technique and this is its primary limitation. Overall, there were several concerns with using the CSK+R pre-extraction method in the context of this study and this led us to consider the alterative option for observing repair protein recruitment to damage: microirradiation.

We found microirradiation to be a more effective technique than pre-extraction. In addition to being more established than pre-extraction in literature, laser microirradiation with a near infrared laser yielded clear NHEJ factor recruitment to DNA DSBs in pre-defined regions within the nucleus. The damage was induced in high levels to a relatively small region in the cell and this created a visible signal of factor recruitment, leaving little doubt as to whether the technique and protein recruitment to the regions in question were stimulated by DNA damage. Furthermore, damaging conditions could be easily validated with staining of γ-H_2AX, which localized clearly to laser tracks. Another major advantage of microirradiation was that the laser used for inducing DNA damage was coupled to a confocal microscope and GFP-tagged protein recruitment in treated cells could be imaged immediately after laser-induced damage. This allowed observation of factor recruitment at several time points through continuous imaging and would permit kinetic studies in the future, since images could be acquired immediately after damage.

One limitation of this technique was that recruitment of NHEJ factors to laser lines was generally apparent, but contrast between the treated and untreated regions was sometimes poor. This could be attributed to competition between GFP-tagged proteins used in this study with endogenous proteins. As GFP tags add substantial weight to proteins as well as potential for disruption of regions close to the tag, it is possible that the GFP-tagged, transfected, repair proteins observed in this study were being outcompeted by their endogenous counterparts. Several microirradiation experiments in past studies were conducted in cells deficient in the GFP-tagged protein being studied and this could

explain why the recruitment signals observed in some papers are stronger than the signal observed in our own work. For example, Mari *et al*. used DNA Ligase IV-deficient and Ku80-deficient cells respectively when studying the proteins' recruitment to microirradiated sites using a laser system similar to our own[92]. This yielded a stronger recruitment signal than the signal we observed with the same constructs. However, Yano *et al*. observed a similar signal to that observed in our study with YFP-XLF in cells with endogenous XLF[109]. Furthermore, GFP-XRCC4 recruitment to laser-induced damage showed higher contrast between irradiated and non-irradiated regions in XRCC4-deficient cells than in epithelial cells that expressed endogenous XRCC4[114,115]. Thus, the low contrast that we observed between treated and untreated regions in GFP-NHEJ factor-expressing cells is common for cells expressing endogenous repair proteins and was anticipated.

It is also possible that studies with stronger recruitment induced more DNA damage to targeted cells. In a past study, laser-induced damage created with a system similar to ours caused more visible recruitment to damage, but also induced between 1000 and 1500 DSBs within a 2.5μm squared region[92]. We estimated that our technique induced only about 185 DSBs across the entire cell (or about 185 DSBs in a 5μm squared region, assuming that MEFs used for the study have a nuclear diameter of about 10μm), making our technique much less damaging than microirradiation described in some previous reports. While this was a limitation to our ability to clearly observe protein recruitment to damage, it was advantageous in that it ensured treated cells were exposed to tolerable levels of damage. Higher levels of damage could lead to sample burning and our methods ensured that repair machinery did not become saturated. Furthermore, a study that we used to model the gray equivalence calculation for our system's laser-induced DNA damage reported a microirradiation dose equivalent to 2.5 Gy of X-ray induced damage in 7.08μm squared regions[108]. This level of damage is similar to what we observed with our system, indicating that damage at the levels we used is not unprecedented in microirradiation studies.

Another explanation for relatively weak recruitment observed in our study is that over-transfection of a given fluorescently-tagged protein prevented clear resolution of damage-

associated protein simply because there were very high levels of protein in the nucleus. This, in combination with the addition of the large GFP tag, could alter recruitment efficiency.

Another limitation of microirradiation was efficiency. Only a small amount of cells could be treated at one time and the process of inducing damage to many cells could be time consuming. Thus, indirect immunofluorescence following microirradiation with our system can be difficult as one must find a small amount of treated cells among hundreds of thousands of untreated cells. However, this was not an issue for us as we used GFP-tagged repair proteins and live imaging for the majority of our experiments.

Additional limitations to microirradiation were that treating cells was more time and resource-consuming the CSK+R pre-extraction method. As well, the NIR laser system used for this study is considerably rare, with only one laser available at our university. A very specific setup with this instrumentation was necessary. Furthermore, the system is delicate and broke down several times during this study. In the end, this prevented us from conducting kinetic studies to compare factor recruitment in wild-type and D192A/D195R-expressing cells. Future work should address this. Overall, despite these limitations, microirradiation appeared to be a much more reliable and convincing technique with more potential applications than the pre-extraction method. For this reason, we employed microirradiation in our study.

4.4 Helix five of the Ku70 vWA domain and the NHEJ complex

4.4.1 The Ku-PAXX interaction

We considered several possible roles of helix five of the Ku70 vWA domain in the assembly of the NHEJ complex, including its ability to interact with the recently identified NHEJ factor PAXX. PAXX, paralog of XRCC4 and XLF, is structurally similar to XRCC4 and XLF at the N-terminus, and promotes DNA DSB repair[29,30]. PAXX does not directly bind DNA but rather, associates with Ku and is required for assembly of the NHEJ complex[29]. This interaction occurs via the PAXX C-terminus, which diverges from XRCC4 and XLF, and is impaired by the mutation of PAXX

F201[30]. Although the region of PAXX required for the Ku-PAXX interaction has been characterized, the domain of Ku required for this is unknown and thus we considered the possibility that helix five of the Ku70 vWA domain could be involved in the Ku-PAXX interaction.

To test this, we assessed the ability of PAXX to bind the Ku70 N-terminus in vitro using a GST pulldown. An interaction between the Ku70 N-terminus and PAXX was not observed, regardless of whether the D192A/D195R mutation was present in the GST-tagged Ku N-terminus. However, full-length Ku immunoprecipitated from mammalian cells displayed binding with His-PAXX. These data suggest that while the Ku heterodimer interacts with PAXX, the Ku70 vWA domain is not sufficient for the Ku-PAXX interaction and that the role of helix five of the Ku70 vWA domain is likely not related to the Ku-PAXX interaction.

It is not surprising that PAXX interacts with a region of Ku beyond helix five of the Ku70 vWA domain. It is known that helix five of the Ku70 vWA domain is highly conserved and mutation of D195 in yeast, which is homologous to residue to D192 in human Ku70, results in a repair defect[40]. Thus, it is likely that helix five of the Ku70 vWA domain, if involved in a protein-protein interaction, would interact with a protein that is also conserved in yeast. A yeast or invertebrate homologue of PAXX has not been identified thus far[30].

This work has shed light on the PAXX-Ku interaction, suggesting for the first time that this interaction is independent of the Ku70 N-terminus. It could be possible that the Ku N-terminus plays a role in PAXX's binding to the heterodimer, but that additional components of Ku are required for the interaction to occur. Many of Ku's interaction interfaces with NHEJ factors, such as XRCC4 and XLF have not been characterized, likely because Ku70 and Ku80 are unstable without their respective binding partners, making it difficult to study (and map interactions within) certain regions of Ku70 and Ku80 independently[49,50]. Overall, future research in characterizing the Ku-PAXX interaction can be conducted with knowledge that the Ku70 N-terminus is not sufficient

for the interaction and regions beyond this in Ku70 and Ku80 should be the focus in future interaction studies.

4.4.2 Helix five and nucleophosmin

Another possibility that we explored was that helix five could mediate a protein-protein interaction with a yet uncharacterized NHEJ factor. Using a large scale GST pulldown with GST-tagged wild-type and D192A/D195R Ku N-termini followed by mass spectrometry identification of proteins, we attempted to identify an NHEJ factor that associated with the wild-type, but not the mutant Ku N-terminus. The only factor of note that we identified was nucleophosmin (NPM1) and this was limited in that we faced uneven loading in the pulldown from which it was identified. Nevertheless, we considered the possibility that Ku and NPM1 interact, as NPM1 has been implicated in DNA repair in a number of past studies[116–119].

NPM1 was initially characterized for its role in ribosome biosynthesis and transport[120]. However, a potential role for nucleophosmin in DNA repair or damage signaling was suggested when NPM1 was identified as a phosphorylation target by mass spectrometry following DNA damage[116]. It has since been implicated in base excision repair, repair of ribosomal DNA (rDNA), and p53 signaling in response to DNA damage[117,119]. In the context of double strand breaks, nucleophosmin was found to be recruited to IR-induced foci in an RNF8-dependent manner[121]. Interestingly, Ku removal from the break is RNF8-dependent, as well[43]. Nucleophosmin's interaction with RNF8 is mediated by phosphorylation of T199 and a substitution mutation at this position conferred a decreased capacity for DSB repair and prolonged presence of the HR protein Rad51 at damage foci[121]. Furthermore, a radiosensitizing drug, YTR107, was shown to prevent NPM1 from localizing to damage foci, again implicating the protein in repair[118]. This evidence supports the notion of an important DSB repair role for NPM1. However, the link between NPM1 and NHEJ has not been clearly established and having pulled down NPM1 with the Ku N-terminus, we considered an interaction with NPM1 to be a potential role of helix five of the Ku70 vWA domain.

However, when we attempted to validate the results in a small-scale pulldown using the GST tagged wild-type and mutant Ku70 N-termini along with GFP-tagged NPM1 that had been transfected into HeLa cells, we did not observe and Ku-NPM1 interaction. While it is possible that the GFP tag used in this experiment interfered with the Ku-NPM1 interaction or that GFP-NPM1 was outcompeted by endogenous protein, the complete absence of signal generated by NPM1 suggested that the NPM1 identified in the original pulldown was an artifact. Thus, we were unsuccessful in identifying a candidate binding partner for helix five using the large-scale GST pulldown approach, but it should be repeated.

4.4.3 Helix five and Ku tetramerization

A recent study has implicated helix five of the Ku vWA domain in Ku heterodimer tetramerization[52]. This was proposed to have an end bridging function in repair. To validate this, we performed GST pulldowns with GST-tagged Ku70 N-termini and nuclear extracts containing full-length Ku from irradiated and non-irradiated HeLa cells or wild-type Ku70 and Ku70 D192A/D195R-expressing MEFs respectively. We did not observe Ku tetramerization. This discrepancy with the literature could be explained by our use of only the Ku N-terminus for the pulldowns, as the previous Ku tetramerization study used full-length Ku[52]. It is possible that while Ku tetramerization is dependent on helix five, as presented in the past study, it could also require regions beyond the Ku N-terminus to be intact for a stabilizing effect. A docking model of tetramerized Ku generated in the past study shows the Ku70 N-terminus in close proximity with regions of Ku80 and it is possible that two Ku80 molecules are required for tetramerization to occur[52]. Since our pulldown only included the Ku N-terminus, it may have lacked a Ku80 molecule necessary for tetramerization. Therefore, while our data show that the Ku N-terminus is not sufficient for Ku tetramerization, we cannot completely rule out the possibility of Ku tetramerization.

Alternatively, tetramerization may not occur at all or may function beyond NHEJ. The original study showing Ku tetramerization posed several limitations, the major being that none of the experiments demonstrating Ku tetramerization were conducted in the context of DNA damage. A second issue with these experiments was that the primary evidence

for Ku tetramerization was an immunoprecipitation system involving differentially tagged Ku peptides with or without a mutation in helix five. These tagged peptides had been cotransfected into cells and thus, the system was highly artificial. Saturation of the system due to overtransfection could have stimulated aggregation or teteramerization of Ku that would not occur naturally. Neither this study, nor our own, answer the question of whether full-length Ku can tetramerize in response to DNA damage and only when this question is answered can the repair function of Ku tetramerization be elucidated. Thus, further work is needed for a full understanding of this potential function of helix five of the Ku70 vWA domain.

4.4.4 Recruitment of the ligation complex in the helix five mutant

We used a targeted microirradiation approach to assay recruitment of known members of the NHEJ complex to laser-induced DNA damage in live cells. Ku recruitment to microirradiated sites was observed in wild-type Ku70 and Ku70 D192A/D195R expressing cells, consistent with previous reports that mutation of helix five does not affect Ku localization to damage in yeast[40]. It was expected that the D192A/D195R mutation could abolish recruitment of an NHEJ factor. Since the D192A/D195R repair defect is conserved in yeast, we expected that the NHEJ factor whose recruitment is helix five dependent would also be conserved in yeast and that it would be a major player in NHEJ[40]. A DNA-PK homologue has not been identified in yeast. Therefore, it was not considered a likely candidate for interacting with helix five[122]. Thus, we turned our attention to members of the XRCC4-XLF-DNA Ligase IV complex. A Ku-DNA ligase IV interaction was previously reported, but the region of Ku required for this was not mapped[123]. We therefore considered the possibility that helix five of the Ku70 vWA domain is important for the Ku-DNA ligase IV interaction. Additionally, the ligation complex carries out the final ligation step of NHEJ, so we expected that if an NHEJ factor's recruitment were disrupted by the Ku70 D192A/D195R mutation, these proteins would not be recruited in the mutant.

Surprisingly, the D192A/D195R mutation did not prevent ligation complex members' recruitment to microirradiated damage. This indicated that while the mutant harbored a repair defect, repair proteins could still be recruited in the presence of the D192A/D195R

mutation -even those involved in final steps of the NHEJ cascade. Overall, we concluded that helix five is not necessary in recruiting the ligation complex to DSBs. However, as pulsed field gel electrophoresis showed impaired DNA repair as a function of time in the D192A/D195R mutant, it is likely that while the ligation complex is recruited in the repair mutant, it or an upstream step in repair does not function normally[61]. NHEJ is often perceived as a stepwise process, but it has been purported that while Ku stimulates recruitment of downstream NHEJ factors, the recruitment order of proteins downstream of Ku is not well-defined and can vary with damage complexity[124]. Thus, while we observed recruitment of proteins involved in the final step of NHEJ in the Ku70 D192A/D195R mutant, we cannot conclude that *all* NHEJ factors are recruited normally in the mutant.

Repair factors may be recruited to a lesser degree than normal in the D192A/D195R mutant, or not be retained normally at damage. Our work was limited in that we did not study recruitment kinetics of each tagged NHEJ factor and a kinetic study is needed to fully assess the D192A/D195R mutant's ability to recruit NHEJ factors. This will provide insights into factor recruitment levels and retention. Images taken in this study were taken with a slow scan speed, in order to visualize tagged NHEJ factor recruitment, which was sometimes low due to competition with endogenous proteins. While slow scan speed improved resolution of factor recruitment, image acquisition took approximately 30 seconds. At this time point, factor recruitment had already peaked and we were not able to measure a buildup of NHEJ factor recruitment over time to compare across wild-type, knockout, and D192A/D195R expressing cells.

Unexpectedly, we observed recruitment of GFP-XRCC4 in Ku-deficient cells. It has been reported that XRCC4's recruitment is Ku-dependent in a past microirradiation study and we had anticipated an absence of XRCC4 recruitment to damage in Ku-deficient cells[92]. However, this work relied on indirect immunofluorescence and it is possible that our GFP system was slightly more sensitive than immunofluorescence, allowing visualization of low levels of protein recruitment. As XRCC4 has been shown to associate with DNA ends independently of Ku in vitro[125], it is possible that Ku is not required for XRCC4's recruitment to breaks. However, it was surprising to see recruitment of XRCC4, but not

other members of the ligation complex, to damage since these proteins normally act together in repair. While it could be argued that Ku is important for the interaction between XLF and XRCC4[126], which explains the absence of XLF recruitment despite XRCC4 recruitment in Ku-deficient cells, we expect that XRCC4's recruitment here was likely an artifact of overexpression of the protein. XRCC4 is more abundant in cells than DNA-Ligase IV, which could explain why the system saturated for XRCC4, but not DNA ligase IV[127].

4.5 Potential for additional roles of helix five of the Ku70 vWA domain

With the importance of helix five of the Ku70 vWA domain in repair documented in both yeast and mammalian cells, it is clear that this region of Ku has an important role in DNA repair function[52,61]. However, our work has shown that this lies beyond recruitment of the ligation complex, the Ku-PAXX interaction, signaling via lysine residues within the helix, and likely Ku tetramerization. Furthermore, as Ku itself is recruited normally in the D192A/D195R mutant it is doubtful that the D192A/D195R mutation is a structure breaking mutation that completely destabilizes the protein. Additional roles if helix five must be explored to understand its repair function.

We attempted to characterize unidentified NHEJ factors that interact with helix five using a GST pulldown approach. However, this technique posed several limitations. A large amount of time, as well as protein, was required for the experiment. Furthermore, the GST pulldown was technically difficult because the GST-tagged Ku70 N-termini bound to glutathione-agarose beads with relatively low affinity, as compared to GST alone and this resulted in the need for use of large amounts of glutathione-agarose beads in the experiment. Large elution volumes were then needed to isolate pulled down proteins from the beads and this was impractical for loading samples on an SDS-PAGE gel. Despite quantifying the protein bound to beads prior to the pulldown, we faced uneven loading in the experiment, suggesting that our quantification was inaccurate or that not all of the protein used in the pulldown was loaded in the SDS-PAGE gel, possibly due to loss of beads during washes. Overall, the pulldown failed to identify any strong candidate

binding partners for helix five, apart from nucleophosmin which was not reproducible in a small-scale experiment.

It is still possible that helix five could interact with an NHEJ factor that has yet to be characterized and that our screen simply did not identify this factor. Although the basics of NHEJ are well-understood, it is a complex pathway and new, important, proteins involved in NHEJ continue to be identified, as exemplified by the recent characterization of PAXX as an NHEJ factor[29]. To identify novel NHEJ factors that interact with helix five, other techniques beyond our GST pulldown for characterizing protein-protein interactions should be pursued. A potential method for this would be the Bio-ID system[128]. Using Bio-ID, one could create wild-type Ku70 and Ku70 D192A/D195R N-termini fused with the biotin ligase BirA and transfect this into cells. In Bio-ID, BirA biotinylates proteins in close proximity to (and likely interacting with) BirA-fused proteins or peptides. Biotinylated proteins are then purified and identified by mass spectrometry. This technique would be favorable over a GST pulldown as it is more physiologically relevant and does not rely on in vitro binding.

It is also possible that helix five of the Ku70 vWA domain recruits an NHEJ accessory factor. The accessory factors Artemis and PNKP are conserved in yeast[129,130], like the helix five repair defect and therefore could be candidate binding partners for helix five. However, the D192A/D195R mutation is fairly severe suggesting that its role involves major NHEJ proteins, rather than accessory factors[61]. Thus, we favor the idea that an unknown yet essential NHEJ factor is recruited to helix five.

Alternatively, helix five's interaction with TRF2 could promote DNA repair. There have been mixed reports about TRF2's role in repair. While TRF2 has been implicated as a downstream phosphorylation target in ATM signalling and is recruited to microirradiated sites, there is some evidence that only complex damage stimulates TRF2 recruitment[131,132]. However, Tbf1, a yeast protein with homology to TRF1 and TRF2 has been implicated in DSB repair[133]. TRF2 has been identified as a binding partner for helix five of the Ku70 vWA domain within the shelterin complex and while this work focused

on the TRF2-Ku interaction in the context of telomeres, it is possible that TRF2 is mediating the helix's repair function in a yet uncharacterized mechanism[52].

Alternatively, helix five of the Ku70 vWA domain may be involved in promoting Ku removal from DNA DSBs, rather than recruiting an NHEJ factor. Perhaps the helix is involved in recruiting factors that stimulate Ku removal from the break, such as MDC1 or RNF8. This could affect repair if prolonged Ku retention at breaks led to absence of free Ku to repair newly formed breaks.

It is also possible that helix five is involved in mediating the cell's DNA repair pathway choice. The primary DSB repair processes in mammals are NHEJ and homologous recombination, with the latter permitted in S and G_2 phases of the cell cycle when a homologous chromosome can act as a template for repair[19]. However, Ku is able to bind DSBs, regardless of cell cycle stage and it has been proposed that Ku removal or loss of Ku affinity for DNA as a result of end resection, which yields single-stranded DNA, is required for HR to occur[134,34]. It is possible that mutation of helix five of the Ku70 vWA domain prevents Ku removal from DNA or that it prevents recruitment of a factor involved in this removal, leading to aberrant regulation of DSB repair pathway choice. Additionally, a third process, called alternative NHEJ (aNHEJ) is employed in cases where NHEJ is dysfunctional. Pathway choice between classical NHEJ and aNHEJ is Ku dependent[135] and it is possible that helix five of the Ku70 vWA domain interacts with a key protein involved in repressing aNHEJ or stimulating classical NHEJ when classical NHEJ *is* functional.

In summary, although we have not identified the function of helix five of the Ku70 vWA domain, several possibilities remain for the helix's role in repair. Whether this is via a protein-protein interaction, as we hypothesized, or a signaling interaction is unclear and further investigation is needed to fully characterize the function of this region despite our efforts.

4.6 Insights into Ku-mediated inhibition of Aurora B

While the primary focus of this project was characterizing the function of helix five of the Ku70 vWA domain, this was a sub-objective within one of our lab's major goals: to identify functions of the poorly-characterized Ku70 vWA domain as a whole. Beyond helix five of Ku70's vWA domain, work in our lab has focused on S155 within helix four of the Ku70 vWA domain. We have shown that phosphorylation of S155 is important for DNA damage signaling[61].

Phosphorylation of this residue in response to DNA damage leads to inhibition of the kinase Aurora B, which is involved in mitosis and cell cycle progression[62]. Aurora B's regulation of Ku is thought to prevent cells from replicating damaged DNA by pausing the cell cycle and giving cells time to repair their DNA. Major, irreparable damage would lead to constitutive Ku70 S155 phosphorylation and senescence of cells that have undergone severe DNA damage. A Ku-Aurora B interaction had been demonstrated by immunoprecipitation and by an immunofluorescence proximity ligation assay (PLA), which generates a signal in fixed cells where two probed proteins exist in close proximity[136,62]. However, we wanted to show evidence of Aurora B being recruited to damage in living cells and microirradiation gave us the ability to do so.

Using this technique, we were able to observe recruitment of Aurora B to laser-induced DNA damage and measure kinetics of this recruitment through live imaging. As a result, we were able to demonstrate, for the first time, that Aurora B is recruited to DNA damage in living cells[62]. While this work stretched beyond the major goal of this project, it illustrates the usefulness of a technique that we optimized in the lab and the wide scope of applications that the technique could be used for.

This work was limited, however, in that we could not fully characterize accumulation kinetics of Aurora B to laser-induced DNA damage. Like other GFP-tagged NHEJ factors used in this study, the GFP-Aurora B in our experiments competed with endogenous protein for DNA damage and the recruitment signal was weak. It could only be detected when relatively high-quality images were acquired through use of a slow scan speed (approximately 16s). As Aurora B was recruited rapidly to damage, protein

recruitment peaked during acquisition of the first image and increasing accumulation of Aurora B at the break over time was not captured. To perform a stronger kinetic study, these experiments should be performed in Aurora B-deficient cells. Without endogenous Aurora B competition, the GFP-Aurora B recruitment signal would be stronger and we would be able to resolve recruitment at a higher scan speed (despite higher scan speed generating lower-quality images), allowing us to capture increasing Aurora B accumulation at earlier time points. However, as Aurora B is involved in cell cycle regulation, Aurora B-deficiency would be problematic in cultured cells and to our knowledge, an immortalized Aurora B-deficient cell line is not available.

4.7 Future directions

We have ruled out several possibilities for the function of helix five of the Ku70 vWA domain. Our work has indicated that mutation of helix five does not affect Ku recruitment to DSBs, does not appear to mediate Ku tetramerization on its own, does not rely on lysine signaling through K182 and K189 alone or together to function in repair, does not mediate the Ku-PAXX interaction, and does not abolish recruitment of members of the ligation complex. However, despite identifying a multitude of things that helix five does not do, we have yet to identify the true function of the helix and this is the primary limitation in this study.

Laser microirradiation provided us with insights into NHEJ complex formation in living Ku70 knockout, wild-type, and D192A/D195R cells. However, recruitment of the GFP-tagged proteins sometimes appeared to be weak and this was another limitation of our work. This occurred despite the fact that damage induction was evident with γ-H_2AX immunostaining. This low level of recruitment can be attributed, to some extent, to high levels of protein transfection. However, using GFP tagged proteins was preferable to immunofluorescence as it allowed live imaging of protein recruitment to DSBs. Another reason for poor recruitment was likely the presence of endogenous protein within cells. Endogenously expressed protein would compete with heavier GFP-tagged protein and reduce the signal at laser-induced damage. If necessary, to surpass this issue, each protein could be depleted from wild-type or mutant-expressing cells by siRNA. However, this would be very time and resource-consuming. Another option would be to increase the

laser power or iterations of the laser to increase levels of damage, as our system induced relatively low amounts of breaks as compared to some studies[92,111]. However, we found that recruitment to laser-induced DNA damage could usually be observed in treated cells, even though levels of protein accumulation did not produce an extremely powerful signal.

While microirradiation yielded information regarding recruitment of NHEJ factors to laser-induced DNA damage, it did not provide us with insights into the activities of each NHEJ factor at the break. We can conclude that the Ku70 D192A/D195R mutation does not abolish NHEJ factor recruitment. However, our system does not provide information beyond recruitment and cannot provide us with insights into each NHEJ factor's activity at the break. Furthermore, as we did not conduct a kinetic study of factor recruitment, we cannot rule out the possibility that an NHEJ factor, although recruited in the D192A/D195R mutant, is recruited to a lesser degree or that a factor is not retained at damage. A kinetic study of NHEJ factor recruitment would greatly strengthen our results and this is highly recommended for future studies.

Another useful future study that could be accomplished by microirradiation would be assessing the retention of GFP-tagged Ku at laser-induced DSBs in wild-type and mutant expressing cells. This would require imaging of GFP-tagged Ku at various time points following damage. As Ku dissociates from damage rapidly within the first 15 minutes of damage and more slowly afterwards, a reasonable time frame for imaging the microirradiated cells would be every ten to fifteen minutes for two hours[104]. If the D192A/D195R mutation conferred a Ku removal defect, this would be made evident by persistence of Ku70 D192A/D195R at the DSB as compared to wild-type Ku70 after fifteen minutes as well as at later time points.

We were unable to identify unknown factors that associated with helix five of the Ku70 vWA domain using a GST pulldown approach. However, this should be further explored. The GST pulldown approach used herein was time-consuming and reagent-heavy and we recommend that a different system, such as the BioID system should be employed for future work[128].

Another aim of future work should be to investigate a potential repair function of the helix five-TRF2 interaction. This could be accomplished using our system of comparing NHEJ factor recruitment to microirradiated sites in wild-type and D192A/D195R-expressing Ku70 knockout MEFs using GFP-tagged TRF2 or indirect immunofluorescence.

4.8 Conclusion

The purpose of this thesis was to characterize the function of helix five of the Ku70 von Willebrand A domain in non-homologous end joining. We evaluated the possibility that two lysine residues within the helix could be involved in repair, finding that they did not play a role in cell survival in response to IR. We also tested the previously reported observation that helix five mediates Ku tetramerization. Surprisingly, we did not observe Ku binding to a GST-tagged Ku N-terminal peptide which suggested that the Ku N-terminus alone, regardless of the integrity of helix five, was not sufficient for Ku tetramerization. We also evaluated the ability of helix five of the Ku70 vWA domain to mediate an interaction between Ku and the newly identified DSB repair protein PAXX. This interaction was found to occur independently of helix five and the Ku70 N-terminus was not sufficient for this interaction to occur, implying that PAXX likely associates with a region of Ku beyond the Ku70 vWA domain. A targeted microirradiation assay revealed that members of the ligation complex, as well as Ku itself, were recruited to DNA DSBs in cells with a D192A/D195R DNA repair mutation in helix five. Since known conserved and essential NHEJ proteins appeared to be recruited normally, this suggested that an uncharacterized repair factor could be involved in helix five's repair function. We were unable to identify novel NHEJ factors that interacted with wild-type, but not mutant, helix five in a large-scale GST pulldown and suggest using a new system to screen for unknown factors that could interact with helix five.

Overall, while we were unable to fully characterize helix five's function in repair, we explored several potential roles of the helix and have narrowed the search for its function. This will simplify future studies in characterizing the role of the helix. This work will provide insights into the mechanisms through which Ku promotes NHEJ and formation of the NHEJ complex, thus aiding in the knowledge of the universal eukaryotic process

of DSB repair. An understanding of DNA DSB repair, in turn, could lead to improvement in cancer therapeutics targeting this processes, allowing for development of alternative strategies to target tumor cells.

CHAPTER 5: REFERENCES

1. Polo, S. E. & Jackson, S. P. Dynamics of DNA damage response proteins at DNA breaks: a focus on protein modifications. *Genes Dev.* **25,** 409–433 (2011).

2. Jackson, S. P. & Bartek, J. The DNA-damage response in human biology and disease. *Nature* **461,** 1071–1078 (2009).

3. Squatrito, M. & Holland, E. C. DNA damage response and growth factor signaling pathways in gliomagenesis and therapeutic resistance. *Cancer Res.* **71,** 5945–5949 (2011).

4. Chapman, J. R., Taylor, M. R. G. & Boulton, S. J. Playing the End Game: DNA Double-Strand Break Repair Pathway Choice. *Mol. Cell* **47,** 497–510 (2012).

5. Helleday, T., Lo, J., van Gent, D. C. & Engelward, B. P. DNA double-strand break repair: from mechanistic understanding to cancer treatment. *DNA Repair (Amst).* **6,** 923–935 (2007).

6. Kastan, M. B. & Bartek, J. Cell-cycle checkpoints and cancer. *Nature* **432,** 316–323 (2004).

7. Hall EJ, G. A. J. *Radiobiology for the Radiologist*. **6,** (Lippincott Williams & Wilkins, 2006).

8. Löbrich, M. & Jeggo, P. A. The impact of a negligent G2/M checkpoint on genomic instability and cancer induction. *Nat. Rev. Cancer* **7,** 861–869 (2007).

9. Povirk, L. F. Biochemical mechanisms of chromosomal translocations resulting from DNA double-strand breaks. *DNA Repair (Amst).* **5,** 1199 (2006).

10. Mistry, A. R. *et al.* DNA topoisomerase II in therapy-related acute promyelocytic leukemia. *N. Engl. J. Med.* **352,** 1529–1538 (2005).

11. Sedelnikova, O. A. *et al.* Role of oxidatively induced DNA lesions in human pathogenesis. *Mutat. Res. Mutat. Res.* **704,** 152–159 (2010).

12. Mehta, A. & Haber, J. E. Sources of DNA double-strand breaks and models of recombinational DNA repair. *Cold Spring Harb. Perspect. Biol.* **6,** a016428 (2014).

13. Reynolds, P., Cooper, S., Lomax, M. & O'Neill, P. Disruption of PARP1 function inhibits base excision repair of a sub-set of DNA lesions. *Nucleic Acids Res.* **43,** 4028–4038 (2015).

14. Caldecott, K. W. DNA single-strand break repair. *Exp. Cell Res* **329,** 2–8 (2014).

15. Inagaki, A., Schoenmakers, S. & Baarends, W. M. DNA double strand break repair, chromosome synapsis and transcriptional silencing in meiosis. *Epigenetics* **5,** 255–266 (2010).

16. Zeng, Z., Cortés-Ledesma, F., El Khamisy, S. F. & Caldecott, K. W. TDP2/TTRAP is the major 5′-tyrosyl DNA phosphodiesterase activity in vertebrate cells and is critical for cellular resistance to topoisomerase II-induced DNA damage. *J. Biol. Chem.* **286,** 403–409 (2011).

17. Ramsden, D. A., Weed, B. D. & Reddy, Y. V. R. V (D) J recombination: born to be wild. in *Seminars in cancer biology* **20,** 254–260 (Elsevier, 2010).

18. Schatz, D. G. & Swanson, P. C. V (D) J recombination: mechanisms of initiation. *Annu. Rev. Genet.* **45,** 167–202 (2011).

19. Shrivastav, M., De Haro, L. P. & Nickoloff, J. A. Regulation of DNA double-strand break repair pathway choice. *Cell Res.* **18,** 134–147 (2008).

20. Deriano, L. & Roth, D. B. Modernizing the nonhomologous end-joining repertoire: alternative and classical NHEJ share the stage. *Annu. Rev. Genet.* **47,** 433–455 (2013).

21. Langerak, P., Mejia-Ramirez, E., Limbo, O. & Russell, P. Release of Ku and MRN from DNA ends by Mre11 nuclease activity and Ctp1 is required for homologous recombination repair of double-strand breaks. *PLoS Genet.* **7,** e1002271 (2011).

22. Simsek, D. & Jasin, M. Alternative end-joining is suppressed by the canonical NHEJ component Xrcc4-ligase IV during chromosomal translocation formation. *Nat. Struct. Mol. Biol.* **17,** 410–416 (2010).

23. Jackson, S. P. Sensing and repairing DNA double-strand breaks. *Carcinogenesis* **23,** 687–696 (2002).

24. Szostak, J. W., Orr-Weaver, T. L., Rothstein, R. J. & Stahl, F. W. The double-strand-break repair model for recombination. *Cell* **33,** 25–35 (1983).

25. Sung, P. & Klein, H. Mechanism of homologous recombination: mediators and helicases take on regulatory functions. *Nat. Rev. Mol. Cell Biol.* **7,** 739–750 (2006).

26. Karran, P. DNA double strand break repair in mammalian cells. *Curr. Opin. Genet. Dev.* **10,** 144–150 (2000).

27. Mahaney, B. L., Meek, K. & Lees-Miller, S. P. Repair of ionizing radiation-induced DNA double-strand breaks by non-homologous end-joining. *Biochem. J.* **417,** 639–650 (2009).

28. Wang, C. & Lees-Miller, S. P. Detection and Repair of Ionizing Radiation-Induced DNA Double Strand Breaks: New Developments in Nonhomologous End Joining. *Int. J. Radiat. Oncol. Biol. Phys.* (2013). doi:10.1016/j.ijrobp.2013.01.011; 10.1016/j.ijrobp.2013.01.011

29. Ochi, T. *et al.* PAXX, a paralog of XRCC4 and XLF, interacts with Ku to promote DNA double-strand break repair. *Science (80-.).* **347,** 185–188 (2015).

30. Xing, M. *et al.* Interactome analysis identifies a new paralogue of XRCC4 in non-homologous end joining DNA repair pathway. *Nat. Commun.* **6,** (2015).

31. Strande, N. T., Waters, C. A. & Ramsden, D. A. Resolution of complex ends by Nonhomologous end joining-better to be lucky than good? *Genome Integr.* **3,** 1–11 (2012).

32. Oike, T. *et al.* Garcinol, a histone acetyltransferase inhibitor, radiosensitizes cancer cells by inhibiting non-homologous end joining. *Int. J. Radiat. Oncol. Biol. Phys.* **84,** 815–821 (2012).

33. Srivastava, M. *et al.* An inhibitor of nonhomologous end-joining abrogates double-strand break repair and impedes cancer progression. *Cell* **151,** 1474–1487 (2012).

34. Fell, V. L. & Schild-Poulter, C. The Ku heterodimer: Function in DNA repair and beyond. *Mutat. Res. Mutat. Res.* (2014).

35. Mimori, T. *et al.* Characterization of a high molecular weight acidic nuclear protein recognized by autoantibodies in sera from patients with polymyositis-scleroderma overlap. *J. Clin. Invest.* **68,** 611 (1981).

36. Mimori, T., Hardin, J. A. & Steitz, J. A. Characterization of the DNA-binding protein antigen Ku recognized by autoantibodies from patients with rheumatic disorders. *J. Biol. Chem.* **261,** 2274–2278 (1986).

37. Griffith, A. J., Blier, P. R., Mimori, T. & Hardin, J. A. Ku polypeptides synthesized in vitro assemble into complexes which recognize ends of double-stranded DNA. *J. Biol. Chem.* **267,** 331–338 (1992).

38. Rathmell, W. K. & Chu, G. Involvement of the Ku autoantigen in the cellular response to DNA double-strand breaks. *Proc. Natl. Acad. Sci.* **91,** 7623–7627 (1994).

39. Grundy, G. J., Moulding, H. A., Caldecott, K. W. & Rulten, S. L. One ring to bring them all—the role of Ku in mammalian non-homologous end joining. *DNA Repair (Amst).* **17,** 30–38 (2014).

40. Ribes-Zamora, A., Mihalek, I., Lichtarge, O. & Bertuch, A. A. Distinct faces of the Ku heterodimer mediate DNA repair and telomeric functions. *Nat. Struct. Mol. Biol.* **14,** 301–307 (2007).

41. Yoo, S. & Dynan, W. S. Geometry of a complex formed by double strand break repair proteins at a single DNA end: recruitment of DNA-PKcs induces inward translocation of Ku protein. *Nucleic Acids Res.* **27,** 4679–4686 (1999).

42. Postow, L. & Funabiki, H. An SCF complex containing Fbxl12 mediates DNA damage-induced Ku80 ubiquitylation. *Cell Cycle* **12,** 587–595 (2013).

43. Feng, L. & Chen, J. The E3 ligase RNF8 regulates KU80 removal and NHEJ repair. *Nat. Struct. Mol. Biol.* **19,** 201–206 (2012).

44. Brown, J. S. *et al.* Neddylation Promotes Ubiquitylation and Release of Ku from DNA-Damage Sites. *Cell Rep.* (2015).

45. Wu, D., Topper, L. M. & Wilson, T. E. Recruitment and dissociation of nonhomologous end joining proteins at a DNA double-strand break in Saccharomyces cerevisiae. *Genetics* **178,** 1237–1249 (2008).

46. Kosova, A. A., Lavrik, O. I. & Khodyreva, S. N. Ku Antigen Interaction with Apurinic/Apyrimidinic Sites: Nonhomologous End Joining Vs Base Excision Repair. *MOJ Proteomics Bioinform* **1,** 18 (2014).

47. Li, H., Marple, T. & Hasty, P. Ku80-deleted cells are defective at base excision repair. *Mutat. Res. Mol. Mech. Mutagen.* **745,** 16–25 (2013).

48. Li, H. *et al.* Deleting Ku70 is milder than deleting Ku80 in p53-mutant mice and cells. *Oncogene* **28,** 1875–1878 (2009).

49. Singleton, B. K. *et al.* Molecular and biochemical characterization of xrs mutants defective in Ku80. *Mol. Cell. Biol.* **17,** 1264–1273 (1997).

50. Gu, Y., Jin, S., Gao, Y., Weaver, D. T. & Alt, F. W. Ku70-deficient embryonic stem cells have increased ionizing radiosensitivity, defective DNA end-binding activity, and inability to support V(D)J recombination. *Proc. Natl. Acad. Sci. U. S. A.* **94,** 8076–8081 (1997).

51. Li, P. *et al.* ABH2 couples regulation of ribosomal DNA transcription with DNA alkylation repair. *Cell Rep.* **4,** 817–829 (2013).

52. Ribes-Zamora, A., Indiviglio, S. M., Mihalek, I., Williams, C. L. & Bertuch, A. A. TRF2 Interaction with Ku Heterotetramerization Interface Gives Insight into c-NHEJ Prevention at Human Telomeres. *Cell Rep.* **5,** 194–206 (2013).

53. Palm, W. & de Lange, T. How shelterin protects mammalian telomeres. *Annu. Rev. Genet.* **42,** 301–334 (2008).

54. Celli, G. B., Denchi, E. L. & de Lange, T. Ku70 stimulates fusion of dysfunctional telomeres yet protects chromosome ends from homologous recombination. *Nat. Cell Biol.* **8,** 885–890 (2006).

55. Sfeir, A. & de Lange, T. Removal of shelterin reveals the telomere end-protection problem. *Science (80-.).* **336,** 593–597 (2012).

56. Stellwagen, A. E., Haimberger, Z. W., Veatch, J. R. & Gottschling, D. E. Ku interacts with telomerase RNA to promote telomere addition at native and broken chromosome ends. *Genes Dev.* **17,** 2384–2395 (2003).

57. Wang, Y., Ghosh, G. & Hendrickson, E. A. Ku86 represses lethal telomere deletion events in human somatic cells. *Proc. Natl. Acad. Sci.* **106,** 12430–12435 (2009).

58. Ciccia, A. & Elledge, S. J. The DNA damage response: making it safe to play with knives. *Mol. Cell* **40,** 179–204 (2010).

59. Tomimatsu, N. *et al.* Ku70/80 modulates ATM and ATR signaling pathways in response to DNA double strand breaks. *J. Biol. Chem.* **282,** 10138–10145 (2007).

60. Zhou, X.-Y. *et al.* Ku affects the ATM-dependent S phase checkpoint following ionizing radiation. *Oncogene* **21,** 6377–6381 (2002).

61. Fell, V. L. & Schild-Poulter, C. Ku regulates signaling to DNA damage response pathways through the Ku70 von Willebrand A domain. *Mol. Cell. Biol.* **32,** 76–87 (2012).

62. Fell, V. L., Rogers, S. R., Aitken, A. S., Hoffer, S. M. & Schild-Poulter, C. Ku70 phosphorylation mediates Aurora B inhibition and activation of the DNA damage response. *Nucleic Acids Res.* **Submitted,** (2015).

63. Bertinato, J., Schild-Poulter, C. & Hache, R. J. Nuclear localization of Ku antigen is promoted independently by basic motifs in the Ku70 and Ku80 subunits. *J. Cell Sci.* **114,** 89–99 (2001).

64. Koike, M., Ikuta, T., Miyasaka, T. & Shiomi, T. Ku80 can translocate to the nucleus independent of the translocation of Ku70 using its own nuclear localization signal. *Oncogene* **18,** 7495–7505 (1999).

65. Nussenzweig, A. *et al.* Requirement for Ku80 in growth and immunoglobulin V (D) J recombination. *Nature* **382,** 551–555 (1996).

66. Manis, J. P. *et al.* Ku70 is required for late B cell development and immunoglobulin heavy chain class switching. *J. Exp. Med.* **187,** 2081–2089 (1998).

67. Gu, Y. *et al.* Growth retardation and leaky SCID phenotype of Ku70-deficient mice. *Immunity* **7,** 653 (1997).

68. Ouyang, H. *et al.* Ku70 is required for DNA repair but not for T cell antigen receptor gene recombination in vivo. *J. Exp. Med.* **186,** 921–929 (1997).

69. Li, H., Vogel, H., Holcomb, V. B., Gu, Y. & Hasty, P. Deletion of Ku70, Ku80, or both causes early aging without substantially increased cancer. *Mol. Cell. Biol.* **27,** 8205–8214 (2007).

70. Difilippantonio, M. J. *et al.* DNA repair protein Ku80 suppresses chromosomal aberrations and malignant transformation. *Nature* **404,** 510–514 (2000).

71. Qiao, B. *et al.* Imatinib radiosensitizes bladder cancer by targeting homologous recombination. *Cancer Res.* **73,** 1611–1620 (2013).

72. Walker, J. R., Corpina, R. A. & Goldberg, J. Structure of the Ku heterodimer bound to DNA and its implications for double-strand break repair. *Nature* **412,** 607–614 (2001).

73. Shin, D. S., Chahwan, C., Huffman, J. L. & Tainer, J. A. Structure and function of the double-strand break repair machinery. *DNA Repair (Amst).* **3,** 863–873 (2004).

74. Downs, J. A. & Jackson, S. P. A means to a DNA end: the many roles of Ku. *Nat. Rev. cell Biol.* **5,** 367–378 (2004).

75. Aravind, L. & Koonin, E. V. Prokaryotic homologs of the eukaryotic DNA-end-binding protein Ku, novel domains in the Ku protein and prediction of a prokaryotic double-strand break repair system. *Genome Res.* **11,** 1365–1374 (2001).

76. Whittaker, C. A. & Hynes, R. O. Distribution and evolution of von Willebrand/integrin A domains: widely dispersed domains with roles in cell adhesion and elsewhere. *Mol. Biol. Cell* **13,** 3369–3387 (2002).

77. Grundy, G. J. *et al.* APLF promotes the assembly and activity of non-homologous end joining protein complexes. *EMBO J.* **32,** 112–125 (2013).

78. Doherty, A. J. & Jackson, S. P. DNA repair: how Ku makes ends meet. *Curr. Biol.* **11,** R920–R924 (2001).

79. Papadopoulos, J. S. & Agarwala, R. COBALT: constraint-based alignment tool for multiple protein sequences. *Bioinformatics* **23,** 1073–1079 (2007).

80. Waterhouse, A. M., Procter, J. B., Martin, D. M. A., Clamp, M. & Barton, G. J. Jalview Version 2—a multiple sequence alignment editor and analysis workbench. *Bioinformatics* **25,** 1189–1191 (2009).

81. Kolas, N. K. *et al.* Orchestration of the DNA-damage response by the RNF8 ubiquitin ligase. *Science* **318,** 1637–1640 (2007).

82. Postow, L. *et al.* Ku80 removal from DNA through double strand break-induced ubiquitylation. *J. Cell Biol.* **182,** 467–479 (2008).

83. Galanty, Y. *et al.* Mammalian SUMO E3-ligases PIAS1 and PIAS4 promote responses to DNA double-strand breaks. *Nature* **462,** 935–939 (2009).

84. Kim, W. *et al.* Systematic and quantitative assessment of the ubiquitin-modified proteome. *Mol. Cell* **44,** 325–340 (2011).

85. Subramanian, C., Hada, M., Opipari Jr, A. W., Castle, V. P. & Kwok, R. P. CREB-binding protein regulates Ku70 acetylation in response to ionization radiation in neuroblastoma. *Mol. Cancer Res.* **11,** 173–181 (2013).

86. Singleton, B. K., Torres-Arzayus, M. I., Rottinghaus, S. T., Taccioli, G. E. & Jeggo, P. A. The C terminus of Ku80 activates the DNA-dependent protein kinase catalytic subunit. *Mol. Cell. Biol.* **19,** 3267–3277 (1999).

87. Ma, Y., Pannicke, U., Schwarz, K. & Lieber, M. R. Hairpin opening and overhang processing by an Artemis/DNA-dependent protein kinase complex in nonhomologous end joining and V (D) J recombination. *Cell* **108,** 781–794 (2002).

88. Mahajan, K. N., Nick McElhinny, S. A., Mitchell, B. S. & Ramsden, D. A. Association of DNA polymerase mu (pol mu) with Ku and ligase IV: role for pol mu in end-joining double-strand break repair. *Mol. Cell. Biol.* **22,** 5194–5202 (2002).

89. Lee, J. W. *et al.* Implication of DNA polymerase λ in alignment-based gap filling for nonhomologous DNA end joining in human nuclear extracts. *J. Biol. Chem.* **279,** 805–811 (2004).

90. Rasouli-Nia, A., Karimi-Busheri, F. & Weinfeld, M. Stable down-regulation of human polynucleotide kinase enhances spontaneous mutation frequency and

sensitizes cells to genotoxic agents. *Proc. Natl. Acad. Sci. U. S. A.* **101,** 6905–6910 (2004).

91. McElhinny, S. A. N., Snowden, C. M., McCarville, J. & Ramsden, D. A. Ku recruits the XRCC4-ligase IV complex to DNA ends. *Mol. Cell. Biol.* **20,** 2996–3003 (2000).

92. Mari, P.-O. *et al.* Dynamic assembly of end-joining complexes requires interaction between Ku70/80 and XRCC4. *Proc. Natl. Acad. Sci.* **103,** 18597–18602 (2006).

93. Costes, S. V, Chiolo, I., Pluth, J. M., Barcellos-Hoff, M. H. & Jakob, B. Spatiotemporal characterization of ionizing radiation induced DNA damage foci and their relation to chromatin organization. *Mutat. Res.* **704,** 78–87 (2010).

94. Mah, L. J., El-Osta, A. & Karagiannis, T. C. γH2AX: a sensitive molecular marker of DNA damage and repair. *Leukemia* **24,** 679–686 (2010).

95. Rogakou, E. P., Boon, C., Redon, C. & Bonner, W. M. Megabase chromatin domains involved in DNA double-strand breaks in vivo. *J. Cell Biol.* **146,** 905–916 (1999).

96. Kong, X. *et al.* Comparative analysis of different laser systems to study cellular responses to DNA damage in mammalian cells. *Nucleic Acids Res.* **37,** e68 (2009).

97. Britton, S., Coates, J. & Jackson, S. P. A new method for high-resolution imaging of Ku foci to decipher mechanisms of DNA double-strand break repair. *J. Cell Biol.* **202,** 579–595 (2013).

98. Darżynkiewicz, Z., Traganos, F., Sharpless, T. & Melamed, M. R. Thermal denaturation of DNA in situ as studied by acridine orange staining and automated cytofluorometry. *Exp. Cell Res.* **90,** 411–428 (1975).

99. Kielbassa, C., Roza, L. & Epe, B. Wavelength dependence of oxidative DNA damage induced by UV and visible light. *Carcinogenesis* **18,** 811–816 (1997).

100. Dinant, C. *et al.* Activation of multiple DNA repair pathways by sub-nuclear damage induction methods. *J. Cell Sci.* **120,** 2731–2740 (2007).

101. Zheng, L. *et al.* MRE11 complex links RECQ5 helicase to sites of DNA damage. *Nucleic Acids Res.* **37,** 2645–2657 (2009).

102. Bekker-Jensen, S. *et al.* Spatial organization of the mammalian genome surveillance machinery in response to DNA strand breaks. *J. Cell Biol.* **173,** 195–206 (2006).

103. Harper, J. V *et al.* Induction of persistent double strand breaks following multiphoton irradiation of cycling and G1-arrested mammalian cells-replication-induced double strand breaks. *Photochem. Photobiol.* **84,** 1506–1514 (2008).

104. Reynolds, P. *et al.* The dynamics of Ku70/80 and DNA-PKcs at DSBs induced by ionizing radiation is dependent on the complexity of damage. *Nucleic Acids Res.* gks879 (2012).

105. Roberts, S. A. *et al.* Ku is a 5′-dRP/AP lyase that excises nucleotide damage near broken ends. *Nature* **464,** 1214–1217 (2010).

106. Andrews, N. C. & Faller, D. V. A rapid micropreparation technique for extraction of DNA-binding proteins from limiting numbers of mammalian cells. *Nucleic Acids Res.* **19,** 2499 (1991).

107. Burgess, A. *et al.* Loss of human Greatwall results in G2 arrest and multiple mitotic defects due to deregulation of the cyclin B-Cdc2/PP2A balance. *Proc. Natl. Acad. Sci.* **107,** 12564–12569 (2010).

108. Kruhlak, M. J. *et al.* Changes in chromatin structure and mobility in living cells at sites of DNA double-strand breaks. *J. Cell Biol.* **172,** 823–834 (2006).

109. Yano, K. *et al.* Ku recruits XLF to DNA double-strand breaks. *EMBO Rep.* **9,** 91–96 (2008).

110. Watanabe, R. *et al.* SWI/SNF factors required for cellular resistance to DNA damage include ARID1A and ARID1B and show interdependent protein stability. *Cancer Res.* **74,** 2465–2475 (2014).

111. Uematsu, N. *et al.* Autophosphorylation of DNA-PKCS regulates its dynamics at DNA double-strand breaks. *J. Cell Biol.* **177,** 219–229 (2007).

112. Sharma, A., Singh, K. & Almasan, A. in *DNA Repair Protocols* 613–626 (Springer, 2012).

113. Chan, D. W. *et al.* Autophosphorylation of the DNA-dependent protein kinase catalytic subunit is required for rejoining of DNA double-strand breaks. *Genes Dev.* **16,** 2333–2338 (2002).

114. Koike, M., Yutoku, Y. & Koike, A. Accumulation of Ku70 at DNA double-strand breaks in living epithelial cells. *Exp. Cell Res.* **317,** 2429–2437 (2011).

115. Koike, M., Yutoku, Y. & Koike, A. Establishment of hamster cell lines with EGFP-tagged human XRCC4 and protection from low-dose X-ray radiation. *J. Vet. Med. Sci.* **74,** 1269–1275 (2012).

116. LEE, S. *et al.* A proteomics approach for the identification of nucleophosmin and heterogeneous nuclear ribonucleoprotein C1/C2 as chromatin-binding proteins in response to DNA double-strand breaks. *Biochem. J* **388,** 7–15 (2005).

117. Gjerset, R. A. DNA damage, p14ARF, nucleophosmin (NPM/B23), and cancer. *J. Mol. Histol.* **37,** 239–251 (2006).

118. Sekhar, K. R. *et al.* The novel chemical entity YTR107 inhibits recruitment of nucleophosmin to sites of DNA damage, suppressing repair of DNA double-strand breaks and enhancing radiosensitization. *Clin. Cancer Res.* **17,** 6490–6499 (2011).

119. Poletto, M., Lirussi, L., Wilson, D. M. & Tell, G. Nucleophosmin modulates stability, activity, and nucleolar accumulation of base excision repair proteins. *Mol. Biol. Cell* **25,** 1641–1652 (2014).

120. Yung, B. Y.-M. & Chan, P.-K. Identification and characterization of a hexameric form of nucleolar phosphoprotein B23. *Biochim. Biophys. Acta (BBA)-General Subj.* **925,** 74–82 (1987).

121. Koike, A. *et al.* Recruitment of phosphorylated NPM1 to sites of DNA damage through RNF8-dependent ubiquitin conjugates. *Cancer Res.* **70,** 6746–6756 (2010).

122. Dasika, G. K. *et al.* DNA damage-induced cell cycle checkpoints and DNA strand break repair in development and tumorigenesis. *Oncogene* **18,** 7883–7899 (1999).

123. Costantini, S., Woodbine, L., Andreoli, L., Jeggo, P. A. & Vindigni, A. Interaction of the Ku heterodimer with the DNA ligase IV/Xrcc4 complex and its regulation by DNA-PK. *DNA Repair (Amst).* **6,** 712–722 (2007).

124. Davis, A. J. & Chen, D. J. DNA double strand break repair via non-homologous end-joining. *Transl. Cancer Res.* **2,** 130–143 (2013).

125. Chen, L., Trujillo, K., Sung, P. & Tomkinson, A. E. Interactions of the DNA ligase IV-XRCC4 complex with DNA ends and the DNA-dependent protein kinase. *J. Biol. Chem.* **275,** 26196–26205 (2000).

126. Yano, K., Morotomi-Yano, K., Lee, K.-J. & Chen, D. J. Functional significance of the interaction with Ku in DNA double-strand break recognition of XLF. *FEBS Lett.* **585,** 841–846 (2011).

127. Hammel, M., Yu, Y., Fang, S., Lees-Miller, S. P. & Tainer, J. A. XLF regulates filament architecture of the XRCC4· ligase IV complex. *Structure* **18,** 1431–1442 (2010).

128. Roux, K. J., Kim, D. I., Raida, M. & Burke, B. A promiscuous biotin ligase fusion protein identifies proximal and interacting proteins in mammalian cells. *J. Cell Biol.* **196,** 801–810 (2012).

129. Bonatto, D., Revers, L. F., Brendel, M. & Henriques, J. A. P. The eukaryotic Pso2/Snm1/Artemis proteins and their function as genomic and cellular caretakers. *Brazilian J. Med. Biol. Res.* **38,** 321–334 (2005).

130. Vance, J. R. & Wilson, T. E. Uncoupling of 3′-Phosphatase and 5′-Kinase Functions in Budding Yeast CHARACTERIZATION OF SACCHAROMYCES CEREVISIAE DNA 3′-PHOSPHATASE (TPP1). *J. Biol. Chem.* **276,** 15073–15081 (2001).

131. Huda, N. *et al.* Recruitment of TRF2 to laser-induced DNA damage sites. *Free Radic. Biol. Med.* **53,** 1192–1197 (2012).

132. Chan, K. Y. K. *et al.* DNA double-strand breaks are not sufficient to initiate recruitment of TRF2. *Nature* **200,** 7

133. Bonetti, D., Anbalagan, S., Lucchini, G., Clerici, M. & Longhese, M. P. Tbf1 and Vid22 promote resection and non-homologous end joining of DNA double-strand break ends. *EMBO J.* **32,** 275–289 (2013).

134. Shao, Z. *et al.* Persistently bound Ku at DNA ends attenuates DNA end resection and homologous recombination. *DNA Repair (Amst).* **11,** 310–316 (2012).

135. Fattah, F. *et al.* Ku regulates the non-homologous end joining pathway choice of DNA double-strand break repair in human somatic cells. *PLoS Genet.* **6,** e1000855 (2010).

136. Söderberg, O. *et al.* Direct observation of individual endogenous protein complexes in situ by proximity ligation. *Nat. Methods* **3,** 995–1000 (2006).

CHAPTER 6: APPENDICES

Appendix A: Confirmation of protein expression by Western blot for constructs used in our studies.

Figure A-1 shows expression of fluorescently tagged proteins used for microirradiation in this study after transfection into HeLa cells. All proteins ran at approximately the predicted size.

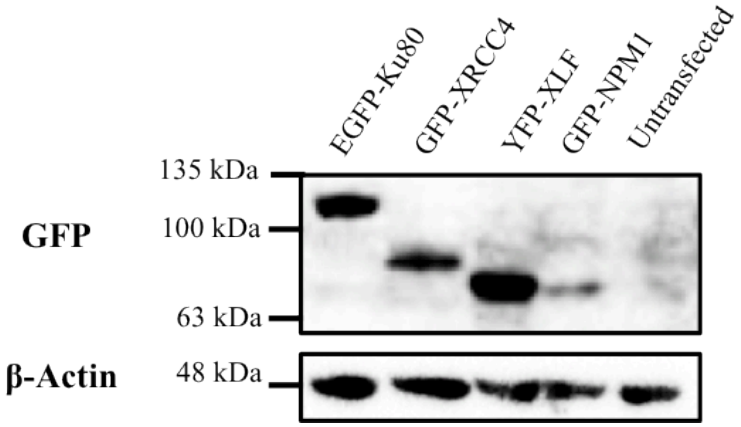

Figure A-1: Expression of fluorescently-tagged DSB repair proteins and candidate repair proteins. HeLa cells were transfected with the indicated fluorescently-tagged proteins. Nuclear extracts were obtained and subjected to analysis by Western blotting for GFP and β-actin.

Figure A-2 illustrates expression of Ku70, the empty pMSCV puro vector, and mutant forms of Ku70 used for this study in infected Ku70 knockout MEFs. Panel A represents single mutants and their expression in comparison to wild-type and empty vector-expressing cells and Panel B represents a double mutant and its expression in comparison to wild-type and empty vector-expressing cells.

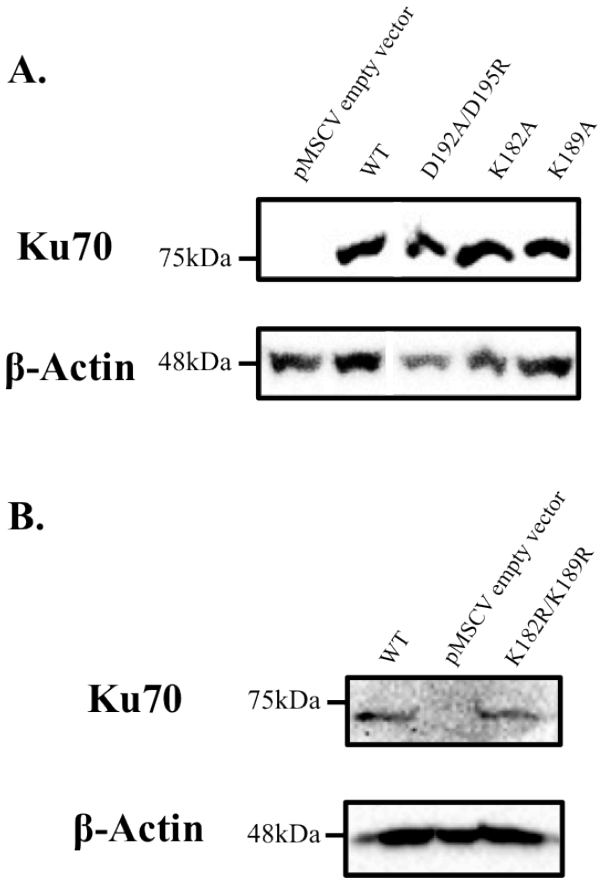

Figure A-2: Expression of Ku70 in Ku70 knockout MEFs infected with various pMSCV-Puro constructs. Ku70 knockout MEFs were infected with the indicated forms of Ku70 or the pMSCV Puro empty vector. Nuclear extracts were collected and subject to Western blotting for Ku70 and for β-actin**.**

Appendix B: Mass spectrometry results from GST Pulldown with the Ku70 and Ku70 D192A/D195R N-terminus showing nucleophosmin as a candidate Ku70 N-terminus binding partner

We used MALDI TOF/TOF mass spectrometry to identify proteins pulled down with the Ku70 N-terminus from irradiated mammalian cell extracts. One of the proteins pulled down was identified as nucleophosmin. Analysis is summarized here:

Concise Summary Report (Project: MALDI_2014, Spot Set: MALDI_2014\... H14, Spot Id: 222732, Peak List Id: 332070, MS Job Run Id: 14022) 2015-06-04 9:49 PM

MATRIX SCIENCE Mascot Search Results

```
User            : kj
Email           : kjurcic@uwo.ca
Search title    : Project: MALDI_2014, Spot Set: MALDI_2014\Michelle_052614, Label: H14, Spot Id: 222732, Peak List Id: 332070, MS Job Run Id: 1402
MS data file    : pmf_H14_140113683148.txt
Database        : NCBInr 20140323 (38032689 sequences; 13525028931 residues)
Taxonomy        : Mus. (174906 sequences)
Timestamp       : 27 May 2014 at 14:50:15 GMT
Top Score       : 52 for gi|55153941, Nucleophosmin 1 [Mus musculus]
```

Mascot Score Histogram

Protein score is -10*Log(P), where P is the probability that the observed match is a random event.
Protein scores greater than 65 are significant (p<0.05).

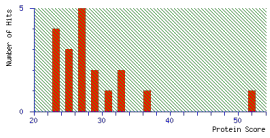

Concise Protein Summary Report

Format As: Concise Protein Summary — Help

Significance threshold p< 0.05 Max. number of hits 5

Preferred taxonomy: All entries

Re-Search All | Search Unmatched

1. gi|55153941 **Mass:** 32739 **Score:** 52 **Expect:** 1.1 **Matches:** 9
   Nucleophosmin 1 [Mus musculus]
   gi|568890274 **Mass:** 32817 **Score:** 52 **Expect:** 1.1 **Matches:** 9
   PREDICTED: nucleophosmin-like [Mus musculus]
   gi|6679108 **Mass:** 32711 **Score:** 52 **Expect:** 1.1 **Matches:** 9
   nucleophosmin isoform 1 [Mus musculus]
   gi|74150401 **Mass:** 32715 **Score:** 42 **Expect:** 9.8 **Matches:** 8
   unnamed protein product [Mus musculus]
   gi|356582426 **Mass:** 28482 **Score:** 38 **Expect:** 25 **Matches:** 7
   nucleophosmin isoform 3 [Mus musculus]
   gi|60551056 **Mass:** 28481 **Score:** 38 **Expect:** 25 **Matches:** 7
   Npm1 protein [Mus musculus]
   gi|148680457 **Mass:** 28919 **Score:** 38 **Expect:** 26 **Matches:** 7
   mCG125894, isoform CRA_b [Mus musculus]
   gi|356582423 **Mass:** 31119 **Score:** 38 **Expect:** 28 **Matches:** 8
   nucleophosmin isoform 2 [Mus musculus]
   gi|148688598 **Mass:** 16038 **Score:** 37 **Expect:** 33 **Matches:** 6
   mCG1037244 [Mus musculus]
   gi|26390517 **Mass:** 25081 **Score:** 34 **Expect:** 62 **Matches:** 6
   unnamed protein product [Mus musculus]

2. gi|148703708 **Mass:** 5332 **Score:** 36 **Expect:** 47 **Matches:** 4
   mCG1037868 [Mus musculus]

3. gi|148679116 **Mass:** 9481 **Score:** 33 **Expect:** 88 **Matches:** 3
   mCG1035992 [Mus musculus]

4. gi|148680755 **Mass:** 111276 **Score:** 32 **Expect:** 1.1e+02 **Matches:** 9
   ATPase, Ca++ transporting, ubiquitous, isoform CRA_b [Mus musculus]
   gi|1438539 **Mass:** 114961 **Score:** 31 **Expect:** 1.3e+02 **Matches:** 9
   sarcoendoplasmic reticulum Ca2+ ATPase SERCA3b [Mus musculus]
   gi|31542159 **Mass:** 114991 **Score:** 31 **Expect:** 1.3e+02 **Matches:** 9
   sarcoplasmic/endoplasmic reticulum calcium ATPase 3 isoform b [Mus musculus]
   gi|148680756 **Mass:** 107170 **Score:** 25 **Expect:** 5e+02 **Matches:** 8
   ATPase, Ca++ transporting, ubiquitous, isoform CRA_c [Mus musculus]

   gi|26354550 **Mass:** 102759 **Score:** 25 **Expect:** 6.1e+02 **Matches:** 8
   unnamed protein product [Mus musculus]

5. gi|26345726 **Mass:** 11917 **Score:** 30 **Expect:** 1.7e+02 **Matches:** 4
   unnamed protein product [Mus musculus]

Search Parameters

```
Type of search        : Peptide Mass Fingerprint
Enzyme                : Trypsin
Fixed modifications   : Carbamidomethyl (C)
Variable modifications : Oxidation (M)
Mass values           : Monoisotopic
Protein Mass          : Unrestricted
Peptide Mass Tolerance : ± 50 ppm
Peptide Charge State  : 1+
Max Missed Cleavages  : 1
Number of queries     : 99
Selected for scoring  : 30
```

Mascot: http://www.matrixscience.com/

Appendix C: Permission for use of copyrighted materials

2015-07-08 10:47 PM

Subject: **Re: Permission to Use Copyrighted Material in a Doctoral/Master's Thesis**
To: Sarah Hoffer

Date: 05/28/15 05:18 PM
From: RUP Permissions Dept.

Dear Sarah,

Thank you for writing. You may reuse the figure in the manner described in your request. The figure must be accompanied by the following citation:

©2013 Britton et al. Journal of Cell Biology. 202:579-595. doi:10.1083/jcb.201303073

With best wishes as you complete your thesis,

RUP Permissions Department

On 5/28/2015 10:34 AM, Sarah Hoffer wrote:

To whom it may concern,

I am a University of Western Ontario graduate student completing my Doctoral / Master's thesis entitled "Characterizing the function of helix five of the Ku70 von Willebrand A Domain in Non-Homologous End Joining". My thesis will be available in full-text on the internet for reference, study and / or copy. Except in situations where a thesis is under embargo or restriction, the electronic version will be accessible through the Western Libraries web pages, the Library's web catalogue, and also through web search engines.I will also be granting Library and Archives Canada and ProQuest/UMI a non-exclusive license to reproduce, loan, distribute, or sell single copies of my thesis by any means and in any form or format. These rights will in no way restrict republication of the material in any other form by you or by others authorized by you.

I would like permission to allow inclusion of the following material in my thesis:

I would like to use two images from Figure 2A (page 582) of the article entitled "A new method for high-resolution imaging of Ku foci to decipher mechanisms of DNA double-strand break repair" from pages 579-595 of JCB volume 202 no. 3.published in 2013 by the Rockefeller University Press in JCB (doi: 10.1083/jcb.201303073).

The material will be attributed through a citation.

Please confirm in writing or by email that these arrangements meet with your approval.

Sincerely,
Sarah Hoffer

Copyright Clearance Center RightsLink®

Home | Create Account | Help | Live Chat

AMERICAN SOCIETY FOR MICROBIOLOGY

Title: Ku Regulates Signaling to DNA Damage Response Pathways through the Ku70 von Willebrand A Domain

Author: Victoria L. Fell, Caroline Schild-Poulter

Publication: Molecular and Cellular Biology

Publisher: American Society for Microbiology

Date: Jan 1, 2012

LOGIN

If you're a copyright.com user, you can login to RightsLink using your copyright.com credentials. Already **a RightsLink user** or want to learn more?

Quick Price Estimate

This permission does not apply to images that are credited to publications other than ASM journals. For images credited to non-ASM journal publications, you will need to obtain permission from the journal referenced in the figure or table legend or credit line before making any use of the image(s) or table(s).

I would like to...	reuse in a dissertation/thesis
Select your currency	CAD – $
Format	Print and electronic
Portion	Figures/tables/images
Number of figures/tables	2
Are you the author of this ASM article?	No
Quick Price	Click Quick Price

QUICK PRICE CONTINUE

This service provides permission for reuse only. Please be advised that obtaining the content you license is a separate transaction not involving RightsLink. We recommend that users contact their librarians or the corresponding author of the article in order to obtain the content. Alternatively, if the article from which you seek to reuse content is under access control, you may purchase a single copy of the article PDF from the individual journal website. Content may be reused according to the terms of your agreement.

To request permission for a type of use not listed, please select "I don't see my intended use" or contact the publisher directly.

Title:	Ku Regulates Signaling to DNA Damage Response Pathways through the Ku70 von Willebrand A Domain
Author:	Victoria L. Fell, Caroline Schild-Poulter
Publication:	Molecular and Cellular Biology
Publisher:	American Society for Microbiology
Date:	Jan 1, 2012

Permissions Request

ASM authorizes an advanced degree candidate to republish the requested material in his/her doctoral thesis or dissertation. If your thesis, or dissertation, is to be published commercially, then you must reapply for permission.

BACK CLOSE WINDOW

NATURE PUBLISHING GROUP LICENSE
TERMS AND CONDITIONS

Aug 17, 2015

This is a License Agreement between Sarah Hoffer ("You") and Nature Publishing Group ("Nature Publishing Group") provided by Copyright Clearance Center ("CCC"). The license consists of your order details, the terms and conditions provided by Nature Publishing Group, and the payment terms and conditions.

All payments must be made in full to CCC. For payment instructions, please see information listed at the bottom of this form.

License Number	3691661384319
License date	Aug 17, 2015
Licensed content publisher	Nature Publishing Group
Licensed content publication	Nature
Licensed content title	Structure of the Ku heterodimer bound to DNA and its implications for double-strand break repair
Licensed content author	John R. Walker, Richard A. Corpina, Jonathan Goldberg
Licensed content date	Aug 9, 2001
Volume number	412
Issue number	6847
Type of Use	reuse in a dissertation / thesis
Requestor type	academic/educational
Format	print and electronic
Portion	figures/tables/illustrations
Number of figures/tables/illustrations	1
Figures	Figure 2a (crystal structure modified in PyMOL)
Author of this NPG article	no
Your reference number	None
Title of your thesis / dissertation	Characterizing the function of helix five of the Ku70 von Willebrand A domain in non-homologous end joining
Expected completion date	Aug 2015
Estimated size (number of pages)	120
Total	0.00 CAD

Terms and Conditions

Terms and Conditions for Permissions

Nature Publishing Group hereby grants you a non-exclusive license to reproduce this material for this purpose, and for no other use,subject to the conditions below:

1. NPG warrants that it has, to the best of its knowledge, the rights to license reuse of this material. However, you should ensure that the material you are requesting is original to Nature Publishing Group and does not carry the copyright of another entity (as credited in the published version). If the credit line on any part of the material you have requested indicates that it was reprinted or adapted by NPG with permission from another source, then you should also seek permission from that source to reuse the material.

2. Permission granted free of charge for material in print is also usually granted for any electronic version of that work, provided that the material is incidental to the work as a whole and that the electronic version is essentially equivalent to, or substitutes for, the print version.Where print permission has been granted for a fee, separate permission must be obtained for any additional, electronic re-use (unless, as in the case of a full paper, this has already been accounted for during your initial request in the calculation of a print run).NB: In all cases, web-based use of full-text articles must be authorized separately through the 'Use on a Web Site' option when requesting permission.

3. Permission granted for a first edition does not apply to second and subsequent editions and for editions in other languages (except for signatories to the STM Permissions Guidelines, or where the first edition permission was granted for free).

4. Nature Publishing Group's permission must be acknowledged next to the figure, table or abstract in print. In electronic form, this acknowledgement must be visible at the same time as the figure/table/abstract, and must be hyperlinked to the journal's homepage.

5. The credit line should read:
   Reprinted by permission from Macmillan Publishers Ltd: [JOURNAL NAME] (reference citation), copyright (year of publication)
   For AOP papers, the credit line should read:
   Reprinted by permission from Macmillan Publishers Ltd: [JOURNAL NAME], advance online publication, day month year (doi: 10.1038/sj.[JOURNAL ACRONYM].XXXXX)

   Note: For republication from the *British Journal of Cancer,* the following credit lines apply.
   Reprinted by permission from Macmillan Publishers Ltd on behalf of Cancer Research UK: [JOURNAL NAME] (reference citation), copyright (year of publication)For AOP papers, the credit line should read:
   Reprinted by permission from Macmillan Publishers Ltd on behalf of Cancer Research UK: [JOURNAL NAME], advance online publication, day month year (doi: 10.1038/sj.[JOURNAL ACRONYM].XXXXX)

6. Adaptations of single figures do not require NPG approval. However, the adaptation should be credited as follows:

   Adapted by permission from Macmillan Publishers Ltd: [JOURNAL NAME] (reference citation), copyright (year of publication)

Note: For adaptation from the *British Journal of Cancer,* the following credit line applies.
Adapted by permission from Macmillan Publishers Ltd on behalf of Cancer Research UK: [JOURNAL NAME] (reference citation), copyright (year of publication)

7. Translations of 401 words up to a whole article require NPG approval. Please visit http://www.macmillanmedicalcommunications.com for more information.Translations of up to a 400 words do not require NPG approval. The translation should be credited as follows:

   Translated by permission from Macmillan Publishers Ltd: [JOURNAL NAME] (reference citation), copyright (year of publication).

   Note: For translation from the *British Journal of Cancer,* the following credit line applies.
   Translated by permission from Macmillan Publishers Ltd on behalf of Cancer Research UK: [JOURNAL NAME] (reference citation), copyright (year of publication)

We are certain that all parties will benefit from this agreement and wish you the best in the use of this material. Thank you.

Special Terms:

v1.1

Questions? **or** **(toll free in the US) or**

Curriculum Vitae

Sarah Hoffer

Education:

2013-Present **Master's Thesis Candidate –Master of Science – Biochemistry**
The University of Western Ontario, London, Ontario, Canada
Department of Biochemistry, Schulich School of Medicine and Dentistry and Robarts Research Instuitute
Thesis: Characterizing the function of helix five of the Ku70 von Willebrand A domain in non-homologous end joining

2009-2013 **Bachelor of Medical Science, Honors Specialization in Biochemistry and Cell Biology**
The University of Western Ontario, London, Ontario, Canada

Honours and Awards:

2013/2014 **Biochemistry 4999E Course Prize**
Awarded for highest grade in Biochemistry 4999E at the University of Western Ontario

2010-2013 **Dean's Honor List**
Awarded to University of Western Ontario students with an average above 80%

2009-2013 **Richmond Beck Scholarship** ($4000)
Awarded to a student attending university who graduated from Springfield Public School

2009 **Western Scholarship of Excellence** ($2000)
Awarded to students beginning studie at the University of Western Ontario with a high school average above 90%

2009 **Kinsmen Club of Aylmer Award** ($200)
Awarded to an East Elgin Secondary School student with strong academic standing

Research Experience:

Master of Science Candidate supervised by Dr. Caroline Schild-Poulter
Department of Biochemistry, University of Western Ontario
London, Ontario Canada
September 2013 – August 2015

Undergraduate Honors Research Project supervised by Dr. Eric Ball
Department of Biochemistry, University of Western Ontario
London, Ontario Canada
April 2012-August 2012

Student Volunteer supervised by Dr. Eric Ball
Department of Biochemistry, University of Western Ontario
London, Ontario Canada
July 2011-April 2012

Publication

Fell, V. L., Rogers, S., Aitken, A., **Hoffer S.**, and Schild-Poulter C. **Ku70 phosphorylation mediates Aurora B inhibition and activation of the DNA damage response.** Submitted to Nucleic Acids Research, (in review).

Abstracts:

Hoffer, S. and Schild-Poulter, C. **Characterizing the function of helix five of the Ku70 von Willebrand A domain in non-homologous end joining** (poster presentation).
12th Annual Oncology Research and Education Day
London, Ontario
2015

Hoffer, S. and Schild-Poulter, C. **Characterizing the function of helix five of the Ku70 von Willebrand A domain in non-homologous end joining** (poster presentation).
Robarts Research Retreat
London, Ontario
2015

Hoffer, S. and Schild-Poulter, C. **Characterizing the function of helix five of the Ku70 von Willebrand A domain in non-homologous end joining** (poster presentation).
London Health Research Day
London, Ontario
2015

Hoffer, S. and Schild-Poulter, C. **Characterizing the function of helix five of the Ku70 von Willebrand A domain in non-homologous end joining** (poster presentation).
11th Annual Oncology Research and Education Day
London, Ontario
2014

Hoffer, S. and Schild-Poulter, C. **Characterizing the function of helix five of the Ku70 von Willebrand A domain in non-homologous end joining** (poster presentation).
Robarts Research Retreat
London, Ontario
2014

Hoffer, S. and Schild-Poulter, C. **Characterizing the function of helix five of the Ku70 von Willebrand A domain in non-homologous end joining** (poster presentation).
2nd Annual Symposium on Telomeres and Genome Integrity
Quebec City, Quebec
2014

Hoffer, S. and Schild-Poulter, C. **Characterizing the function of helix five of the Ku70 von Willebrand A domain in non-homologous end joining** (poster presentation).
London Health Research Day
London, Ontario
2014

Hoffer, S. and Schild-Poulter, C. **Characterizing the function of helix five of the Ku70 von Willebrand A domain in non-homologous end joining** (poster presentation).
Biochemistry Department Annual Research Showcase
London, Ontario
2014

Extracurricular Activities

Participation House Support Services-London and Area, London, ON
Volunteer (2014-2015)

Special Olympics Ontario/London, London, ON
Coach (2014-2015)

Alzheimer Outreach Services of McCormick Home, London, ON
Volunteer (2014-2015)

Biochemistry Social Committee, Department of Biochemistry, University of Western Ontario, London, ON
Fundraiser event organizer (2014)

Cancer Awareness Society, University of Western Ontario, London, ON
Promotions executive, (2011-2012)

Violence Prevention Program, Thames Valley District School Board London, ON
Volunteer/Instructor, (2011)

War Child Western, The University of Western Ontario, London, ON
First year representative (2009-2010) and event coordinator (2011)